Protein Capture by Cation Exchange Membranes

by

Anna-Katharina Josefine Hassel

A thesis
presented to the University of Waterloo
in fulfillment of the
thesis requirement for the degree of
Doctor of Philosophy
in
Chemical Engineering

Waterloo, Ontario, Canada, 2015

Author's Declaration

I hereby declare that I am the sole author of this thesis. This is a true copy of the thesis, including any required final revisions, as accepted by my examiners.

I understand that my thesis may be made electronically available to the public.

A. Katharina J. Hassel

Abstract

Monoclonal antibodies (mAbs) are large recombinant proteins produced in CHO (Chinese hamster ovary) cell culture with a multiplicity of applications such as ligands for affinity chromatography material, medical applications for disabling toxins and especially as cancer therapeutics. They have the prospect of novel mechanisms for improved tumor targeting in local therapeutic applications.

The bottleneck in mAb supply lies not with their production but in their purification. Hence new mAb purification operations are necessary due to the complexity in their purification and the significant cost of antibody downstream procedures which can represent up to 80 % of the total production cost. The predominant mAb purification process relies on a series of resin chromatography steps with Protein-A affinity chromatography as the initial capture step. Protein-A resins display an excellent specificity for mAbs but are extremely costly, limited by pore diffusion mass transfer and may lead to leaching of the Protein-A ligand in the eluted product stream. To overcome these issues, alternative strategies without Protein-A or resin chromatography, are being investigated to achieve similar or improve mAb recovery.

This PhD project investigated the potential of a weak cation exchange macroporous hydrogel membrane material developed by NATRIX Separations^{TM} for model protein capture as first step towards mAb purification. The weak cation exchange material consists of a polymeric matrix and functionalized groups which display different charge characteristics according to ionic strength or pH.

The project was divided in three overall objectives: In a first part a variety of model proteins and antibodies were characterized for their hydrophobic character with a fluorescence probe. Secondly, the membrane was characterized, to contribute new knowledge for this novel weak cation exchange membrane such as its swelling behaviour, surface charge, ion exchange capacity and average pore size. Lastly, the interaction between membrane and proteins was investigated. Static and dynamic conditions as well as membranes in different formats were characterized for their binding behaviour and mass transfer limitations present in the material with model proteins lysozyme and IgG.

This work shows a promising avenue towards a simpler, cheaper and faster purification process with high protein capture and yield, addressing the downstream bottleneck for many proteins especially mAbs and make the successful cancer drug accessible for a broader audience of patients.

Acknowledgements

I would like to take this opportunity to thank several people for their support and guidance. Without them, this thesis would not have been possible.

Firstly, I would like to convey my heartfelt gratitude and appreciation to my supervisor Dr. Christine Moresoli. Her support and patience throughout this project went far beyond finding time for meetings and answering questions. She is truly an inspiration to me and I appreciate all the opportunities for professional and personal growth she provided over the years. I am thankful to have found such a kind mentor with high ethical values that I aspire towards.

I would like to thank my committee members, Dr. Marc Aucoin, Dr. Boxin Zhao, Dr. Brendan McConkey and Dr. Grant Allen for all their comments and assistance with my work.

I am grateful to the amazing staff in the Chemical Engineering Department: Rose Guderian, Ingrid Sherrer, Judy Caron, Liz Bevan, Ralph Dickhout, Bert Habicher, Rick Hecktus, Tom Dean and Jennifer Moll for their help with technical and organizational problems or for just lending me an ear at times.

Furthermore I would like to thank Dr. Sigrid Peldszus for the use of the electrokinetic analyser and Dr. Marc Aucoin for access to the AKTA machine.

I am grateful to MabNet (Monoclonal Antibody Network) for an amazing journey and fruitful scientific exchange over the years. Thank you also to NSERC (Natural Sciences and Engineering Research Council Canada) for funding my research and Natrix Separations Inc. (Burlington, Canada) for supplying membrane and accessory materials. Thanks to DAAD RISE (German Academic Exchange for Research Internships in Science and Engineering) for funding multiple students over the years to join our group from Germany and support my research.

A rewarding part of my responsibilities over the past few years has come from training and supervising several young and talented students. I would like to thank the students who made considerable contributions to my research and personal growth: Sarah Armbruster, Dorothee Kurz, Nicholas Cober, Ross Arnold, Max Fondyga, Nils Wagner, Dominika Kidon, Dhiren Patel, Tyler Sennema, Gianmarco Ferrari, Kamyar Ghofrani, Karthik Ramesh, Michelle Huang, Olivia Kwik, Kayleigh Kuindersma and Rawle Groothuizen.

I would like to thank all of my friends for being there for me especially Michaela, Jennifer, Annika, Barbara, Katja and Tina. And to my amazing family, particularly my sister Jasmin, my parents Annemarie and Erwin, my parents-in-law Roberta, Bob and Don and my loving husband William. Your belief gave me strength.

For Peter and all the precious souls we have lost to cancer

Für Peter und alle kostbaren Seelen, die wir durch Krebs verloren haben

Table of Contents

List of Tables

List of Figures

List of Equations

List of Abbreviations

ϵ	Dielectric constant of electrolyte (-)
ϵ_0	Vacuum permittivity (F/m)
η	Electrolyte viscosity (kg/ms)
σ	Protein steric factor (-)
ζ	Zeta potential (mV)
°C	Degree Celsius
A	Cross-section of the streaming channel (m^2)
aa	Amino acids
ADCC	Antibody-dependent cell-mediated cytotoxicity
ANS	1-anilino-8-naphthalene sulfonate
BHK	Baby hamster kidney
BSA	Bovine serum albumin
BTC	Breakthrough curve
C	Carboxymethyl
c	Concentration (g/l)
c_0	Initial protein concentration (g/l)
c_e	Eluted protein concentration (g/l)
c_f	Final protein concentration (g/l)
CDC	Complement-dependent cytotoxicity
CDRs	Complementary determining regions
cHCAb	Chimeric heavy chain antibody
CHO	Chinese hamster ovary
CLSM	Confocal Laser Scanning Microscopy
COS	African green monkey kidney
CPA	Cis-parinaric acid
D_{ax}	Axial dispersion coefficient (m^2/second)
Da	Dalton
DBC	Dynamic binding capacity (mg/ml)

DEAE	Diethylaminoethyl
EEM	Excitation-emission
EG2	Monoclonal antibody recognizing the human EGFR
EGFR	Epidermal growth factor receptor
ESEM	Environmental scanning electron microscopy
Ex	Example
ex/em	Excitation/emission
Fab	Antigen binding fragment
Fc	Crystallisable fragment
FESEM	Field Emission Scanning Electron Microscope
FI	Fluorescence intensity (-)
FPLC	Fast protein liquid chromatography
Gal	Galactose
GlcNAc	N-acetylglucosamine
H_s	Membrane relative swelling (-)
HCl	Hydrochloric acid
HCP	Host cell protein
HEK	Human embryonic kidney
HIC	Hydrophobic interaction chromatography
IEC	Ion exchange capacity (meq/g)
Ig	Immunoglobulin
IgG	Immunoglobulin G
IS	Ionic strength (mS/cm)
K	Equilibrium constant (ml/mg)
KCl	Potassium chloride
L	Length of the streaming channel (m)
m_{dry}	Mass of dry membrane (g)
$m_{swollen}$	Mass of swollen membrane (g)
M_S	Molarity of solution (mol/l)
mAbs	Monoclonal antibodies
Man	Mannose
NaCl	Sodium chloride
NaOH	Sodium hydroxide
Neu5Ac	Sialic acid
PES	Polyethersulfone
pH	Power of hydroxide
pI	Isoelectric point
PRODAN	6-propionyl-2-(N,N-dimethylamino)

PVDF-PAA	Polyvinylidene fluoride poly(acrylic acid)
Q	Quaternary ammonium
q	Binding capacity (mg/ml)
q_S	Swelling factor (-)
q_{max}	Saturation capacity of the solid matrix (mg/ml)
$q_{s,buffer}$	Membrane swelling factor in buffer (-)
$q_{s,I70}$	Membrane swelling factor in 70% isopropanol (-)
QAE	Quaternary aminoethyl
R^2	Coefficient of determination
rpm	Revolutions per minute
S	Methyl sulphonate
S_0	Hydrophobicity index (-)
SBC	Static binding capacity (mg/ml)
sdAb	Single-domain antibody
SDS-PAGE	Sodium dodecyl sulfate polyacrylamide gel electrophoresis
SE2	Secondary electron signal
SMA	Steric mass-action
SOM	Small organic molecules
SP	Sulphopropyl
SpA	Recombinant Staphylococcal Protein-A
SSR	Residual sum of squares
UV	Ultraviolet
v	Characteristic protein charge (-)
V_e	Elution volume (l)
V_m	Volume of dry membrane (l)
V_s	Volume of solution (l)
$V_{10\%}$	Volume at which absorbance is 10% of C_0 absorbance (l)
w/v	Weight by volume (%)

Chapter 1

Thesis Overview

1.1 Research Aim

For many years SOM (small organic molecules) have been the foundation of the pharmaceutical sector. Lately more and more biologics (biological based drugs) have found their way into clinical therapeutics [1]. Types of recombinant biologics (created with genetic recombination in laboratories) include hormones, growth factors, enzymes, inhibitors, vaccines and monoclonal antibodies (mAbs) [2].

The importance of mAbs has increased over the last decade. In 2001/2002, 16% of newly FDA approved biologics were mAbs, 3.5% of all pharmaceuticals, whereas in 2011/2012 this ratio increased to 35% and 9% for biologics and overall therapeutics respectively [1]. mAbs as therapeutics are mainly used in the the oncology sector (51%) and the autoimmune/inflammatory sector (38%). Forecasts for 2015 for a subset of 50 companies, accounting for approximately 70% of annual industry sales, predict that mAb sales will exceed 60 billion dollars [3].

The rise of recombinant medicine is facing many challenges predominantly the increasing demand for large scale productions and higher yields [1]. The existing bottleneck however is a downstream purification technique that can deal with the larger volumes and mAb concentrations currently achieved. The technique presently used to purify mAbs due to its high yield and purity is Protein-A resin chromatography. This technique however has many drawbacks including high ligand cost and poor bed utilization [4].

This PhD thesis will discuss an alternative purification technique for mAbs (and other proteins): cation exchange membrane chromatography.

1.2 Objectives

The main objective of this PhD work was to evaluate the potential of a weak cation exchange macroporous hydrogel membrane to capture monoclonal antibodies (mAbs) from cell culture. Multiple steps needed completion in order to achieve this assessment as seen in Figure 1.1. The flow chart represents the main steps of this project.

The first step was the characterization of selected proteins. Proteins of interest were model proteins bovine serum albumin, lysozyme, polyclonal Immunoglobulin G and a monoclonal antibody (EG2). Details such as charge and hydrophobicity characteristics affect the interaction between molecules (aggregation) and will have an effect on their interaction with the membrane chromatography material.

The second step mirrored this objective for the membrane material of interest. Charge and hydrophobicity characteristics of the membrane affect the interaction with proteins. Ion exchange capacity was determined as well as maximum amount of protein able to be captured. Further characteristics such as swelling and pore size were estimated.

With these two preliminary steps, objective 3 could be approached: Capture of model proteins IgG and lysozyme. Protein membrane interactions were evaluated in a static and dynamic mode. Conditions for binding and elution steps were investigated to achieve high binding capacities as well as recoveries. Research focus was on potential transport limitations of the material as well as the type of interaction with different proteins conducted through isotherm adsorption models.

1.3 Structure

This chapter (1.3) gives an overview of the thesis structure. Chapter 1.1 presents the research aim and motivation of the thesis. The objectives of the thesis are presented in Chapter 1.2. Most important literature and state of the art methodology are presented in Chapter 2. The results and discussion are presented in Chapters 3 to 5 as manuscript format. Some of the information especially in the introduction and materials and methods section may contain similar information. The overall conclusions and recommendations are presented in Chapter 7. In the following paragraphs, the major topics of Chapters 3, 4 and 5 are described. Each of these chapters start with a synopsis to summarize the aim of the respective chapter and standing as part of the whole thesis.

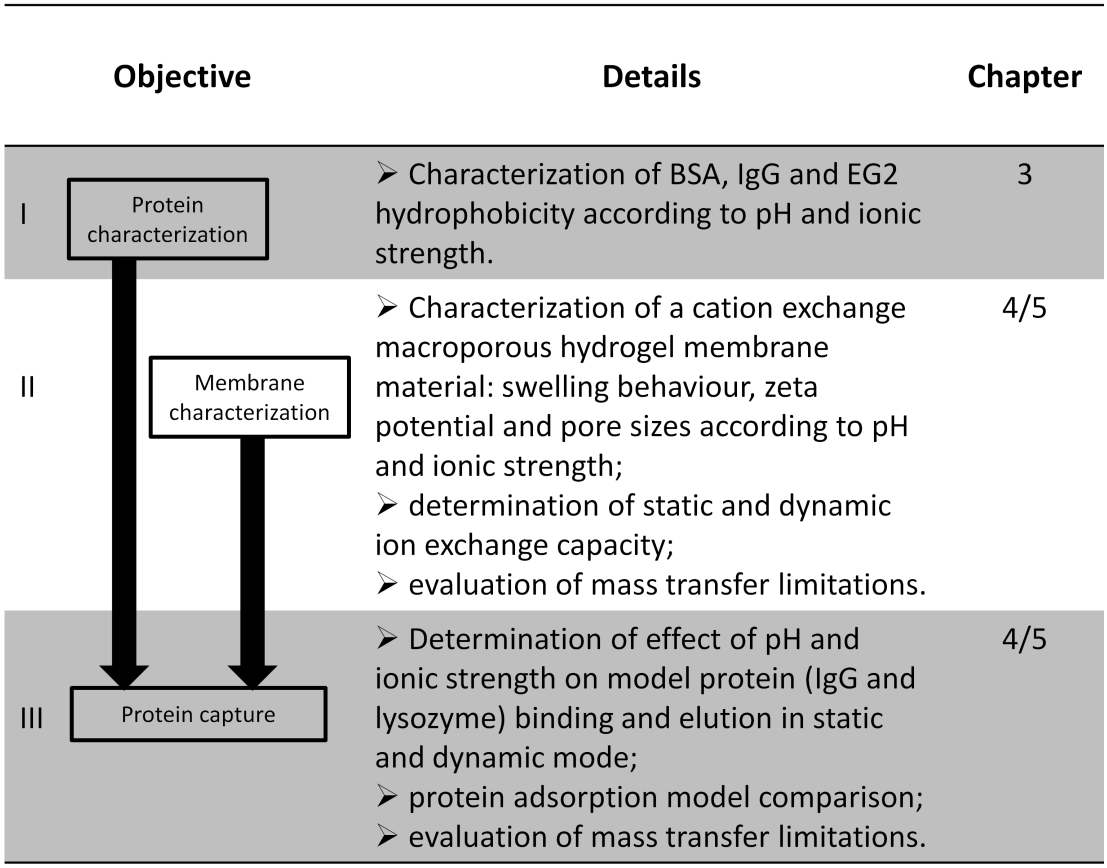

Figure 1.1: Flowchart of the objectives of the PhD thesis

Chapter 3
This chapter discusses protein hydrophobicity characterization (objective 1). Bovine serum albumin (BSA) was used as model protein to establish the ANS (1-Anilino-8-Naphthalene Sulfonate) method. Polyclonal Immunoglobulin G (IgG) and a monoclonal antibody (EG2) were investigated for their hydrophobic properties. This chapter was prepared for submission to the Talanta Journal.

Chapter 4
This chapter presents the physicochemical properties of a weak cation exchange macroporous hydrogel membrane. Characterization includes zeta potential measurement, pore size analysis, swelling and hydrophobicity behaviour in addition to static protein binding

and elution capacities with IgG (objective 2, 3). This chapter was submitted to the Journal of Membrane Science.

Chapter 5

This chapter deals mainly with protein and membrane interactions by considering capture of IgG and lysozyme as model proteins (objective 3). Ion exchange capacity (objective 2) was conducted and compared to protein interactions. Weak and strong cation exchange membranes were investigated and compared. This chapter was prepared for submission to the Journal of Membrane Science.

Chapter 2

Literature Review

2.1 Antibodies

2.1.1 Structure and Function

Antibodies or immunoglobulins are Y-shaped glycoproteins, containing a protein and a carbohydrate component, are produced by white blood cells (B cells) and play an important role in the human defence system.

Most antibodies are tetramers consisting of two heavy and two light chains (Figure 2.1). Disulfide bonds link the different chains together. The two heavy and two light chains are identical which gives the glycoprotein the option to bind simultaneously to two different antigens. Each chain has constant and variable regions. The constant regions of the heavy chains can be one of five isotypes which form the five different immunoglobulin classes: lgA, lgD, lgE, lgG and lgM [5] with IgG being the most important and therefore predominantly used in research. Light chains are distinguished as either kappa (κ) or lambda (λ) type. The two types exist in all major antibody classes but in recombinant antibody the kappa light chains are present [6].

Antibodies can be split by the protease enzyme papain at the cleavage site or hinge region, leaving two identical Fab (fragment, antigen binding) fragments consisting of one light chain, one heavy chain and one Fc (fragment, crystallisable) fragment consisting of two heavy chains. Fab is responsible for specific antigen binding whereas Fc consists of a ligand interaction site that induces clearance mechanisms. The complementarity determining regions (CDRs) of immunoglobulins are part of their variable regions and facilitate specific antigen binding.

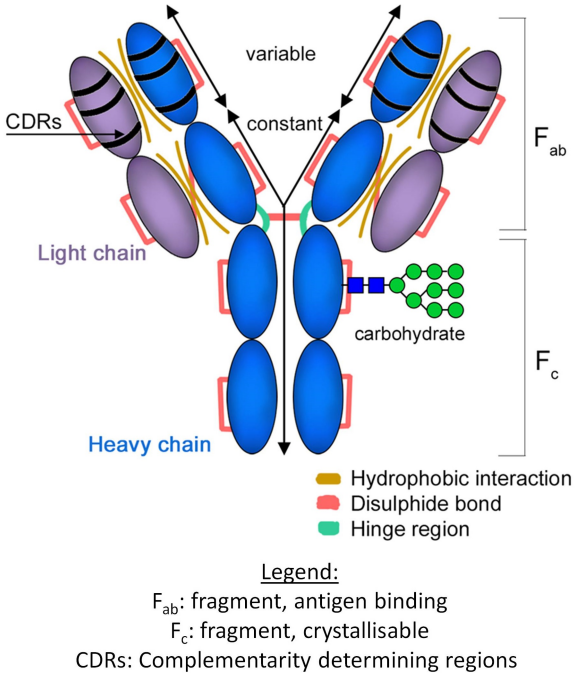

Figure 2.1: Antibody structure (lgG)

Antibodies possess three main functions: neutralize pathogens by binding to a specific epitope, a region on the antigen (the enemy cell surface); agglutinate, which means to link pathogens to a complex which are then easier to remove by phagocytes and activate the innate immune system (opsonisation) [7].

Different forces are involved in antibody-antigen binding. All of these are noncovalent interactions and are therefore reversible. For example high salt concentration, extreme pH and detergents can release the antigen. Table 2.1 shows the different forces responsible for antibody-antigen binding.

2.1.2 Glycoforms

The variable carbohydrates attached to the constant Fc region of IgG (Figure 2.1) lead to multiple potential isoforms (different forms of the same protein) of IgG. The attachment process is called glycosylation which is an enzyme based mechanism where oligo- or polysaccharides are attached to the antibodies. In this specific case, the isoforms are called

Table 2.1: Noncovalent forces forming the antibody-antigen-binding

Noncovalent forces	**Characteristics**
Electrostatic forces	Attractive forces between opposite charged molecules.
Hydrogen bonds	Interaction between two electronegative atoms like N and O that then share one hydrogen atom.
Van der Waals forces	Attractive and repulsive forces between molecules. The Lennard-Jones-potential is a model used for the van der Waals forces as a function of distance.
Hydrophobic forces	Hydrophobic molecules aggregate in order to keep out water molecules.

glycoforms (protein with different attached glycans or polysaccharides attached glycosidically). There are different classes of glycans for example N-, O-, and C-linked glycans, named after the element in the amino acid where binding takes place. With the addition of these glycans, proteins in general gain structural and functional abilities.

For antibodies, these changes may achieve specific changes in solubility, stability or aggregation behaviour. Studies indicate that the composition of cell cultures, along with other factors such as cell line, expression system and reactor types have a significant effect on the glycoforms [6]. Potential glycan side chains, as illustrated in Figure 2.2, can be classified as monoforms (e.g. high mannose), complex forms (e.g. variable monosaccharides) or hybrid forms. It is unknown as of yet if these changes have an impact on purification behaviour.

2.1.3 Monoclonal and Polyclonal Antibodies

Monoclonal antibodies (mAbs) come from a single clone of antibody producing cells (B cells). Therefore all antibodies are uniform and act against one specific epitope on one antigen. Unfortunately single cell clones are not very stable and have only a short half life. As a result Milstein and Koehler [8] invented a method to insure the longer survival of these cell clones. By combining B lymphocytes and myeloma (tumor) cells, immortal hybridoma cells were created.

Their high specificity make mAbs a valuable tool in fields such as tracking molecules in cells, purification in affinity chromatography and predominantly in medical applications

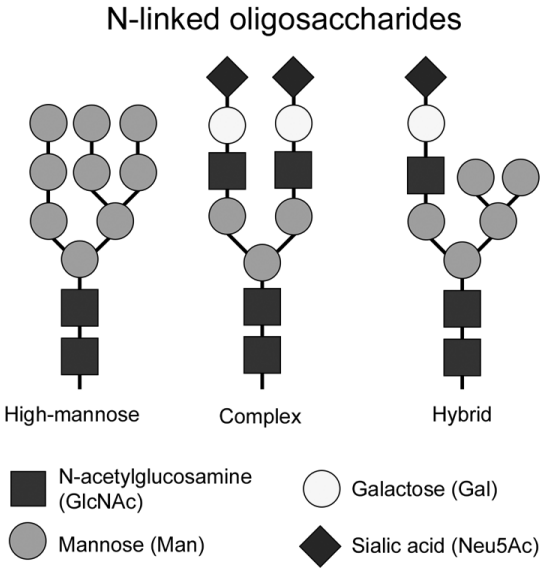

Figure 2.2: Example of potential glycan side chains for the modification of antibodies

for disabling toxins and as a cancer therapeutics. Monoclonal antibody based drugs are designed to target a specific antigen.

Polyclonal antibodies on the other hand come from different B cells and are therefore not identical but are more tolerant against changes on the epitope surface and can maintain their binding to the antigen. They are also used when the specific epitope is not yet known. However, due to their production in animals and their heterogeneity, polyclonal antibodies will likely show unspecific and undesired reactions and will likely require significantly higher doses and will limit their medical use.

Antibodies exist in a variety of sizes: large antibodies (> 100 kDa), medium size antibodies (30-100 kDa) and small antibodies (< 30 kDa) as summarized in Table 2.2. Antibody size is influencing characteristics such as half life and tumor penetration. The larger the antibody, the longer the half life but the more limited the tumor penetration.

IgG is an example for a large antibody. Many commercial mAbs are IgG based, for example Herceptin. EG2-hFc belongs to the medium sized antibodies and is a chimeric heavy chain antibody (cHCAb) that can be constructed by fusing a small, single-domain antibody (sdAb) EG2 with the fragment crystallisable (Fc) of human IgG. The advantage of an incorporated Fc domain is the induced antibody-dependent cell-mediated cytotoxicity (ADCC) and complement-dependent cytotoxicity (CDC) [9]. There is a potential

Table 2.2: Examples and characteristics of different size antibodies (ab)

Characteristics	**Small Ab**	**Medium Ab**	**Large Ab**
Example	sdAb (single domain antibodies)	cHCAb (chimeric heavy chain antibodies)	Ig (Immunoglobulin antibodies)
Size (kDa)	∼15	∼80	∼150
Half life	Low	Medium to high	High
Tumor penetration	High	Medium to high	Low
Potential or commercial mAbs	EG2 (potential)	EG2-hFc (potential)	Herceptin (IgG based, commercial) [9]

commercial application for antibodies containing the EG2 sequence since it recognizes the human epidermal growth factor receptor (EGFR), which is overexpressed or dysregulated in certain tumor types such as breast, lung and pancreatic cancer.

2.1.4 Antibody Production

The increasing demand for mAbs brings the need for efficient large-scale production. Therefore in vivo production is not sufficient and production by mammalian cell culture is preferable [10]. Most of the antibodies currently approved are not made in hybridomas but by recombinant DNA technology. During the last 20 years, when mAb production first started in mammalian cells, the industrial scale (up to 25,000 l bioreactors) titres increased about 30 fold up to 5 g/l. Laboratory scale titres up to 30 g/l have been reported [11–13].

HEK 293 (Human embryonic kidney) and CHO DG44 (Chinese hamster ovary) are the predominant cell lines used for transient expression of mAbs. Other known cell lines like COS (African green monkey kidney) and BHK (baby hamster kidney) are used to a lesser extent. The reasons that antibodies for pharmaceutical applications are predominantly produced in mammalian cell cultures include high producing, high stable cell lines, proper protein folding, post-translational modifications (e.g. glycosylation) and product secretion into the cell culture broth. Table 2.3 gives a brief overview of FDA approved mAbs from CHO cells [11].

Table 2.3: FDA approved mAbs from CHO cells (selected)

Product	**Manufacturer**	**Year**	**Treatment**	**Target**
Rituxan	Genentech	1997	Non-Hodgkin's lymphoma	CD20
Herceptin	Genentech	1998	Breast cancer	Her2
Zevalin	Spectrum Pharmaceuticals	2002	Non-Hodgkin's lymphoma	CD20
Vectibix	Amgen	2006	Colorectal cancer	EGFR

2.1.5 Antibody Recovery Techniques

The purification sequence for antibody recovery contains three major steps (Figure 2.3). The first step, cell harvest, is for the removal of cells via filtration or centrifugation. The second step, Protein-A chromatography, is targeting the antibodies. Additional polishing steps such as viral inactivation, ion exchange chromatography or filtration conclude the process. Additional chromatography steps assure that the leached and aggregated Protein-A is removed (cation exchange) and only monomers are further processed (size-exclusion). Higher order oligomers lose affinity towards antigens [14, 15]. The process of Protein-A affinity has been optimized for throughput, cleaning and re-use. To be purified, proteins need to consist of a C_H2/C_H3 region which interacts with Protein-A (Figure 2.4) [4].

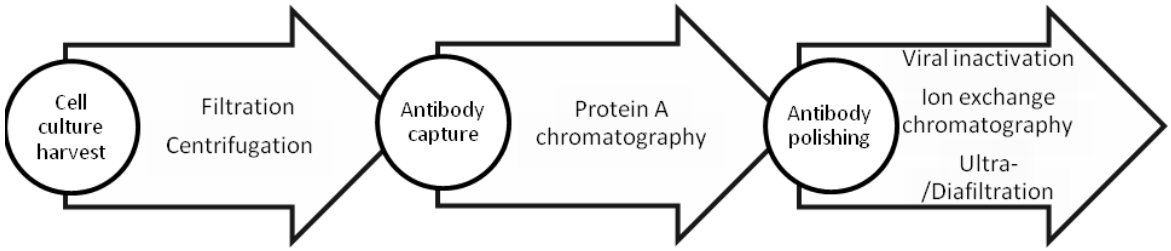

Figure 2.3: Antibody purification steps

Separation of antibodies via affinity chromatography happens on the basis of a reversible interaction between the antibody and Protein-A ligand, immobilized on the matrix. The interactions between Protein-A and the antibody can be a result of electrostatic or hydrophobic interactions, Van der Waals forces and/or hydrogen bonding (Table 2.1). For

elution of the antibody, the interaction is disrupted by using a competitive molecule, or by changing the pH, ionic strength or polarity.

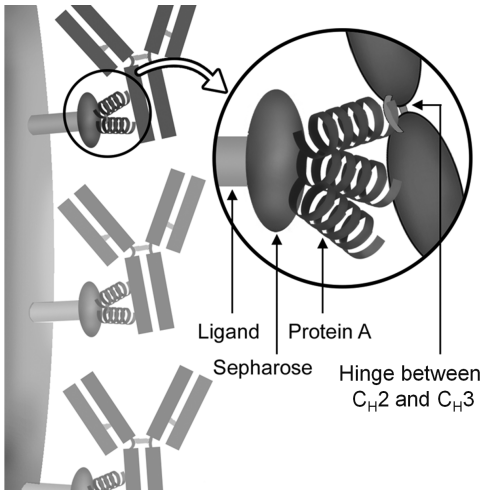

Figure 2.4: Schematic representation of interactions between Protein A ligand and C_H2/C_H3 antibody region

The advantages of antibody capture by Protein-A affinity purification consist of the specificity of the operation and significant time-saving (single step purification) compared to less selective multistep sequences. Large volumes can be processed. The major disadvantage is the expensive Protein-A ligand. Other serious problems include Protein-A ligand leaching and the limited lifetime of the Protein-A ligand material. Antibody capture by Protein-A affinity chromatography consists of the following major steps [16]:

1. Adsorption of the antibody (C_H2/C_H3 region) to Protein-A immobilized on a solid phase
2. Removal of bound contaminants by washing
3. Recovery of the antibody from the solid phase

Recombinant Staphylococcal Protein-A (SpA) is a 42 kDa protein. It is a component of *Staphylococcus aureus* cell surface. It has 5 homologous residues (about 58 aa) for the immunoglobulin binding and a C-terminal region for the attachment to the cell wall. By binding to immunoglobulins, it is slowing down the immune system and gives the microorganism a higher pathogenicity. Binding sites are predominantly the Fc fragment

of IgG1, IgG2 and IgG4 but also the Fab fragment of human IgG, IgM, IgA and IgE that contain V_H3 [16].

SpA consists of three different regions:

- S: signal sequence that is processed during secretion
- E, D, A, B and C: five homologous IgG binding domains
- XM: a cell-wall anchoring region

Every domain can independently bind to the Fc-part of IgG1, IgG2 and IgG4, with an estimated affinity constant (K_A) of $3.1*10^8$ M^{-1} (at 15°C). For interaction with IgG3, only a weak interaction can be measured [17].

Recent research has identified the binding motif between Protein-A and human IgG [18]. For human IgG1, the key amino acid residues are Isoleucine I253, Histidine H310, Glutamine Q311, Aspartic acid D315, Lysine K317, Glutamic acid E430 and Asparagine N434 and their counter components for SpA are Phenylalanine F132, Tyrosine Y133, Histidine H137, Glutamic acid E143, Arginine R146 and Lysine K154. Some of these amino acids have slightly basic or acidic side chains, Isoleucine and Phenylalanine have nonpolar side chains. Research groups found that 80% of the binding behaviour was due to hydrophobic interactions and less than 20% due to electrostatic forces [17, 18].

2.1.6 Protein Quantification Assays

2.1.6.1 Total Protein Quantification

Total protein quantification is commonly obtained by UV spectrophotometry and absorption at 280 nm (A_{280}) which represents the Tyrosine, Tryptophan and disulfide bonds content of the proteins. The value obtained depends on the path length of the cuvette. According to the Lambert-Beer law (Equation 2.1) [19]:

$$A(absorbance) = \epsilon * c * l \tag{2.1}$$

With ϵ = extinction coefficient ($M^{-1} * cm^{-1}$), c = concentration (mol/l) and l = optical path length (cm).

2.1.6.2 Protein Analysis by Molecular Weight Estimation

SDS-PAGE (sodium dodecyl sulfate polyacrylamide gel electrophoresis) is the most widely used method for qualitatively analyzing protein mixtures according to the molecular weight of their polypeptide chains. It is very useful for monitoring protein purification, and because the method is based on the separation of proteins according to size, the method can also be used to determine the relative molecular mass of proteins using a size standard [19]. The SDS-labelled proteins travel under an applied electric field with the same mobility. However, as proteins pass through the separating gel separation occurs: the smaller protein pass easily through the pores of the gel, whereas large proteins are retarded by frictional resistance owing to the sieving effect of the gel. Once the run is completed, the gel can be stained with Coomassie Blue and polypeptides are visible as blue bands on a clear background [20].

2.2 Chromatography Principles for Protein Purification

Chromatography is a technique where components of a mixture are carried in a mobile (liquid or gas) phase through a stationary phase (e.g. resin or membrane). Differences in their chemical structure will allow components to interact differently with the matrix and is used for their separation. Chromatography has five main steps: equilibration (preparation of the matrix), binding (introduction of the mixture containing the compound to be purified), washing (removal of unwanted bound substances), elution (recovery of desired compounds) and re-equilibration (restoring of matrix). Depending on the purpose of the separation, some steps will be more pronounced or steps might be dropped or interlaced.

Protein purification exploits the characteristics of the protein amino acid composition which will possess different hydrophobicity, charges and influence the overall net charge of the protein. The isoelectric point (pI) of a protein resembles an overall net charge of zero for the protein. Protein size can also be used for their separation. Protein mixtures can be purified using a variety of chromatography purification techniques. Only those techniques relevant to antibody purification will be discussed in the next sections with ion exchange chromatography presented in more detail.

2.2.1 Affinity Chromatography

In affinity chromatography, a specific ligand is coupled to the chromatography matrix and reversibly interacts with the target protein only. The technique is therefore highly selective, with high resolution, capacity and recovery. It is the only method that allows purification on the basis of biological function or chemical structure which is advantageous for the separation of active from denatured or highly aggregated proteins. Biological interaction between ligand and proteins can be reversed by using a competitive ligand (specific elution) or by changing the pH, ionic strength or polarity (non-specific elution). The major limitation of this effective separation technique is the cost of the affinity ligand and/or matrix cleaning procedures to prolong ligand life [16]. Protein-A is the major affinity ligand used for capturing antibodies. The technique is widely used in industry and leads to high yields and purities [18].

2.2.2 Size Exclusion

Size exclusion or gel filtration chromatography is based on the separation of proteins by size. Protein mixtures may differ in size and when applied to a porous gel matrix, small proteins can penetrate these pores and are delayed while large proteins are excluded and leave the matrix first. A potential drawback is poor resolution when proteins are very similar in size, which can be rectified by increasing retention time or matrix length which in turn increases time and mobile phase needs. Correct pore size of the matrix is very important [21]. Size exclusion can be used as a polishing step for antibody production when separating antibody monomers from aggregated antibodies [15].

2.2.3 Hydrophobic Interaction Chromatography

In hydrophobic interaction chromatography or HIC, a nonpolar matrix attracts proteins with hydrophobic patches. Organic solvents, change of pH or temperature can affect this interaction. Mild conditions are used and biological activity can be retained [21]. HIC has recently been considered for the separation of mAbs monomers from their aggregates [22].

Table 2.4: Functional groups in ion-exchange materials

Anion exchangers	**Functional group**
Diethylaminoethyl (DEAE)	$-O-CH_2-CH_2-N^+H(CH_2CH_3)_2$
Quaternary aminoethyl (QAE)	$-O-CH_2-CH_2-N^+(C_2H_5)_2-CH_2-CHOH-CH_3$
Quaternary ammonium (Q)	$-O-C_2-CHOH-CH_2-O-CH_2-CHOH-CH_2-N^+(CH_3)_3$
Cation exchangers	**Functional group**
Carboxymethyl (C)	$-O-CH_2-COO^-$
Sulphopropyl (SP)	$-O-CH_2-CHOH-CH_2-O-CH_2-CH_2-CH_2SO_3^-$
Methyl sulphonate (S)	$-O-CH_2-CHOH-CH_2-O-CH_2-CHOH-CH_2SO_3^-$

2.2.4 Ion Exchange Chromatography

2.2.4.1 Anion and Cation Exchange Chromatography Principles

Ion exchange chromatography is based on electrostatic interactions which involves reversible adsorption of charged solute proteins to immobilized ion exchange groups of the opposite charge. There are two types of ion exchange materials, cation and anion exchange. In anion exchange the matrix is positively charged whereas the counterions are negatively charged, leading to the binding of anions. Oppositely for cation exchange, the matrix is negatively charged, the counterions positively charged resulting in the binding of cations.

There are two approaches for protein purification with ion exchange. One can bind proteins of interest and wash out contaminants or bind the contaminants and let the desired proteins pass through. The first approach is more useful because it may also concentrate the protein of interest.

Table 2.4 [23] gives examples of potential functional groups of ion exchangers. The nature of the functional group will affect the type and strength of interactions between components and matrix whereas their number and availability will affect the capacity.

Sulfonic (SP, S) and quaternary amino groups (QAE, Q) are present in strong ion exchanger materials; DEAE and C are present in weak ion exchange material. The terms strong and weak do not refer to the strength in binding but to the extent of the variation of ionization with pH (Equation 2.2). Strong exchanger materials therefore are completely ionized over a wide pH range and very stable. The exchange capacity of weak exchangers on the other hand varies noticeably according to pH but this effect may provide slightly different selectivity and maybe preferred in some situations. The effect of pH and ionization

of the functional groups can be represented with the Henderson-Hasselbalch equation:

$$pH = pKa + \log\left(\frac{[A^-]}{[AH]}\right) \longleftrightarrow [A^-] = \left(\frac{10^{(pH-pKa)}}{10^{(pH-pKa)}+1}\right) * 100 \tag{2.2}$$

Most ion exchange operation consists of five steps (major three seen in Figure 2.5):

1. Equilibration to a start pH and ionic strength, specific to the binding of the desired protein
2. Sample addition, start of adsorption/binding –>counter ions bind reversibly to the matrix, unbound substances get washed out
3. Start of elution by changing conditions, increase in pH –>the matrix becomes more negative, proteins less positive or increase in ionic strength –>the matrix becomes less negative, more ions in solution shield proteins, release happens in order of their strength of binding, weakest first
4. Removal of the residual bound substances
5. Regeneration of matrix (re-equilibration) for next purification

Capacity of ion exchange material represents the ability to adsorb counterions. There are different ways to express the capacity [23]:

- Total ionic capacity: number of charged substituent groups per gram dry (or swollen) matrix
- Available capacity: amount of protein that can be bound under defined conditions
- Dynamic capacity: amount of protein bound when the feed flow rate is included

2.2.4.2 Surface Charge Properties

Ion exchange surfaces will change their surface charge according to pH and will interact differently with charged proteins. Surface charge properties can be obtained from zeta potential measurements.

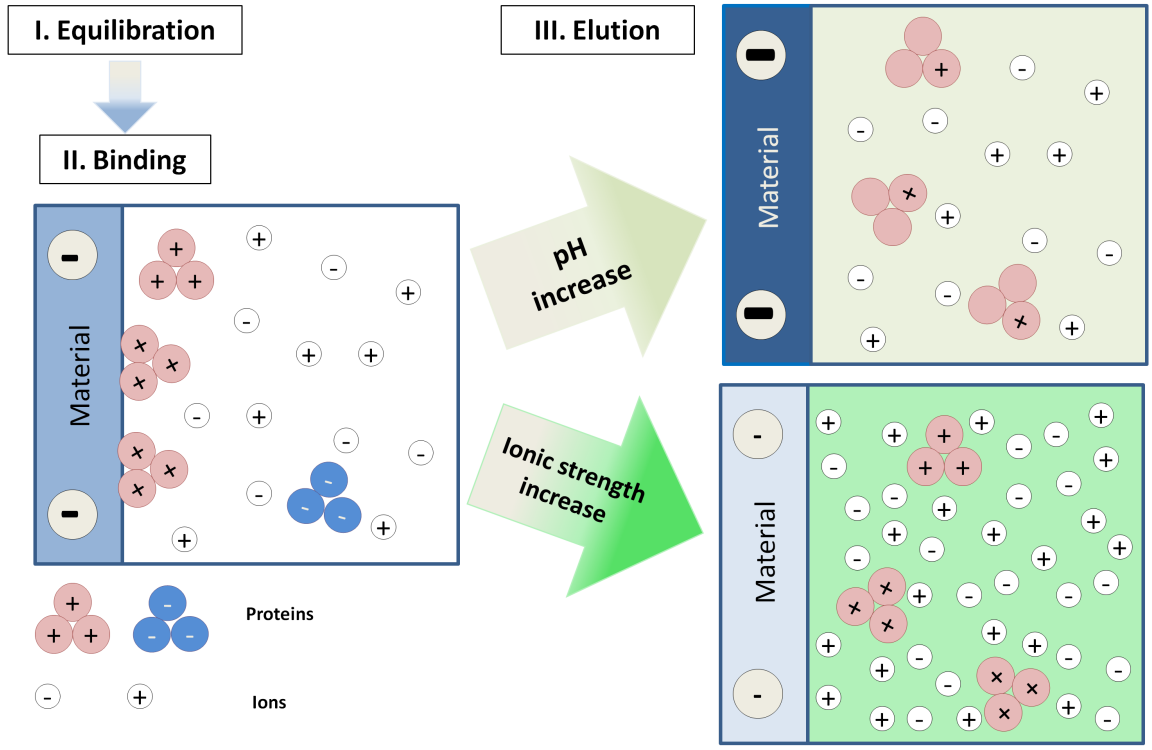

Figure 2.5: Cation exchange operation (3 major steps)

A charged surface will affect the distribution of ions in its surrounding area, called the interfacial region, resulting in a larger amount of counter ions close to the surface. This leads to the creation of the electrical double layer. This layer has three distinct regions: the surface potential on the surface of the particle or stationary phase, the stern potential in the centre of the electrical double layer and the zeta potential at the outer influence point of the electrical double layer, as seen in Figure 2.6.

The zeta potential magnitude gives an indication of the stability of the system. A system with high potential (negative or positive, >30 mV) has molecules that repel each other and is therefore stable. A zeta potential close to 0 indicates an instable system in which molecules tend to aggregate.

Zeta potential can be estimated from the streaming potential measurements obtained at different pressures (Equation 2.3).

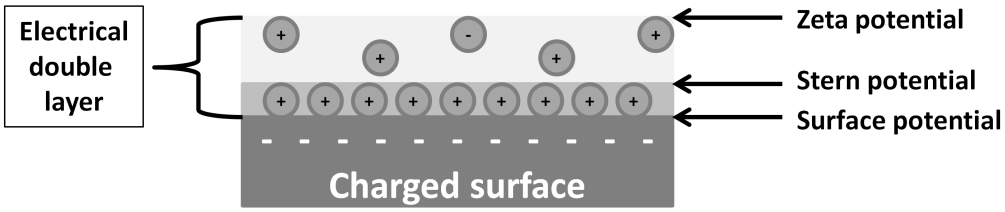

Figure 2.6: Electrical double layer and zeta potential

$$\zeta = \frac{dl}{dp} * \frac{\eta}{\epsilon * \epsilon_0} * \frac{L}{A} \tag{2.3}$$

With: dl/dp = slope of the streaming potential versus pressure curve; η = electrolyte viscosity (kg/ms); ϵ = dielectric constant of electrolyte (-); ϵ_0 = vacuum permittivity (F/m); L = length of the streaming channel (m); A = cross-section of the streaming channel (m^2).

2.2.4.3 Ion Exchange Capacity

Ion exchange capacity (IEC) represents the ability of a material to displace or exchange ions that were previously attached to the charged groups of the material. Table 2.5 presents published IEC characteristics (overall range from 0.22-2.8 meq/g) for exchange materials (focus on membranes) performed with the titration method.

Titration methods for determination of IEC with both cation and anion exchange membranes is commonly mentioned in literature [24–30]. The ion exchange membrane is first equilibrated to ensure that all the functional groups are protonated. Then a salt is introduced to displace the protons with the salt ions. Afterwards this solution can be titrated to determine the quantity of protons displaced which therefore indicates the equivalent number of functional groups that are active. The pH or conductivity of the solution according to volume of titration solution added can be used to determine the equivalence point and the corresponding ion exchange capacity according to Equation 2.4.

$$IEC(\frac{meq}{g}) = \frac{M_S * V_S}{m_{membrane}} \tag{2.4}$$

Table 2.5: Published IEC characteristics estimated by titration for ion exchange membrane materials

Membrane Material	**Exchange Group**	**IEC (meq/g)**
Polyvinylchloride/polycarbonate [24]	Strong cation	1.35-1.76
Poly(vinylchloride) [25]	Strong cation	1.2-2.8
Polyethylene and styrene-divinyl benzene [26]	Cation/Anion	1.40/0.78
Poly(vinylchloride) [27]	Cation	1.27-2.71
Sulfonated polysulfone [28]	Cation	0.66-0.72
Poly(vinylchloride) + styrene-divinvylbenzene [29]	Weak Cation	0.22
Poly(vinylchloride) + styrene-divinvylbenzene [29]	Strong Cation	0.28
Sulfonated poly(ether ester ketone) [30]	Cation	0.71-1.52

Where M_S is the molarity of titration solution (mol/l), V_S is the volume of solution added during the titration to reach the equivalence point (ml) and $m_{membrane}$ is the initial mass of the membrane, prior to hydration (g). The equivalence point can be estimated using the 1^{st} derivative method. The method uses the experimental data to generate a first derivative function with the maximum turning point being the equivalence point.

2.2.4.4 Protein Adsorption

The distribution of a solute between two phases of a chromatographic system can be described by equilibrium isotherms. Equilibria in the area of gas-solid and vapor-solution adsorption have been studied in detail, the former one for more than 230 years. The equilibrium isotherm plot shows the amount of a component in a known amount of the stationary phase versus its concentration in the carrier phase. There are five types of plots known (see Figure 2.7) [31]. Type I called Langmuir isotherm is the most frequent type. Here the pore size of the microporous adsorbent is not much greater than the diameter of the sorbate molecule. If there is a wide range of adsorbent pore sizes, types II and III can be observed showing characteristic vertical asymptotes. The increase in capacity at higher pressures (which is the equivalent to concentration in gas-solid interactions) can be explained with the increasing pore diameters with raising pressure. Types IV and V show a two step increase; this could be due to adsorption to surface layers in pores that are much wider than the diameter of the sorbate in addition to the normal diameters, or to filling of smaller pores after a few adsorption layers are formed.

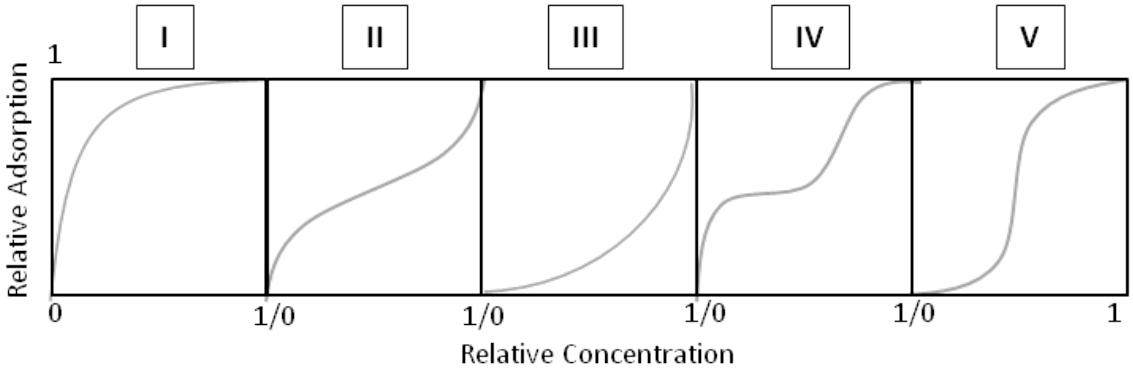

Figure 2.7: Adsorption isotherms profile types: I (Langmuir), II+III (asymptotic) and IV+V (step increase)

The study of phase equilibria in liquid-solid adsorption is more recent. Starting in the 1950ies, researchers adapted gas-solid adsorption principles to liquid-solid phenomena. This approach will be reviewed in the context of protein (adsorbate) adsorption to ion exchange material (adsorbent). Three of the adsorption isotherms presented in Figure 2.7 are valid for liquid-solid adsorption, types I, IV and V. Adsorption isotherm types II and III do not have an equivalent in liquid-solid studies. In general, liquid-solid equilibria are more complex but common gas-solid isotherms such as Langmuir, Bi-Langmuir and Freundlich have been extended to this newer area (describing shapes like Figure 2.7-I). Other adsorption isotherm models such as the steric mass-action (SMA) model and spreading model have been developed specifically for liquid-solid interactions (capture isotherm shapes I and V in Figure 2.7). All five models will be described in the next sections.

2.2.4.4.1 Satic Binding Capacity Static binding capacity represents equilibrium conditions and can be described with the following models:

Langmuir model The Langmuir model is the simplest description (Figure 2.8) of adsorption at solid-fluid interfaces. The assumptions are a homogeneous surface, monolayer coverage of proteins and that the occupation of one binding site does not affect the adsorption of a new protein. This is only true when the binding site density is low and the proteins are small. Equation 2.5 states the Langmuir isotherm [32]:

$$q(c) = q_{max} * \frac{K_L * c}{1 + K_L * c} \tag{2.5}$$

With q = binding capacity (mg/ml) at a certain c = concentration of protein (mg/ml), K_L = Langmuir equilibrium constant and q_{max} = saturation capacity of the solid matrix (mg/ml). The plot q/c versus q shows a linear trend. The equilibrium constant K_L (ratio of k_a and k_d in Figure 2.8) describes the shape of the isotherm. Many adsorption situations for protein binding to chromatography materials (especially membranes) do not follow the Langmuir isotherm since the assumptions may not represent reality.

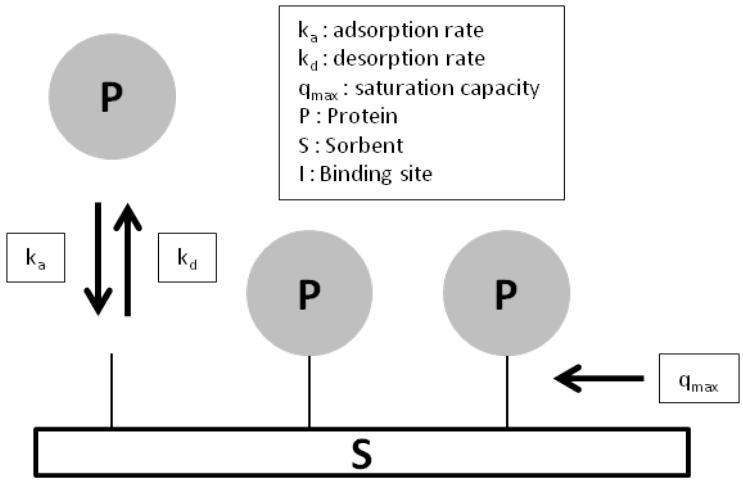

Figure 2.8: Schematic representation of the Langmuir adsorption principles

Bi-Langmuir model The Bi-Langmuir model is an expansion of the Langmuir model for chromatographic separations that do not possess a homogeneous surface. In cases where two different binding sites can interact with the proteins the Langmuir isotherm changes to two independent contributions as seen in Figure 2.12 and Equation 2.7 [32].

$$q(c) = q_{max,1} * \frac{K_{B,1} * c}{1 + K_{B,1} * c} + q_{max,2} * \frac{K_{B,2} * c}{1 + K_{B,2} * c} \tag{2.6}$$

With q = binding capacity (mg/ml) at a certain c = concentration of protein (mg/ml), $K_{B,i}$ = Bi-Langmuir equilibrium constant for sites 1 and 2 and $q_{max,i}$ = saturation capacity of the solid matrix (mg/ml) for sites 1 and 2. The Bi-Langmuir model is used instead when the plot q/C versus q is too strongly curved to fit the Langmuir model.

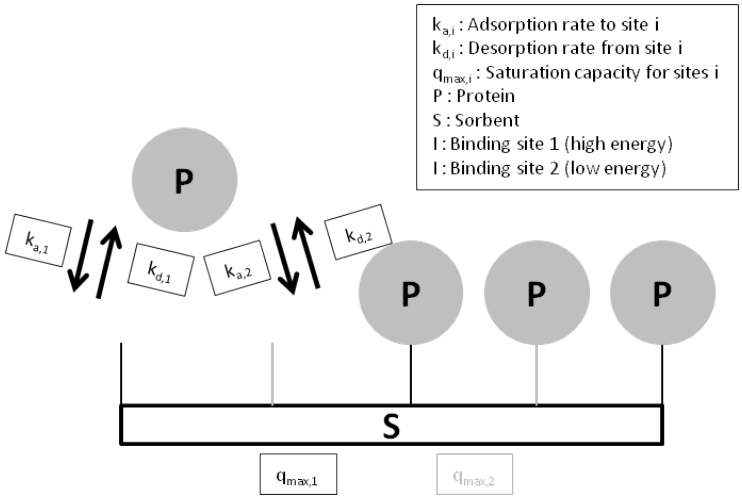

Figure 2.9: Schematic representation of the Bi-Langmuir adsorption principles

Freundlich model The Freundlich model is an empirical derivation from the Langmuir model. It takes into account that with increasing protein surface coverage the rate of protein adsorption slows down (see Figure 2.10). Equation 2.7 will take this new development into account [32, 33]:

$$q(c) = K_F * c^{\frac{1}{n}} \tag{2.7}$$

With q = binding capacity (mg/ml) at a certain c = concentration of protein (mg/ml), K_F and n = Freundlich constants. The exponent 1/n has to be between 0 and 1, resulting in $n \geq 1$. For n = 1, a linear isotherm is obtained. With increasing n, the initial tangent of the isotherm is getting sharper but the maximum binding capacity decreases.

Steric mass-action model The steric mass-action (SMA) model was proposed to describe strong non-linear adsorption in ion-exchange systems. Assumptions for the model are (1) spherical proteins that have uniform size and density, (2) protein binding is dependent on the characteristic charge v, (3) steric hindrance of the counterions bound to the solid matrix occurs and (4) model parameters do not change during adsorption process [34]. Figure 2.11 shows a representation of the principles.

The SMA isotherm can then be described as in Equation 2.8:

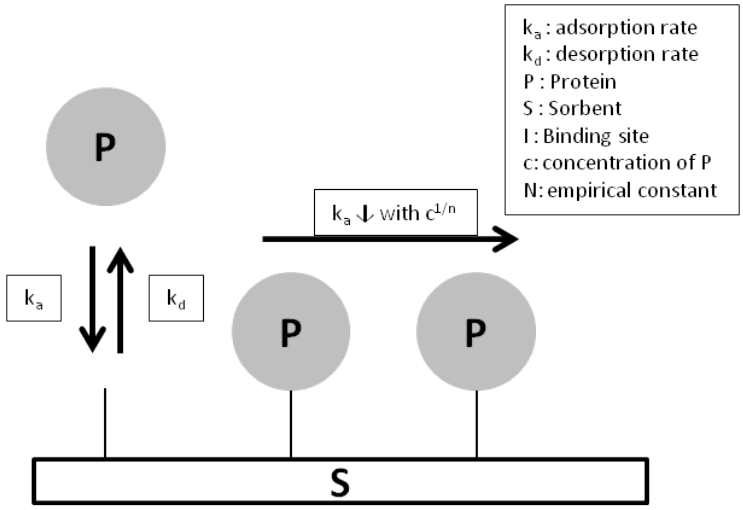

Figure 2.10: Schematic representation of the Freundlich adsorption principles

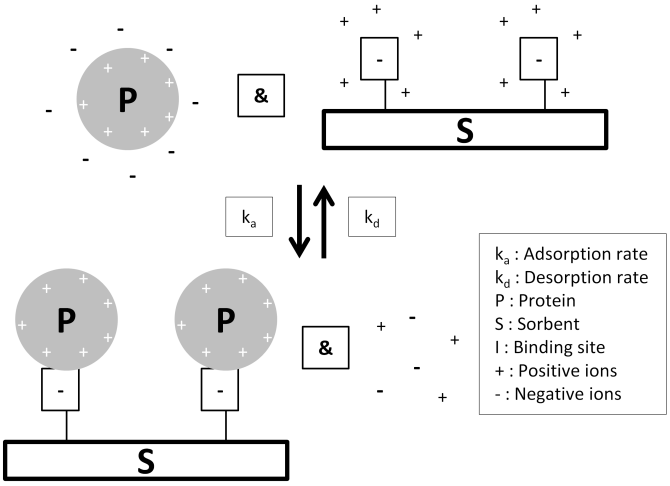

Figure 2.11: Schematic representation of the SMA adsorption principles

$$c = \frac{q}{K_{SMA}} * \frac{n * c_S}{A - (v + n * \sigma) * q}^{\frac{v}{n}} \tag{2.8}$$

With c = concentration of proteins (mg/ml) for a given q = binding capacity (mg/ml), K_{SMA} = equilibrium constant for SMA model, A = ion exchange capacity of monovalent

salt counterions (mmol/l), n = value of valence of salt counterions, c_S = salt counterion concentration in bulk phase (mmol/l), v = characteristic charge, σ = protein steric factor. The equation can be simplified in two extreme cases, low concentration (c) (Equation 2.9) and high concentration (c) (Equation 2.10).

$$\frac{q}{c} = K_{SMA} * \frac{A}{n * c_S}^{\frac{v}{n}} \tag{2.9}$$

$$q_{max} = \frac{A}{v + n * \sigma} \tag{2.10}$$

To solve the isotherm, assumptions of A, n, C_S and q_{max} need to be made according to experimental set-up and with that parameters K_{SMA}, v and σ can be estimated.

Spreading model Limitations for the previously discussed models are that proteins are not considered to change conformation after adsorption. This however may not happen in reality where orientation and/or conformation of proteins may change after adsorption (see Figure 2.12).

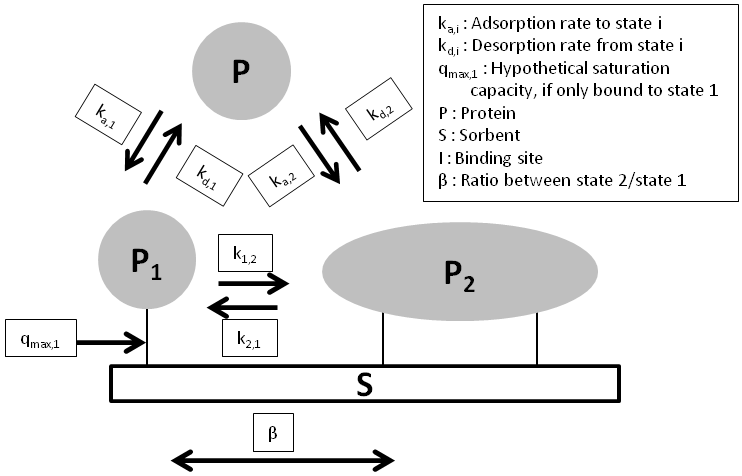

Figure 2.12: Schematic representation of the spreading adsorption principles

Desorption from P_2 to P is negligible most of the time, so in addition to q_{max} and β only equilibrium constants K_1 and K_{12} need to be determined [33].

2.2.4.4.2 Dynamic Binding Capacity Dynamic binding capacities do not deal with equilibrium conditions but focus on the kinetics of a system. Breakthrough curves (BTC) are used to analyze dynamic protein binding capacity. To describe the BTC all previous adsorption models above can be used.

Breakthrough Curves Breakthrough curves (BTC) play an important role in analyzing adsorption behaviours in a dynamic mode where a protein feed solution flows through a resin/membrane chromatography system. Figure 2.13 [35] shows a typical BTC which has similarities to type V of the adsorption isotherms (Figure 2.7). Since BTC are important, its characteristics will be discussed in detail. BTC represent the change of the protein concentration at the exit of the chromatography system over time or volume of the effluent. Theoretical BTC show a sharp peak from 0 to feed protein concentration. Everything is being retained by the chromatography material and once the material is saturated, the effluent stream reflects the feed protein concentration. In reality BTC is not as sharp. BTC is more curved as seen in Examples 1 and 2. One characteristic of BTC is 10% breakthrough which denotes the feed solution volume when 10% of the feed protein concentration is measured at the exit of the chromatography system. The later (or at larger volumes) this occurs, the higher the dynamic binding capacity (DBC) of the material will be (here $\mathrm{DBC}_{Ex2} > \mathrm{DBC}_{Ex1}$). But that is not the only important consideration. The shape of the BTC gives information of the binding behaviour. The closer the shape to the theoretical shape the better since it means the material captures more before it is saturated and does not leak proteins continually (here Ex1 closer to theoretical than Ex2). Mathematically, the area above the BTC resembles the captured and retained protein whereas the area below the BTC can be used to calculate the amount lost due to breakthrough.

To determine 10% breakthrough, Equation 2.11 can be used:

$$q_{DBC10\%} = \frac{c_0 * V_{10\%}}{V_{membrane}} \tag{2.11}$$

With $q_{DBC10\%}$ = dynamic binding capacity at 10% breakthrough in mg protein/mg membrane, c_0 = feed protein concentration (mg/ml), $V_{10\%}$ = volume (ml) at which absorbance is 10% of c_0 absorbance and $V_{membrane}$ = volume of membrane (ml).

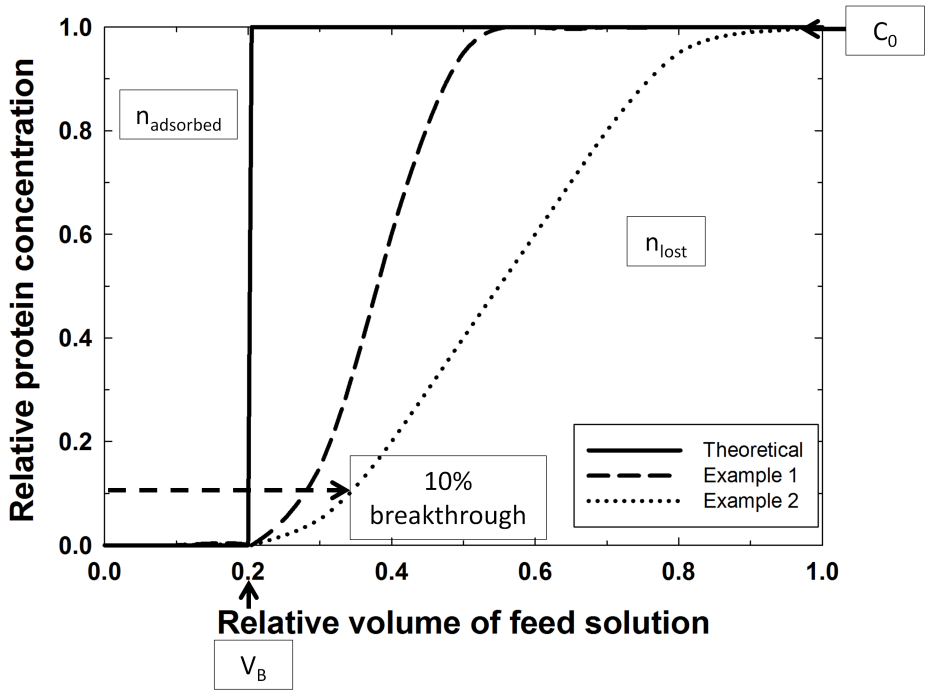

Figure 2.13: Typical breakthrough curve and important parameters with: V_B: breakthrough volume, c_0: analyte concentration, $n_{adsorbed}$: amount retained in membrane, n_{lost}: amount lost due to breakthrough

2.3 Membrane Chromatography

Packed bed resin chromatography has been widely used for protein purification for over 50 years. It yields a high resolution separation of mixtures and can be, depending on the application, low cost and high throughput.

The matrix of resin chromatography can be based on inorganic materials, synthetic materials or polysaccharides. The matrix determines properties such as efficiency, capacity and recovery but also chemical stability, mechanical strength and flow properties. The matrix will also affect the type of binding and may influence the biological activity of the purified protein [23, 36].

Limitations of packed bed resin chromatography are multifold. Examples include pres-

sure drop across the packed bed which is increasing during the process due to media deformation and accumulation of colloidal material and intra-particle diffusion for binding between media and targeted molecule (Figure 2.14) [37]. Channelling is another problem which occurs when cracks in the material or poor packing lead to short-circuiting flow and therefore poor bed utilization.

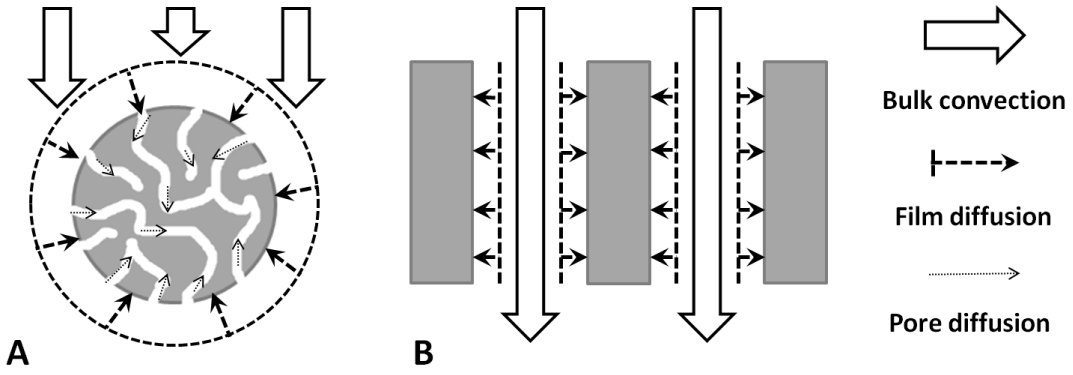

Figure 2.14: Transport in resin (A) versus membrane chromatography (B)

Membrane chromatography also called membrane adsorbers are porous membranes containing functional groups [38]. Their advantages include their 3D-structures with open pores, negligible limitations due to diffusion and high capacity and flow rates. Since the transport is mainly achieved by convection, reduced time and recovery liquid volume can be obtained. Protein binding capacity is almost independent of flow rate over a wide range so that high flow rates can be used. Compared to packed bed columns, a lower pressure drop is reported. It is easy to scale-up and advantageous for large proteins. There are different types of membrane adsorbers that could be used in purification of mAb. PES (polyethersulfone) membranes are charged, hydrophilic polymers that can be functionalized. Other base materials are regenerated cellulose and polyolefins. Table 2.6 presents common commercial ion exchange membranes and their characteristics. Pore size diameter reflects the base material properties and range from 0.3 to 3 μm. Binding capacity depends on material and protein to be captured with a range from 20 to 300 mg/ml.

Dynamic binding capacity for membrane chromatography materials (up to 100 mg/ml hIgG and up to 300 mg/ml BSA, Table 2.6) are higher than for resins (10 mg/ml IgG and 20-60 mg/ml BSA [40] for ion exchange resins, about 50 mg/ml IgG for affinity resins [41]). Binding capacity for membranes remains constant over increasing flow rate (up to 40 x bed volumes) whereas binding capacity for resins decreases with increasing flow rate. When looking at the size of proteins, binding capacity for membrane chromatography

Table 2.6: Commercial ion exchange membranes and their characteristics

Company	**Membrane**		**Characteristics**[a]		
Product name	*Base Material*	*Exchange group*	*Pore size*	*Dynamic binding capacity (10%)*	*Ligand density*
Natrix					
Natrix Q	Polyolefin	Strong anion-exchange	0.45 μm	>300 mg/ml BSA [39]	n/a
Natrix C	Polyolefin	Weak cation-exchange	0.3 μm	>100 mg/ml IgG	n/a
Natrix S[b]	Polyolefin	Strong cation-exchange	0.45 μm	>250 mg/ml lysozyme [39]	n/a
Pall					
Mustang Q	Modified PES	Strong anion-exchange	0.8 μm	70 mg/ml BSA	n/a
Mustang S	Modified PES	Strong cation-exchange	0.8 μm	47 mg/ml lysozyme, 60 mg/ml hIgG	n/a
Satorius					
Sartobind Q	Regenerated cellulose	Strong anion-exchange	>3 μm	29 mg/ml BSA	4-6 μ/cm^2
Sartobind C[b]	Regenerated cellulose	Weak cation-exchange	>3 μm [39]	21 mg/ml lysozyme [39]	4-6 μ/cm^2 [39]
Sartobind S	Regenerated cellulose	Strong cation-exchange	>3 μm	29 mg/ml lysozyme	4-6 μ/cm^2
Sartobind D	Regenerated cellulose	Strong cation-exchange	>3 μm	22 mg/ml BSA	4-6 μ/cm^2

[a]Manufacturer data unless otherwise stated
[b]No longer commercially available

only decreases slightly when purifying proteins over 500 kDa while resins show significant binding capacity decrease for large proteins [42].

There are still some major limitations for membrane chromatography in large-scale applications. For example a poor inlet flow distribution, non-identical membrane thickness or pore size distribution. These disadvantages can be reduced by using multiple membrane layers or optimal membrane holder device configurations.

The three configuration types are flat sheet, hollow fibre and radial flow devices (Figure 2.15) [37]. Flat sheets are generally employed as stacked sheets. The flow is normal (perpendicular) to the membrane material. An additional benefit of hollow fibres membrane chromatography systems is a high surface area and reduced accumulation of particles due to cross flow. The flow is parallel to the surface at first and then pressed through the pores. Flat sheets and hollow fibre systems are used in laboratory scale experiments. The radial devices are used for large scale productions and are widely used in industry. The flow is convective for axial transport but diffusive for radial transport [43]. The commercially available membranes in Table 2.6 come as cut disc, syringe filter ready or cross-flow cassette (Natrix only).

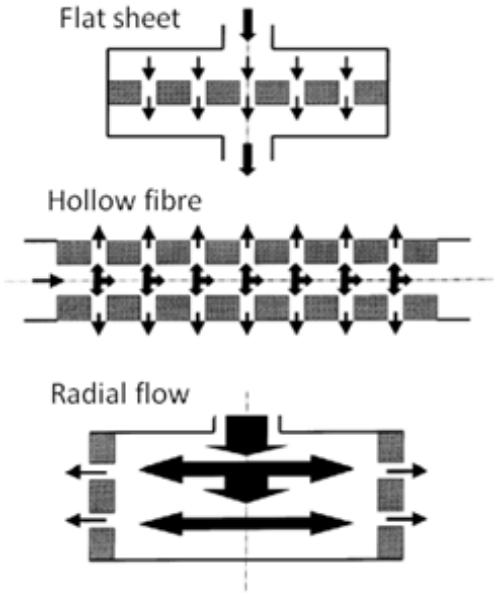

Figure 2.15: Flow in membrane adsorbers

2.3.1 Structural Characterization of Membranes

Several methods are available for characterization of the pore structure of membrane materials. Liquid intrusion porosimetry uses a non-wetting liquid such as mercury. The pressure needed to force the liquid into the pores can be related to the pore size of the material. This technique however does not represent the pore size distribution in a hydrated state which is a major limitation for hydrogel materials [44]. To overcome this disadvantage, inverse size exclusion chromatography could be used where the membrane materials are equilibrated in buffer and therefore represent hydrated conditions. The technique uses multiple probes of different sizes and performs binding experiments [45]. The binding capacities of different probes reflect on the pore size distribution. The estimated pore size may not represent the actual pore size distribution if the full pore space is not accessible to the probe [46].

To visualize membrane surfaces field emission scanning electron microscopy (FESEM) imaging can be used. It offers larger depth of field than a stereo microscope and higher resolution. Samples must be dry and conductive. Most biological samples are non-conductive and will require coating with a thin layer of gold which makes this technique complex and expensive. The magnification is up to 250 000 x. 3D surfaces are also possible to create. For wet samples, environmental scanning electron microscopy (ESEM) could be an alternative technique where samples can be maintained hydrated during imaging. Resolution however is diminished compared to FESEM and therefore a sample freeze drying step prior to FESEM analysis could be an alternative to capture the morphology of the hydrated sample while meeting the dried requirements of FESEM [44, 47].

2.3.2 Mass Transfer in Membranes

Mass transfer in chromatography operations for protein purification reflects the multistep process of protein transport in the bulk phase and in the porous material. Protein transport will involve convective flow from the bulk to the liquid film interface, within the liquid film, internal material transport and ultimately protein adsorption with the ligands of the material.

Convective flow is described by axial dispersion and represented by a protein mass balance in the mobile phase for a membrane section of thickness z given by Equation 2.12:

$$D_{ax} * \frac{\delta c^2}{\delta z^2} = \epsilon * \frac{\delta c}{\delta t} + (1 - \epsilon) * \frac{\delta s}{\delta t} + u_{sf} * \frac{\delta c}{\delta z} \tag{2.12}$$

With ϵ = porosity of the membrane (-), c = protein concentration in the mobile phase (mg/ml), s = protein concentration in the stationary phase (mg/ml), u_{sf} = interstitial velocity (m/second), D_{ax} = axial dispersion coefficient (m^2/second), z = axial position in the membrane (m).

The axial dispersion coefficient, reflects flow non-uniformities, axial diffusion and turbulence in the liquid within the membrane pores which can be estimated from tracer experiments and the first and second moment of its residence time distribution [48] or correlations [49]. The term $\delta s/\delta t$ represents the sink term and is given by protein adsorption on the material surface (discussed in section 2.2.4.4).

Transport within the liquid film in membrane chromatography is represented as follows:

$$\frac{\delta s}{\delta t} = k_f * (c - c_f) \tag{2.13}$$

With k_f = lumped liquid film mass transfer coefficient (s^{-1}), c = protein concentration in mobile phase (mg/ml), c_f = protein concentration within the film (mg/ml). Liquid film mass transfer can be estimated from correlations.

Intra material protein transport includes diffusion in the pores with the protein concentration gradient in the pore liquid as driving force and diffusion in the adsorbed phase with the protein concentration gradient in the adsorbed phase as driving force. Its importance in 3D membrane chromatography materials has long been recognized [49] and observed qualitatively but the interplay between mass transfer and adsorption has limited its analysis.

Qualitative analysis of mass transfer in membrane chromatography can be obtained from visual observations, microscopy or breakthrough curve profiles in dynamic conditions. Modeling approaches have been developed to investigate mass transfer with unique model framework based on combinations of convective flow and mass transfer and protein adsorption considerations and in some instances considerations of liquid film mass transfer and internal material mass transfer considerations [33, 48–50].

Gebauer et al. [49] considered internal material diffusion mass transfer with Langmuir isotherm for strong cation exchange Sartorius membranes with different base materials and functional layer grafting density and proteins (lysozyme and BSA). Their model estimates could reproduce very closely the full breakthrough curves (BTC). Surface diffusion was identified as limiting step for the high grafting density functional layer membrane material while pore diffusion was the limiting step for the low grafting density functional layer membrane material.

In contrast, Yang and Etzel [33] did not consider mass transfer limitations but considered more elaborate binding mechanisms, Langmuir model, steric hindrance model and spreading model for custom made anion exchange microporous poly(vinylidene difluoride) membranes with alpha-lactalbumin and thyroglobulin. Their work indicated that the spreading model provided the best representation of the experimental BTC. But one cannot rule out that the spreading model may have also captured internal mass transfer effects.

Recently, Francis et al. [48] reported on the modeling of protein capture with Mustang Q anion exchange membranes and ovalbumin as target protein. Their modeling approach considered flow non-idealities in the external volume, convection, liquid film mass transfer and four different protein adsorption models, Langmuir, Bi-Langmuir, steric mass-action and spreading model. Their model parameters were estimated from the fitting of experimental breakthrough curves for four different feed flowrates. Consideration of external flow non-idealities with the zonal rate model was able to capture the breakthrough curve broadening due to increasing feed flowrate. Their analysis of the liquid film mass transfer, based on dimensionless group analysis, height equivalent to a theoretical plate and empirical correlation, indicated that the liquid film mass transfer was not limiting and thus could be neglected. Comparison of the four different adsorption models outlines the difficulty in capturing the strong non-linear behavior of the breakthrough curve, sharp initial increase and slow increase near saturation. Only the spreading model was able to capture the strong asymmetry of the experimental BTC obtained at four different flowrates.

Van Beijeren et al. [50] considered the steric mass-action adsorption model, liquid film mass transfer and convection to investigate the effect of flowrate, pH and salt on protein and ion exchange type for commercial strong anion and cation exchange Sartorius membranes with BSA and lysozyme. Their results point to the difficulty in capturing experimental breakthrough curve for range of salt concentrations and feed flowrates and the different behavior according to protein and ion exchange type. The need to incorporate salt effect in model parameter is also suggested.

The status of modeling of protein purification by membrane chromatography was recently reviewed by van Beijeren et al. [51] where the complexity and limited understanding of these operations was reiterated together with the difficulty in accurately representing the full breakthrough curve and the lack of correlations and analysis tools available for these materials.

Mass transfer in membrane chromatography and key literature findings point to the complexity of the mechanisms involved and the difficulty in clearly understanding the phenomena taking place in the functional layer of the membrane material. As details of protein

internal transport and protein adsorption are included, model parameter identifiability and discrimination becomes challenging. Multiple combinations of parameters can reproduce the experimental breakthrough curve to the same accuracy. It may be possible that complex adsorption models may capture internal mass transfer elements in their representation of experimental data when internal mass transfer is not considered. Thus experimentation to better understand mass transfer mechanisms is needed to account for functional layer architecture and for the development of accurate models.

Chapter 3

Challenges for the Determination and Comparison of Protein Hydrophobicity with 1-Anilino-8-Naphthalene Sulfonate (ANS) as Fluorescence Probe

3.1 Synopsis

To analyse the interaction between proteins and membrane adsorber, one has to understand all participants involved and predict their behaviour in different environmental conditions such as pH and ionic strength. Chapter 3 therefore is focussing on the hydrophobic characterization of proteins (BSA, IgG and EG2). To estimate their surface hydrophobicity in different buffers, a characterization method based on ANS as fluorescence probe with affinity to hydrophobic patches on the protein surface, was adapted from the literature for the characterization of BSA as model protein and IgG and EG2 as antibodies.

The ANS technique was established by Sarah Armbruster under the direct supervision of Katharina Hassel, extensive testing with BSA was performed by Ross Arnold and Dorothee Kurz. Technique optimization and antibody characterization was done by Katharina Hassel with support from Gianmarco Ferrari. Data analysis was performed by Katharina Hassel with support from Sarah Armbruster (fluorescence intensity profile), Dorothee Kurz (hydrophobicity estimation model) and Ross Arnold (standardization of data). Writing

was done by Katharina Hassel in collaboration with Ross Arnold (literature comparison). Experimental planning, data analysis and writing were supervised, reviewed and revised by Christine Moresoli.

This chapter has been formatted for future submission to Talanta by Katharina Hassel, Dorothee Kurz, Ross Arnold, Sarah Armbruster and Christine Moresoli, Challenges for the Determination and Comparison of Protein Hydrophobicity with 1-Anilino-8-Naphthalene Sulfonate (ANS) as Fluorescence Probe.

3.2 Abstract

Hydrophobicity of proteins can influence significantly their recovery. Relative surface hydrophobicity of proteins can be obtained with the fluorescence probe 1-anilino-8-naphthalene sulfonate (ANS). ANS does not solely interact with proteins via hydrophobicity but can also interact with proteins by charge interactions.

The first objective of this study was to review and adapt the ANS methodology for comparison between independent studies with the model protein bovine serum albumin (BSA). The second objective was to investigate surface hydrophobicity characteristics of immunoglobulin G (IgG) and EG2 (monoclonal antibody) for pH and ionic conditions representative of cation exchange chromatography operations. Hydrophobicity analysis with ANS was modified by expanding the protein concentration beyond the linear range, using a single reciprocal linear plot (Scott plot) to extract hydrophobicity index (S_0) and by standardization of the data for comparison between conditions and studies. S_0 estimates of BSA from different studies indicated highest relative hydrophobicity at pH 3, lower hydrophobicity at pH 5 and divergent hydrophobicity estimates at pH 7. The magnitude of the hydrophobicity index for BSA, IgG and EG2 was affected by pH (5 and 7) and ionic strength (0 and 1 M KCl). Differences were protein specific and could be related to reported ANS binding sites for BSA and IgG or used to propose ANS binding sites for EG2. The higher S_0 index for EG2 compared to IgG suggest the presence of ANS binding sites on its Fab fragment. Further work is needed to confirm the location of the ANS fragments for EG2, relate hydrophobicity to cation exchange chromatography operations and to extend this method to other types of monoclonal antibody.

3.3 Introduction

Hydrophobicity of proteins is a phenomenon describing the tendency of their non-polar regions to interact with each other which may lead to aggregation [52]. Proteins display various hydrophobic characteristics according to their amino acid content. When a protein is placed in an aqueous environment, the amino acids with hydrophobic side chains [53] will be predominantly buried inside the protein inner region. As the protein structure is sensitive to environmental conditions such as pH, ionic strength or temperature, these conditions may affect the accessibility of the hydrophobic amino acids that are then partially exposed at the surface of the protein [54]. As downstream processing of proteins reflects the protein structure and its amino acid composition, protein hydrophobicity may become important in these operations [55]. The characterization of hydrophobicity for proteins can assist with the development of efficient protein recovery operations.

Protein hydrophobicity can be estimated relatively quickly with fluorescent dyes as probes. Fluorescent dyes bind to hydrophobic patches at the surface of proteins. These interactions can be monitored by changes of fluorescence intensity. The principle of hydrophobicity measurement is simple but the interpretation of hydrophobicity characteristics is not as straightforward as each fluorescent dye possesses unique charge, solubility characteristics and associated solvent requirements. ANS (1-anilino-8-naphthalene sulfonate), (Figure 3.1[1]), is an aromatic dye used extensively for the assessment of protein hydrophobicity [56–61]. ANS has an anionic character and can be solubilised in aqueous solutions. CPA (cis-parinaric acid) is also an anionic dye but with negligible aqueous solubility. Unlike ANS, CPA requires ethanol for solubilization [56]. The charge of ANS and CPA can contribute to the interactions of these dyes with proteins, thus complicating the interpretation of the results. PRODAN (6-propionyl-2-(N,N-dimethylamino) naphthalene) [54, 56, 62, 63], which has no charge, can facilitate the investigation of hydrophobicity but is limited by its low aqueous solubility and the need for an alcohol based solvent.

As mentioned above, the dye protein interaction measured with ANS consists of hydrophobic interaction but may also include electrostatic interaction leading to an overestimation of hydrophobicity. But the charge character of ANS is advantageous in that the analysis is conducted in an aqueous environment which represents the natural environment where proteins are generally found. This is a unique and major advantage of ANS and explains its use in hydrophobicity studies of proteins. The process of ANS binding to a protein is generally observed as blue shift in the location of the maximum fluorescence intensity (∼390/470 nm excitation/emission) and by its magnitude. Binding sites

[1] http://www.sigmaaldrich.com/content/dam/sigma-aldrich/structure2/144/mfcd00012560.eps/_jcr_content/renditions/large.png

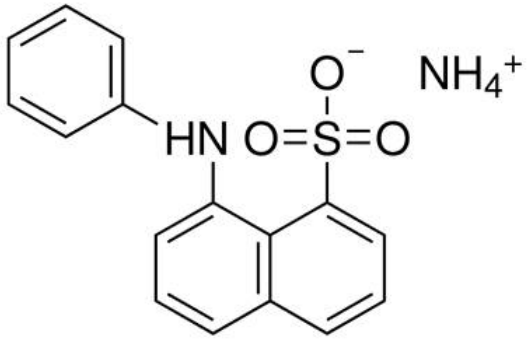

Figure 3.1: Chemical structure of ANS

are naphthalene and aniline residues that form hydrophobic cavities or ion pairing between the sulfonate group and a close positively charged side chain [56, 58].

Hydrophobicity estimates obtained with the ANS method are deduced from changes of the fluorescence intensity at different protein concentrations expressed as the slope of fluorescence intensity and protein concentration [64]. This estimation method has a number of limitations. Firstly, sufficient difference in fluorescence intensity is required to capture the interactions between ANS and the protein. This will generally require a wide range of protein concentration. Depending on the availability of protein, the number of protein concentration conditions and replicates may be limited. One also has to keep in mind potential fluorescence signal quenching at high protein concentration causing non-linear relationship between the fluorescence intensity and protein concentration. Research groups so far have reduced protein concentration and only operated in the linear range, or increased ANS concentration to expand the linear range which is wasteful and cannot be extended infinitively due to quenching effects.

Hydrophobicity estimates, deduced from the slope of fluorescence intensity and protein concentration, may be confounded with equipment characteristics which limits its comparison between different instruments. In this context, the capture of non-linear relationship and standardization of the hydrophobicity estimates are desired. Methods for the capture of non-linear relationship have been developed for saturation kinetics by converting the non linear relationship to a linear format. Linearization can be obtained by double reciprocal plots as developed for the estimation of enzyme kinetic parameters. But this linearization approach may include bias according to the range of experimental data. Alternative linearization methods include single reciprocal linear plot, such as the Scott plot [65]. The application of the Scott plot for the representation of ANS protein fluorescence intensity

data according to protein concentration will generate a plot of the protein concentration divided by the fluorescence intensity versus the protein concentration, with the slope as the inverse of the hydrophobicity index.

Hydrophobicity estimates of proteins with ANS have focused extensively on bovine serum albumin (BSA), [57, 58, 61]. In these studies, ANS concentration was in the range of 10^{-4} to 10^{-6} M (final concentration) and BSA concentrations up to 0.025% w/v. The number of ANS binding sites on BSA is not clear. Togashi [60] reports five binding sites per BSA molecule whereas Cattoni et al. [58] reports six ANS molecules bound to BSA. Cattoni et al. [58] also proposed that differences of ANS binding sites on BSA could be explained by conformational transformation of BSA taking place under specific experimental conditions where surface sites turn into hydrophobic cavity. It is important to note that these observations do not exclude the contribution of electrostatic interactions to the observed ANS and BSA binding.

Seeing the challenge and dynamic nature of ANS and protein interaction for small protein molecules, one can imagine the complexity for larger protein molecules such as antibodies. For example, polyclonal human IgG is an antibody mixture of unlike molecules identifying different parts of an antigen. Antibodies consist of two light and two heavy chains where each chain contains variable and constant regions. The chains are connected by disulfide bonds which, when split, lead to two antigen binding fragments (Fab) and one crystallisable fragment (Fc) – each of these fragments being a potential site for interaction with ANS. Studies are divergent in terms of the location and number of ANS binding sites to IgG. One study reported two binding sites on the Fab region and indicated the presence of potential additional ANS binding sites in the Fc region [66]. Another study confirmed the existence of two weak hydrophobic binding sites on the Fc region (C_H2 area) [67]. A further report indicates the higher amount of hydrophobic surface patches available for ANS after heat treatment of the IgG [68].

Monoclonal antibody differs from polyclonal antibody (IgG), by their identical chains. For example, EG2 is a chimeric heavy chain antibody containing only heavy chains which are furthermore shorter than the ones found in IgG, as described by Bell et al. [18]. No previous hydrophobicity studies with ANS and EG2 have been reported. But ANS and the monoclonal antibody adalimumab showed higher ability to bind to ANS than polyclonal IgG [68].

The aim of this study was to use ANS and estimate the relative hydrophobicity for a number of proteins. The first step was based on ANS and BSA, as model protein, and clarification of the fluorescence intensity profile over a broad excitation/emission range and BSA concentration. The presence of fluorescence saturation and the analysis of non-linear

fluorescence intensity profiles were considered. Attention was also given to the standardization of hydrophobicity estimates such that comparison with independent studies could be achieved. Lastly, the technique was extended to polyclonal antibody (IgG) and monoclonal antibody, EG2, with respect to their pH and ionic conditions for better knowledge of their downstream processes.

3.4 Material and Methods

3.4.1 Reagents and Solutions

The ammonium salt of 8-anilino-1-naphthalenesulfonic acid (ANS), fluorescence grade, 97.0% purity (# 10417) and bovine serum albumin (BSA), lyophilized powder, 96.0% purity (# A3912) were obtained from Sigma-Aldrich (St. Louis, MO, USA). Immunoglobulin G (IgG) was obtained from Equitech-Bio, Inc. (Kerrville, TX, USA). For the buffer preparation, citric acid, anhydrous (EMD, Tokyo, Japan) and sodium phosphate, dibasic, heptahydrate (EMD, Darmstadt, Germany) were used. The ionic strength of the buffer was adjusted with either sodium chloride (NaCl) (BDH, Toronto, ON, CA) or potassium chloride (KCl) (EMD, Billerica, MA, USA). EG2 was supplied by Dr. Durocher, Biotechnology Research Institute, Montreal, Canada.

3.4.2 Buffer, Protein and ANS Preparation

All protein samples were prepared in a phosphate-citrate buffer (pH 3, 5 or 7). The desired pH was obtained with 0.1 M citric acid and 0.2 M sodium phosphate, dibasic, heptahydrate. A BSA stock solution was prepared at a concentration of 0.02% w/v and diluted with the appropriate buffers to obtain solutions with at least four different BSA concentrations in the range of 0.0025%-015% (all w/v). IgG stock solution was 0.16% w/v and used to prepare solutions with concentrations in the range of 0.005%-0.08% w/v (four additional concentrations). Due to the limited supply of EG2, four different concentrations were investigated (0.005%-0.02% w/v). NaCl (0.5 and 1 M) was selected for BSA as means to compare with literature values while for EG2 and IgG, KCl was selected (1 M). A 10 x ANS stock solution (1.62 mM in MilliQ water) was freshly diluted with the appropriate buffer on each experiment day and could be kept for four weeks when stored in the fridge and without light.

3.4.3 Fluorescence Analysis

Fluorescence of all samples was measured with quartz cuvettes using a Cary Eclipse Fluorescence Spectrophotometer (Agilent Technologies). PMT was set to 575 and both excitation and emission slits were set at 5 nm. All conditions were run in triplicate. Fluorescence intensity for EEM (excitation/emission) spectra was obtained for a range of 250-430 nm excitation and 300-600 nm emission. All solutions were prepared in pH 7 phosphate citrate buffer with concentrations of 0.08 mM ANS and 0.2% w/v BSA. Contour plots were produced in MATLAB. Fluorescence intensity for hydrophobicity estimation was measured at an excitation wavelength of 390 nm and an emission wavelength of 470 nm. The fluorescence intensity (FI) of a 3.5 ml protein sample at different concentrations (%w/v) was measured before and after addition of 20 μl of 0.162 mM ANS and subsequent mixing. The difference between the fluorescence intensity of the protein solution with and without ANS was referred to as net fluorescence intensity (Equation 3.1) representing the fluorescence change due to the binding of ANS to the protein.

$$FI_{net} = FI_{+ANS} - FI_{-ANS} \tag{3.1}$$

With FI_{net}: net fluorescence intensity (-); FI_{+ANS} fluorescence intensity with ANS (-); FI_{-ANS}: fluorescence intensity without ANS (-);

3.4.4 Protein Hydrophobicity Estimation

Protein hydrophobicity estimation (for more information see Appendix 1), given as hydrophobicity index (S_0), was adapted from Haskard and Li-Chan, 1998 [54] without modifications for IgG and EG2 and with modifications for BSA. For IgG and EG2, a plot of the net fluorescence intensity against protein concentration had a linear relationship and its slope was used to estimate the protein hydrophobicity index (S_0). For BSA, the net fluorescence intensity according to protein concentration exhibited a non-linear relationship and saturation behaviour. To account for this non-linear behavior and use all FI_{net} values, the Scott plot (Equation 3.2) was adopted. Mathematically, hydrophobicity index S_0 can be extracted from the first derivative at small protein concentrations. Alternatively, the authors used FI_{max} directly to compare hydrophobicity between different conditions.

$$\frac{c}{FI_{net}} = \frac{K_M}{FI_{max}} + \frac{c}{FI_{max}} \tag{3.2}$$

With c: Protein concentration (%w/v); FI_{net}: net fluorescence intensity (-); FI_{max}: maximum fluorescence intensity (-); K_M: protein equilibrium constant (-).

As the hydrophobicity index represents the change of fluorescence intensity for a given protein concentration change, its comparison between independent studies is limited but could be improved by standardization of the data as will be discussed in this study.

3.4.5 Data Analysis

To determine if data sets were significantly different from each other, the Student t-test was used assuming a two tailed distribution and a confidence level of 95% ($\alpha = 0.05$).

3.5 Results and Discussion

3.5.1 Fluorescence Characteristics of BSA and ANS

Different excitation/emission (ex/em) values are reported in the literature to capture the fluorescence intensity of the ANS-BSA complex. Reported values include 390/470 nm ex/em [54, 56], 350/480 nm ex/em [57] and 380/480 nm ex/em [58, 60]. In order to compare these values and identify the location of the maximum fluorescence intensity for the ANS-BSA complex, the emission profile at different wavelength and for different excitation conditions was conducted. Fluorescence intensity according to excitation and emission conditions is presented in Figure 3.2 for ANS, BSA and the ANS-BSA complex respectively. A ridge of fluorescence intensity located at the bottom region of the fluorescence excitation emission profile was observed for all samples and corresponds to the Rayleigh light scattering region which will not be considered in this study. As expected, ANS by itself (Figure 3.2 a)) had very low fluorescence intensity (FI < 15) at concentrations below 0.1 mM. Fluorescence intensity was located predominantly at 350/520 nm excitation/emission, as previously stated by Cardamone and Puri [57] and to a lower extent at 290/520 nm ex/em. In contrast, the fluorescence profile of BSA (Figure 3.2 b) had a distinct FI maximum at 280/340 nm ex/em which reflects the intrinsic fluorescence of aromatic amino acid residues (tryptophan, tyrosine and phenylalanine) [69]. The fluorescence profile of the ANS-BSA complex (Figure 3.2 c) resembled the profile of ANS (Figure 3.2 a) but not those of BSA (280/340 nm ex/em). The fluorescence intensity of the ANS-BSA

complex increased significantly compared to ANS (Figure 3.2 a) and a shift of the fluorescence emission to 470 nm at 390 nm excitation was observed as previously reported [54]. The second peak at 290/470 nm ex/em has not been reported in literature. The ANS-BSA complex had no fluorescence in the 250-300/300-400 nm ex/em region, static quenching between the fluorophore ANS and the quencher BSA may have occurred as previously described by Togashi and Ryder [60]. Based on these observations, 390/470 nm ex/em was selected to quantify the effect of ANS on protein hydrophobicity.

3.5.2 Estimation of Protein Hydrophobicity

Protein hydrophobicity estimated from net fluorescence intensity (FI_{net}) for ANS-protein complexes assumes a linear relationship between FI_{net} and protein concentration. This linear relationship should exist for a sufficiently wide range of protein concentration for reliable estimates. As illustrated in Figure 3.3 (a and b), the relationship between FI_{net} and BSA concentration at pH 3 and pH 5 is not clear. There is a levelling of FI_{net} at BSA concentration above 0.01% w/v. The impact of such relationship on the estimation of the fluorescence index (S_0) can be drastic. When FI_{net} for the entire BSA concentration was considered, estimated S_0 values were 2979 ($R^2 = 0.961$) and 1703 ($R^2 = 0.864$) for pH 3 and 5 respectively. When FI_{net} for BSA concentration up to 0.01%w/v was considered, estimated S_0 values were 4296 ($R^2 = 0.983$) for pH 3 and 3179 ($R^2 = 0.955$) for pH 5 (Figure 3.3 a). An alternative approach to exploit FI_{net} over the entire protein concentration range and capture the non-linear profile is to generate a linear relationship by transforming FI_{net} according to Equation 2. Estimated hydrophobicity indices (here FI_{max}) according to equation 2, were 115 at pH 3 and 69 at pH 5 with the best fit resulting in R^2 of 0.996 and 0.999 respectively (Figure 3.3 b). Based on the higher R^2 obtained for hydrophobicity estimates with all FI_{net} values and the Scott plot, this approach was adopted in this study, FI_{max} was used as a measure of S_0.

3.5.3 Standardization of BSA Hydrophobicity Index and Effect of pH and Ionic Strength

The comparison of published hydrophobicity index for BSA based on ANS interactions and fluorescence intensity can be affected by the characteristics of the spectrofluorometer instrument and BSA, differences in experimental conditions and potential non-linear fluorescence relationships (Table 3.1 and 3.2). Hydrophobicity index (S_0) reported in the literature for BSA according to pH and ionic strength range significantly. Alizadeh-Pasdar

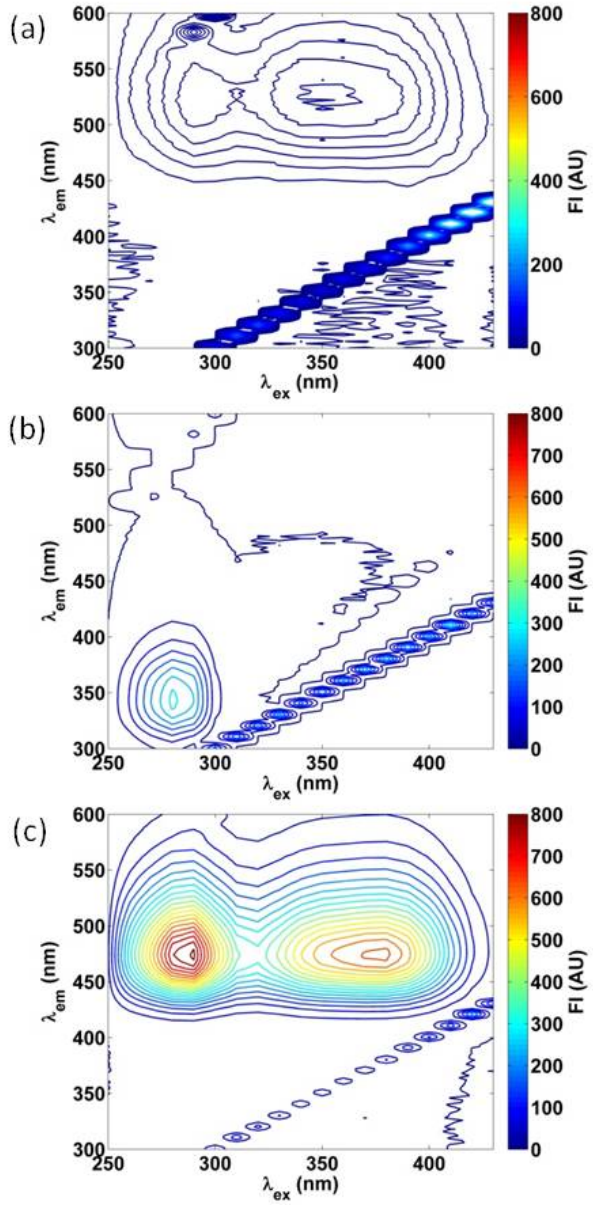

Figure 3.2: Fluorescence intensity according to excitation and emission conditions (a) 0.08 mM ANS solution (b) 0.2% w/v BSA solution (c) 0.08 mM ANS with 0.2% w/v BSA solution. All in pH 7 phosphate citrate buffer.

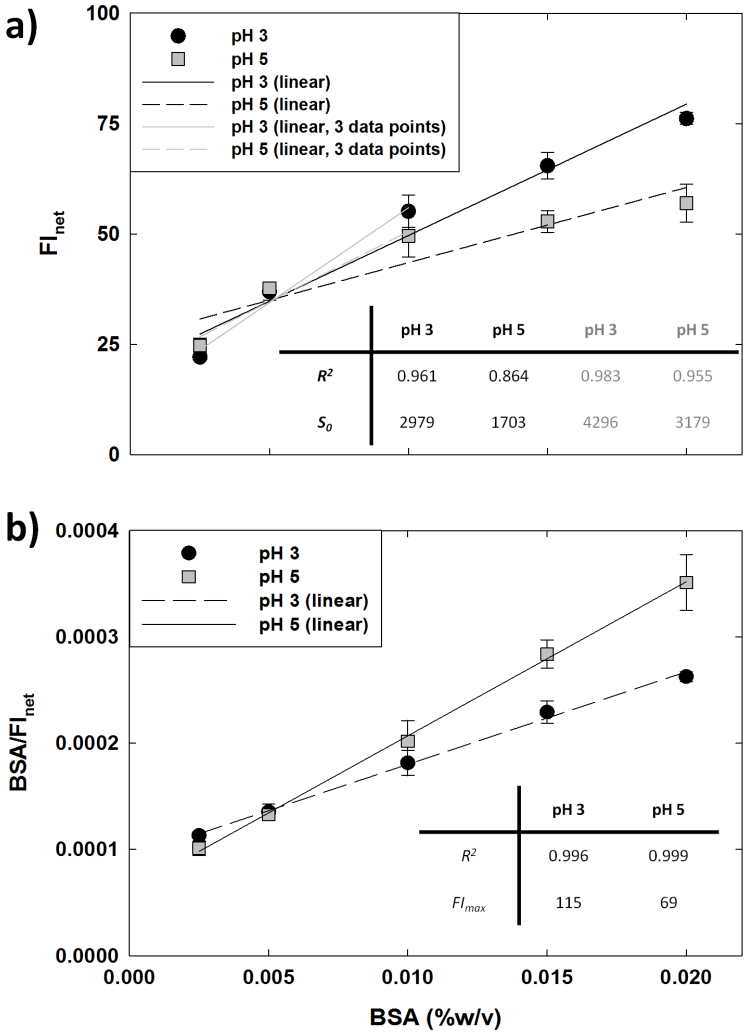

Figure 3.3: Net fluorescence intensity (FI_{net}) according to BSA concentration (%w/v) and pH (pH 3 • and pH 5 □). a) FI_{net}, linearised over complete BSA concentration range (black) and FI_{net}, linearised BSA concentration ≤ 0.01 %w/v (grey) and c) modified data according to Equation 2 (Scott plot) and linearised. Inserts show R^2 values and hydrophobicity index (S_0) or FI_{max}.

and Chan [56] reported S_0 values of 3020 for BSA at pH 3 while Matulis and Lovrien [59] reported S_0 values of 95 for BSA at the same pH but with a different buffer. The comparison

of hydrophobicity estimates from different laboratory may be possible by standardization and modulating the differences of a given laboratory. Relative values are obtained by assigning 100 to the highest hydrophobicity index and other values as fractions of this maximum.

Standardization of published S_0 values for BSA (Table 3.1) was adopted to understand the effect of pH on BSA hydrophobicity. The highest reported hydrophobicity for BSA was at pH 3 and was assigned to be 100%. The lower relative S_0 value at pH 5 compared to pH 3 observed in this study agrees with previous studies. Relative hydrophobicity index S_0 decreased to 66%, 64% and 60% (Alizadeh-Pasdar, Matulis and this study respectively). There are however distinctive differences for the hydrophobicity at pH 7 with Alizadeh-Pasdar being significantly different from this study. Matulis et al. reported a hydrophobicity index similar to their value found at pH 5 (62%), another study indicated that the relative hydrophobicity index at pH 7 further reduced to 30% of its original value (Alizadeh-Pasdar) whereas this study reported an increase to 71%. Increasing ionic strength (up to 1 M NaCl) reduced S_0 values for BSA to 73.3% (Haskard) and 80.7% (this study) as seen in Table 3.2.

The effect of pH and ionic strength on BSA-ANS interactions and their relative hydrophobicity index can be related to the charge of BSA and its isoelectric point (pI) (Table 3.3). Knowing that BSA has a pI of 4.7 [70], its overall charge will be negative at pH above its pI. For these conditions, higher proportion of hydrophobic patches per protein molecule could be accessible to ANS. Conditions close to its pI (e.g. pH 5) lead to an overall charge close to zero. Under these conditions, hydrophobic interactions will predominate and BSA is more likely to aggregate or attach to non charged surfaces leaving fewer hydrophobic patches available to interact with ANS. Therefore the lowest relative hydrophobicity index observed at pH 5 could reflect the close vicinity of the pH to the pI of BSA. Increased relative hydrophobicity index observed at pH 3 and pH 7 reflects the charge of BSA and charge of ANS. The relative hydrophobicity index at pH 3 (100%) and pH 7 (71.4%) was quite different even though both pH are approximately the same distance from the pI. This could be due to the anionic character of ANS and the overall positive charge that BSA has at a pH below its isoelectric point, leading to binding opportunities based on charge interaction as well as hydrophobic interactions. Furthermore, literature reports that at acidic pH, the tertiary BSA structure loosens which would expose more hydrophobic regions accessible to the ANS probe [71]. The influence of ionic strength on the relative hydrophobicity index reflects the stabilizing effect of ions on proteins, preventing ANS from docking to the hydrophobic cavities leading to lower hydrophobicity index values.

Comparable results to literature values were achieved when using FI_{max} as S_0, extracted

Table 3.1: BSA hydrophobicity index (S_0) and [Relative S_0 (%)] according to pH

Experimental conditions and observations	**Alizadeh-Pasdar [56]**	**Matulis [59]**	**This study**
[BSA]	0.005-0.025%	3 μM	0.0025-0.02%
[ANS]	20 μl of 8x10^{-3} M in 4 ml	33 mol ANS/ mol BSA	20 μl of 0.162 mM in 3.5 mL
Buffer	0.1 M sodium citrate	30 mM: sodium formate (pH 3), sodium acetate (pH 5), sodium phosphate (pH 7)	0.1 M sodium citrate
Equipment type	Shimadzu RF-540	Perkin-Elmer 650-10S	Cary Eclipse (Agilent)
Ex/Em/slit width(nm)	390/470/5	No information	390/470/5
pH 3	3020[1] [100]	9.5[1] [100]	114.8±2.3* [100±2.0*]
pH 5	2000[1] [66.2]	6.1[1] [64.2]	68.9±1.7* [60.0±2.4*]
pH 7	900[1] [29.8]	5.9[1] [62.1]	82.0±0.4* [71.4±0.4*]

[1]Extracted from tables and figures and converted to relative values;
*denotes significant ($\alpha = 0.05$) influence of pH on H.

from the saturation curve. However mathematically, S_0 is defined as FI_{max}/K_M (compare Appendix 1). This is questioning the method of extracting hydrophobicity and the meaning of S_0 and might explain differences in reported values.

3.5.4 Hydrophobicity Index of BSA, Immunoglobulin G (IgG) and EG2

Hydrophobicity of proteins has a critical role in protein recovery operations where hydrophobicity can be detrimental to the operation and protein quality. Knowledge of hydrophobicity characteristics for therapeutic proteins such as monoclonal antibody is required for proper design of purification operations.

Table 3.3 presents the hydrophobicity index of BSA, polyclonal IgG and a monoclonal EG2. S_0 values were selected for comparison within the same study. There was no need to

Table 3.2: BSA hydrophobicity index (S_0) and [Relative S_0 (%)] according to ionic strength (NaCl)

Experimental conditions and observations	**Haskard and Chan[2] [54]**	**This study**
[BSA]	0.005-0.025%	0.0025-0.02%
[ANS]	20 μl of 8x10^{-3} M in 4 ml	20 μl of 0.162 mM in 3.5 mL
Buffer	0.1 M sodium citrate pH 7	0.1 M sodium citrate
Equipment type	Perkin-Elmer LS 50B, Shimadzu RF-540	Cary Eclipse (Agilent)
Ex/Em/slit width(nm)	390/470/5	390/470/5
0 M	2250[1] [100]	82.0 0.4* [100 0.4*]
0.5 M	1750[1] [77.8]	70.1±1.3* [85.5±1.9*]
1 M	1650[1] [73.3]	66.2±0.4* [80.7±0.5*]

[1]Extracted from tables and figures and converted to relative values;
[2]study was conducted at 30°C instead of room temperature (21±1°C);
*denotes significant ($\alpha = 0.05$) differences of ionic strength on H.

standardize these values. Conditions are reflecting bind and elute ion exchange chromatography operations. Noted changes of hydrophobicity reflected the changes in hydrophobic region accessibility to the ANS probe in different environmental conditions.

Hydrophobicity index (S_0) at pH 5 and 0 M KCl was 25 for IgG and 45 for EG2 compared to 69 for BSA. The value of S_0 of BSA and IgG at pH 5 was not statistically different when the ionic strength increased to 1 M KCl. In contrast, increasing pH to 7 at 0 M KCl influenced significantly H. In the case of BSA, S_0 increased to 82, for IgG, S_0 decreased to 11 and S_0 decreased to 13 for EG2. Increasing the ionic strength at pH 7 to 1 M KCl, S_0 decreased to 62 for BSA but remained relatively similar for IgG and EG2. Therefore pH influenced significantly the hydrophobicity index for all proteins whereas the influence of ionic strength was significant only for BSA at pH 7. The magnitude of the fluorescence index according to protein type was $H_{BSA} > H_{EG2} > H_{IgG}$ at pH 3 with and without KCl and for pH 5 and pH 7 and 0 M KCl. At pH 5 and 1 M KCl, the magnitude of the fluorescence index was $H_{BSA} = H_{EG2} > H_{IgG}$. At pH 7 and 1 M KCl, the hydrophobicity index at pH 7 was similar for EG2 and IgG and statistically significantly lower than BSA.

Table 3.3: Characteristics of BSA, IgG and EG2 and their hydrophobicity index according to pH (5 and 7) and ionic strength (0 and 1 M KCl)

Characteristics		**BSA**	**IgG**	**EG2**
MW (kDa)		66.4	150	84
pI (-)		4.7	5.5-10 (with 80% above pH 7)	7.7
# ANS binding sites		5 [60] or 6 [58]	2 Fc + 2 Fab [67] or 2 Fc [66]	unknown
Experimental conditions		**Hydrophobicity index S_0 (-)**		
pH 5	*0 M KCl*	$68.9\pm1.7^{*+}$	$25.0\pm0.1^{*+}$	$45.0\pm1.8^{*+}$
	1 M KCl	59.7 ± 0.7	$24.0\pm0.6^{*+}$	$51.4\pm9.8^{*}$
pH 7	*0 M KCl*	$82.0\pm0.4^{*-+}$	$11.2\pm0.1^{*+}$	$12.5\pm0.1^{*+}$
	1 M KCl	$62.0\pm0.8^{-+}$	$8.8\pm0.8^{*}$	$10.1\pm5.4^{*}$

*Denotes statistically significant ($\alpha = 0.05$) influence of pH at constant ionic strength;
$^{-}$denotes statistically significant ($\alpha = 0.05$) influence of ionic strength at constant pH;
$^{+}$denotes statistically significant ($\alpha = 0.05$) differences between proteins.

The increased standard deviation for EG2 at high ionic strength could be due to the lower number of concentrations used (limited supply) or due to an increased influence of salt on the monoclonal antibody and needs further investigation.

The differences in pI of IgG and EG2 (above 7) and the pI of BSA (4.7) may explain the opposite effect that pH had on their fluorescence index. When pH increased from 5 to 7, the hydrophobicity index for IgG and EG2 decreased significantly at the two ionic strength conditions due to their overall charge close to zero at pH 7. The same pH increase had different effect for BSA as its overall charge was near 0 at pH 5 and negative at pH 7. The pH conditions were well below the pI of the antibodies, the biomolecules were already stabilized by pH, a further stabilizing effect over additional salt ions did not lead to a significant effect.

The differences in the magnitude of the hydrophobicity index according to protein type could also be related to the number of ANS binding sites. Literature indicates that the number of ANS binding sites for BSA is 5 [60] or 6 [58] whereas for IgG only 2 weak binding sites at the Fc region are reported and the number of ANS binding sites for the Fab region is not clear [66,67]. There is no information available on the ANS binding sites for EG2. The number of binding sites per protein supports the magnitude of the protein hydrophobicity index observed in this study ($H_{BSA} > H_{EG2} > H_{IgG}$). BSA has more ANS

binding sites (up to 6 (3 weak + 3 strong)) than IgG (4 (2 weak Fc + 2 weak/strong Fab)) leading up to seven times higher hydrophobicity index values. The fluorescence intensity as well as the hydrophobicity index value of EG2 was significantly higher when compared to IgG. Based on the fluorescence characteristics of the EG2-ANS complex, proposed ANS binding sites for EG2 are presented in Figure 3.4.

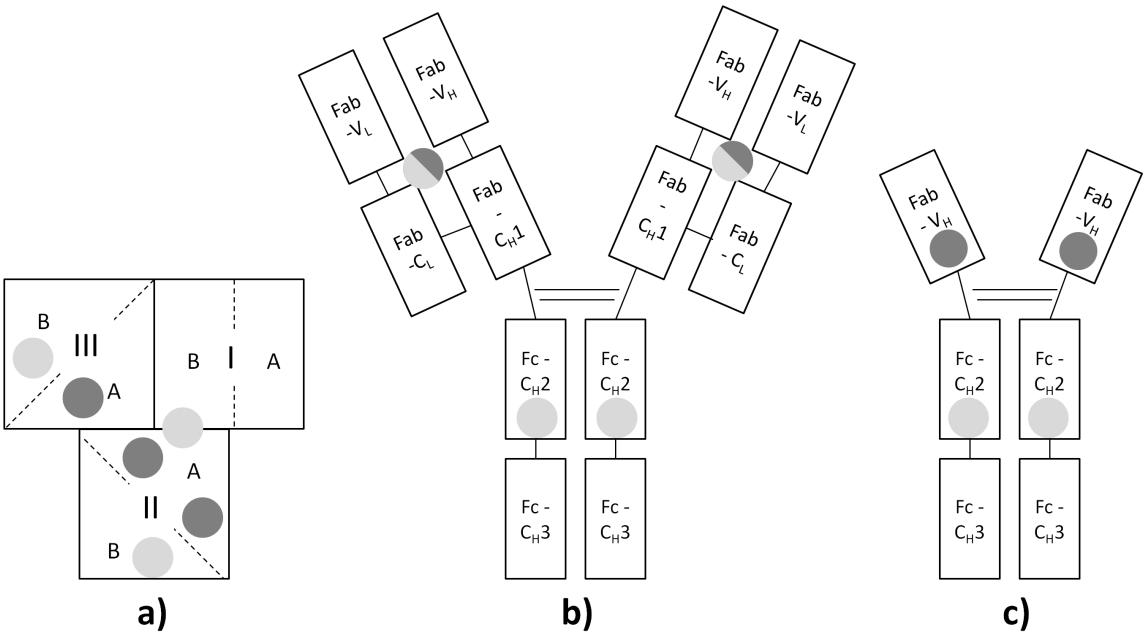

Figure 3.4: Schematic representation of a) BSA with its three domains (I, II and III) and subdomains (A and B each), b) IgG and c) EG2 with Fab (Fragment antigen binding), Fc (Fragment crystallisable), V (Variable region), C (Constant region), H (Heavy chain) and L (Light chain). ANS binding sites found in literature (a and b) and proposed binding sites (c) are represented as dots with strong ANS-Protein interaction (dark grey) and weak ANS-Protein interaction (light grey).

The discrepancy between the reported number of ANS binding sites in the Fab region of IgG may be due to its polyclonal character [68]. Polyclonal antibodies possess antigen binding fragments with different amino acid sequences. These small changes might affect ANS interaction. In a polyclonal mixture, only a fraction of the molecules will possess the ANS binding sequence leading to small fluorescence intensity as observed in this study and others [66,67]. Monoclonal antibody, on the other hand, is made up of identical molecules. Since FI_{net} values were higher with EG2, one can assume that it must possess a sequence

with stronger interactions with ANS. Furthermore it is not only a fraction of molecules but all of them due to the identical character.

3.6 Conclusion

Characterization of hydrophobicity of proteins with the ANS fluorescence probe was selected because of the aqueous solubility of ANS and the extensive work conducted with ANS. Fluorescence characteristics and analysis were first reviewed and refined and subsequently used to characterize the hydrophobicity of three proteins, BSA, IgG and EG2 at different pH and ionic strength conditions. Using ANS as fluorescence probe did not allow to distinguish between hydrophobic and electrostatic interactions between the proteins and the probe.

Major outcomes of this study are as follows:

1. Fluorescence excitation/emission conditions for ANS and BSA were established by mapping the fluorescence intensity according to excitation and emission wavelength.

2. The range of protein concentration and ANS concentration affect their interaction and their relationship which may be linear (known) or show saturation behaviour (not discussed in literature). Linearization of fluorescence intensity according to the full protein concentration range was achieved by creating Scott plot (single reciprocal plot) and then extracting the hydrophobicity index from the inverse slope of the Scott plot (FI_{max}). Mathematically this was not identical to the initial slope S0 ($= FI_{max}/K_M$) but led to best comparable results with literature. More analysis is proposed to address the problematic of defining hydrophobicity as an index.

3. The instrument, BSA characteristics, experimental conditions and data analysis have a significant impact on the magnitude of hydrophobicity index values. A comparison of hydrophobicity index generated in independent studies was obtained for BSA by standardization of the data.

4. Hydrophobicity index according to pH and ionic conditions common to chromatography purification operations for BSA, IgG (polyclonal antibody) and EG2 indicate that pH had significant effect on the hydrophobicity index of all proteins while ionic strength was only significant for BSA at pH 7. The magnitude of the hydrophobicity index for most pH and ionic strength conditions was $H_{BSA} > H_{EG2} > H_{IgG}$.

(a) IgG, a polyclonal antibody, showed low fluorescence intensity which may be due to its different Fab sequences resulting in different interactions with ANS.

(b) Monoclonal antibody will interact with ANS in the same way for all its molecules. If ANS binding sites exists in its Fab region, its fluorescence intensity will be higher than polyclonal antibodies.

3.7 Acknowledgements

Financial support from the Monoclonal Antibody Network (MabNet) of the Natural Sciences and Engineering Research Council (NSERC) is acknowledged. Funding from DAAD RISE worldwide scholarship (Sarah Armbruster and Dorothee Kurz) and NSERC USRA scholarship (Ross Arnold) is acknowledged.

3.8 Appendix

3.8.1 Hydrophobicity estimation and the meaning of a hydrophobicity index

Early methods to determine hydrophobicity include analysis of the primary structure of proteins and their content of hydrophobic amino acids. This however does not resemble the three dimensional structure of proteins and the so called surface or effective hydrophobicity when proteins interact with each other or with a hydrophobic surfaces. Better techniques include the definition of a hydrophobic coefficient (Δ log K) that is describing the difference in partition of proteins in an aqueous two-phase system. With increasing amounts of hydrophobic patches on the protein surface, the affinity to the apolar phase will increase as well [72]. This technique however is not only time consuming, but also limited to the number of conditions used in the two-phase system. In protein purification, hydrophobicity is an important tool since protein surface hydrophobicity can change according to pH and ionic strength, two factors that are frequently adjusted in protein downstream processes. A detection of changing protein hydrophobic tendencies with changing buffer conditions can be followed with fluorescence probes. Previous studies reported the use of various fluorescence probes to determine a hydrophobicity index by extracting the initial slope (S_0) when plotting fluorescence intensity versus protein concentration. This initial slope is proportional to the amount of bound protein [73] and a linear correlation between Δ

log K and was S_0 found [64] indicating that the initial slope, under conditions of excess probe, can be used as hydrophobicity index or effective hydrophobicity of proteins [54]. The authors understand the physical meaning of S_0 to be the extinction coefficient of the protein-probe complex at equilibrium. The linear relationship between fluorescence and protein concentration however is not indefinite. Either a limit of ANS availability or a quenching effect of either ANS or protein concentration will lead to saturation kinetics similar to the one found in enzyme kinetics.

$$FI_{net} = \frac{FI_{max} * c}{K_M + c} \tag{3.3}$$

With FI = fluorescence intensity (-), c = protein concentration (%w/v) and K_M = protein equilibrium constant.

When operating in the linear region a very narrow range of protein concentrations might be observed leading to a low resolution and potentially high error of the test. To avoid these problems the saturation curve might be used as well by analyzing the initial slope with the first derivative of equation (1) at low protein concentrations:

$$S_0 = \lim_{c \to 0} \frac{dFI_{net}}{dc} = \frac{FI_{max}}{K_M} \tag{3.4}$$

Chapter 4

Role of pH and Ionic Strength on Macroporous Hydrogel Weak Cation Exchange Membrane and IgG Capture

4.1 Synopsis

This chapter focuses on weak cation exchange macroporous hydrogel membrane material characterization and IgG adsorption. Zeta potential, global and relative swelling as well as membrane pore structure visualization is discussed. Static IgG binding and elution studies were performed at different pH and ionic strength conditions to identify pH and ionic conditions for maximum IgG binding and recovery and to relate these conditions to material properties.

All experimentation was performed by Katharina Hassel. Sample preparation for the Field Emission Scanning Electron Microscopy (FESEM) image analysis was done by Katharina Hassel and imaging performed by Nina Heinig (Chemistry Department, University of Waterloo). Zeta potential measurements were performed with the electrokinetic analyzer from Dr. Sigrid Peldszus (Civil and Environmental Engineering, University of Waterloo). Data analysis and writing was completed by Katharina Hassel with contribution from Kamyar Ghofrani and Maximilian Fondyga for the FESEM image analysis. Experimental planning, data analysis and writing were supervised and reviewed by Christine Moresoli.

This chapter was submitted to Journal of Membrane Science (December 2014), Katharina Hassel, Christine Moresoli, Role of pH and ionic strength on weak cation exchange macroporous hydrogel membranes and IgG capture.

4.2 Abstract

The surface charge of weak cation exchange membranes, consisting of functionalized macroporous hydrogel coated nonwoven support material, was related to its global swelling. Pore size visualization and analysis by Field Emission Scanning Electron Microscopy (FESEM) of hydrated membranes subjected to freeze drying preserved the hydrogel macroporous structure and showed pores generally an order of magnitude larger than Immunoglobulin G (IgG). At pH 6 and higher, the membrane average pore size was high reflecting the strong negative charge of the carboxylic acid groups. At pH below 5.5, the membrane average pore size was lower reflecting the nearly zero surface charge of the membrane material. The charge of IgG was the predominant factor responsible for IgG binding and elution. Maximum IgG binding capacity was observed at pH 4.8 and 0 M KCl, whereas highest IgG elution was obtained at pH 7 and 0 M KCl. The presence of KCl at pH 4.8 decreased IgG binding capacity while KCl addition at pH 7 did not affect IgG recovery but KCl addition was required for IgG elution at pH 4.5.

4.3 Introduction

Purification of biopharmaceuticals is predominantly achieved in packed-bed chromatography columns with affinity or ion exchange ligands [15]. Recently, membrane chromatography has attracted attention as potential alternative to resin chromatography for recombinant protein purification [37, 43, 74]. Membrane chromatography also referred to as membrane adsorber, typically consists of functionalized porous membrane materials with ligands, increasing the range of membrane separation applications beyond pure size partition [75–77].

The major advantage of membrane adsorbers, when compared to resin chromatography, is their open pore structure offering convective flow, which provides direct access to the ligands, offers negligible diffusion limitation, high flow rates, reduced processing times and decreased elution volumes [37, 76]. The binding capacity becomes nearly independent of flow rate allowing the use of high flow rates and achieving high productivity [78]. The major disadvantage of membrane chromatography resides in the reduced binding capacity caused

by the low functionalized surface to bed volume ratio and uneven inlet flow distribution conditions. The reduced binding capacity can become a significant limitation particularly in the bind and elute capture mode while having less pronounced effect in the flow through mode for impurity removal.

Membrane chromatography can be distinguished according to the structural organization of the functionalized material, polymeric coated or surface grafted porous materials such as Mustang® and Sartobind® and polymer support with pore filled functionalized hydrogel layer like Natrix® materials [39, 79, 80]. Polymer supported hydrogel membrane adsorbers are expected to have superior binding capacity. Their high binding capacity is believed to be caused by the increased functional group density of the gel layer.

The fibrous backbone material of hydrogel filled membranes provides a large pore network. By introducing the functionalized hydrogel, the relative pore size is dependent on the crosslink density. With increasing crosslink density, the average pore size decreases [81]. Hydrogels with ion exchange capacities furthermore have the ability to change their pore size according to environmental settings [82]. Visualization and characterization of the pore structure for hydrogel materials is challenging because of the sensitivity of the material to the environmental conditions but remains important when predicting membrane performance [82–84].

Cation exchange membrane adsorbers containing methyl sulphonate (S) and carboxymethyl (C) functional groups have attracted significant interest as potential replacement for the expensive Protein-A affinity resin chromatography currently used in the capture of monoclonal antibodies. Carboxymethyl (C) functional groups, referred as weak cation exchange, offer variable ionization according to pH conditions while methyl sulphonate groups (S), referred as strong cation exchange, are completely ionized over a wide pH range and very stable [85, 86]. The modulation of the exchange capacity for weak cation exchangers according to pH can generate different selectivity which can be advantageous in some purification applications [87].

In cation exchange chromatography, protein capture results from electrostatic interactions where binding capacity and recovery is maximized by manipulating pH and ionic strength conditions [88–90]. Protein binding will occur when the protein net charge is positive and the matrix has negative charge. Protein elution will occur when electrostatic interactions are disrupted, such as increasing ionic strength by salt addition. Some studies have shown that hydrophobic forces may also be present and contribute to non-specific protein binding [91, 92]. Such interactions may reflect the hydrophobicity of the material or the presence of hydrophobic patches in protein. For example, Hofstee suggested that accessible hydrophobic groups on protein molecules (BSA, lysozyme) interact with agarose

adsorbents containing hydrophobic domains leading to collective hydrophobic and electrostatic forces making difficult protein elution due to the strong nature of the collective binding [93]. To our knowledge, the effect of surface charge profile, swelling and surface pore characteristics of cation exchange membrane material has not been investigated for IgG capture. Published studies have focused on material development or optimization of pH and ionic strength conditions for protein binding and elution.

In the present study, the contribution of electrostatic interactions, membrane swelling and pore size to the capture of IgG with commercial weak cation exchange macroporous hydrogel membrane was assessed by decoupling IgG binding and elution according to pH and ionic strength conditions.

4.4 Experimental

4.4.1 Membrane Material

Weak cation exchange (C) hydrogel membranes (47 mm diameter discs with 275 μm average thickness and 0.399 ml total volume) were provided by Natrix Separations Inc. (Burlington, Ontario, Canada). These membranes are macroporous crosslinked polyacrylate hydrogels containing a high density of pendant carboxylate (carboxyethyl) binding groups physically reinforced by an inert polymeric (polyolefin) web. Detail of their manufacture is proprietary information.

4.4.2 Membrane Zeta Potential

Zeta potential (ζ) estimation was adapted from Ariza et al. [94]. The zeta potential was estimated from the streaming potential measurement obtained with a SurPASS electrokinetic analyzer (Anton Paar, Austria). The experiments were conducted with deionized water adjusted to different pH (4.5-7). The membrane sample, positioned in the sample holder, was placed in the electrokinetic analyzer, where the streaming potential was measured between the clamping cell and the membrane material. Measurement points were taken between 0 and 500 mbar. Measurements were done in triplicates in two independent experiments. The pH adjustment was achieved directly in the system beaker, so that membrane rearrangement in the holder would not influence the measurement or increase the error. Equation (4.1) was used to estimate the zeta potential.

$$\zeta = \frac{dl}{dp} * \frac{\eta}{\epsilon * \epsilon_0} * \frac{L}{A} \tag{4.1}$$

With: dl/dp = slope of the streaming potential versus pressure curve; η = electrolyte viscosity (kg/ms); ϵ = dielectric constant of electrolyte (-); ϵ_0 = vacuum permittivity (F/m); L = length of the streaming channel (m); A = cross-section of the streaming channel (m^2).

4.4.3 Membrane Global Swelling

Membrane global swelling was estimated by immersion in phosphate citrate buffer and gravimetry. Global swelling estimates represent fluid retention via absorption in the bulk of the hydrogel and within the open pore structure of the material. Phosphate citrate buffer with different pH were prepared with 0.1 M citric acid, anhydrous (EMD, Tokyo, Japan) and 0.2 M sodium phosphate, dibasic, heptahydrate (EMD, Darmstadt, Germany) stock solutions. A section of a 47 mm membrane disc, 0.025 g (±0.002) dry mass (with a Mettler AE 100 balance, readability 0.1 mg), was immersed in 20 ml conditioning buffer for 36 hours. The mass of the membrane sample was estimated again after 10 minutes equilibration at 23°C and 32% relative humidity. Two independent experiments with triplicate measurements were conducted for pH between 4.5 to 7 and ionic strength 0 to 1 M (achieved by KCl addition (EMD, Billerica, MA, USA)). The equilibrium swelling ratio (q_s) was calculated according to Equation (4.2) [95].

$$q_s = \frac{m_{swollen}}{m_{dry}} \tag{4.2}$$

Where q_S is the swelling factor (-), $m_{swollen}$ is the mass of swollen membrane (g), and m_{dry} is the mass of dry membrane (g).

4.4.4 Membrane Relative Swelling

Membrane relative swelling (H_s) was analyzed with the same immersion methodology as for the global membrane swelling (4.4.3) with the exception that the membrane sample was immersed in aqueous 70% isopropanol (Sigma Aldrich, St. Louis, MO, USA). Membrane relative swelling was estimated as the ratio between the membrane swelling in aqueous

70% isopropanol to the membrane swelling in phosphate citrate buffer and different pH and ionic strength conditions (Equation (4.3)) [96].

$$H_s = \frac{q_{s,I70}}{q_{s,buffer}} \tag{4.3}$$

Where H_s is the membrane relative swelling (-), $q_{s,I70}$ is the membrane swelling factor in 70% isopropanol (-), and $q_{s,buffer}$ is the membrane swelling factor in buffer conditions (-).

4.4.5 Membrane Pore Size Analysis

Membrane pore structure was visualized by Field Emission Scanning Electron Microscopy (FESEM) [44]. Membrane samples (5x5 mm) were mounted on small FESEM sample stands, sputter coated with a fine layer of gold particles (FESEM gold coating unit Desk II, Denton Vacuum, USA) for conductivity, and placed in the FESEM (Leo 1530, Carl Zeiss AG, Germany) for image acquisition. The working parameters for the FESEM were 10 kV and the secondary electron signal (SE2). The magnification was 5000 x (unless stated otherwise) and three images at different positions on the membrane sample were taken for each sample.

As FESEM imaging can only handle non-hydrated materials, water removal was required prior to the analysis of the samples. Two water removal techniques were considered and compared, air drying (24h, room temperature (21±1°C)) and freeze-drying (Epsilon 1-4 Freeze Dryer [Martin Christ, Germany] during 22 hours). Native non-hydrated membrane samples subjected to air drying and freeze-drying and hydrated (24 hours while being shaken at 80 rpm in phosphate citrate buffer at pH 4.5, 6.0 and 7.0 with 0 M and 1 M KCl addition) membrane samples subjected to air drying, freeze-drying or air drying with subsequent freeze-drying were investigated. The pore diameter distribution and average pore diameter were estimated with *Pore Image Processor* in MATLAB. The black and white contrast of the FESEM images was corrected with the *Background Correction* function. Light areas of the image were identified as pores, therefore black and white areas were inverted prior to processing. Binary operations were used to further refine the pores recognized by the program. Correction and threshold values affect pore size estimates and should therefore be selected carefully and use consistently to all images. A *background correction value* of 100, and a *threshold value* of 200 were selected. The validity of the correction values was verified by comparing the pore shape and size before and after correction [44]. A *Majority* followed by two *Erode*, and one *Dilate* operations were selected.

4.4.6 Static Immunoglobulin G (IgG) Binding and Elution

Immunoglobulin G (IgG) was obtained from Equitech-Bio, Inc., Kerrville, TX, USA. All experiments were performed in closed 20 ml vials at room temperature (21±1°C). Static IgG binding experiments were conducted in phosphate citrate buffer (see 4.4.3) with 0.5 g/l IgG initial concentration and desired pH (4.5 to 5.5) and KCl concentration (0 to 100 mM). Elution of IgG was conducted in phosphate citrate buffer (see 4.4.3) with desired pH (4.5 to 7) and KCl concentration (0 to 1 M). A membrane sample, 0.025 g (±0.002) dry weight, was first conditioned by equilibration for 2 hours in 5 ml of phosphate citrate buffer of the desired pH and KCl concentration (without IgG) and shaking (120 rpm) with a Gyrotory®Shaker-Model G2 (New Brunswick Scientific Co. Inc, Edison, NJ, USA). After equilibration, the membrane sample was removed and transferred to a new vial containing 10 ml of 0.5 g/l IgG phosphate citrate buffer of the desired pH and KCl concentration and incubated with shaking at 120 rpm. After 5 hours incubation, the membrane sample was removed. The IgG concentration in the supernatant was estimated by UV absorbance at 280 nm with a Spectronic^{TM} GENESYS^{TM} 5 UV-vis spectrophotometer (Milton Roy, now under Thermo Scientific, Waltham, MA, USA). The amount of bound IgG per membrane volume (ml) was obtained by difference according to Equation (4.4).

$$q = (c_0 - c_f) * \frac{V_s}{V_m} \tag{4.4}$$

With: q = IgG binding capacity (mg IgG/ml membrane), c_0 = initial IgG concentration (mg/ml), c_f = final IgG concentration (mg/ml), V_s = volume of solution (ml), V_m = volume of dry membrane (ml).

Elution was achieved by transferring the membrane sample to a new vial containing 15 ml of elution buffer. After 2 hours of incubation with shaking at 120 rpm, the IgG concentration of the solution was determined by UV absorbance at 280 nm. The IgG recovery from the membrane was determined with Equation (4.5).

$$\%Recovery = \frac{(c_e * V_e)}{(c_0 - c_f) * V_s} * 100 \tag{4.5}$$

With c_e = IgG concentration eluted from membrane (mg/ml), V_e = elution volume (ml).

4.4.7 Data Analysis

To determine if two data sets were significantly different from each other, the Student t-test was used assuming a two tailed distribution and a confidence level of 95% ($\alpha = 0.05$).

4.5 Results and Discussion

4.5.1 Membrane Apparent Zeta Potential

Charge characteristic of the membrane material, obtained as apparent zeta potential at 0 M KCl, is shown in Figure 4.1 (a). The apparent zeta potential profile reflects the ionization of the carboxylic acid ligands. Slightly positive apparent zeta potential was observed at pH 4.5, 6.8 mV, which decreased with increasing pH, becoming zero at pH 5.3 and strongly negative at pH 7, -40 mV. The observed zero apparent zeta potential at pH 5.3 is in agreement with the pKa value of the membrane material reported by the manufacturer, between pH 4.7 and 5.3. Strong negative zeta potential, -50 mV at pH 7, was reported previously by Tzoneva et al. [97] for carboxylic acid functionalized poly(ether imide) membranes.

4.5.2 Membrane Global Swelling

Membrane global swelling was affected by pH and ionic strength (Figure 1 (b)). Membrane swelling increased linearly with increasing pH for pH 4.5 to pH 6.0. A less pronounced increase was observed from pH 6 to pH 7. The global swelling increase observed with increasing pH (nearly twofold) closely follows the profile of the negative surface charge of the membrane material (Figure 4.1 (a)) reflecting the increasing charge repulsion of the carboxylic acid groups and the flexibility of the hydrogel structure. The increase in swelling with increased pH was significant ($\alpha = 0.05$) for all ionic strength conditions.

The effect of KCl concentration was less pronounced. At any given pH, membrane global swelling decreased slightly with increasing KCl concentration. At pH 4.5, the membrane global swelling was 3.4 (0 M KCl) and 2.74±0.03 (1 M KCl) while at pH 7, the membrane global swelling was 4.53±0.03 (0 M KCl) and 4.0 (1 M KCl). The observed decrease with increasing KCl was significant ($\alpha = 0.05$) for pH 5.5 and higher and may reflect the shielding effect of the salt ions resulting in less water uptake.

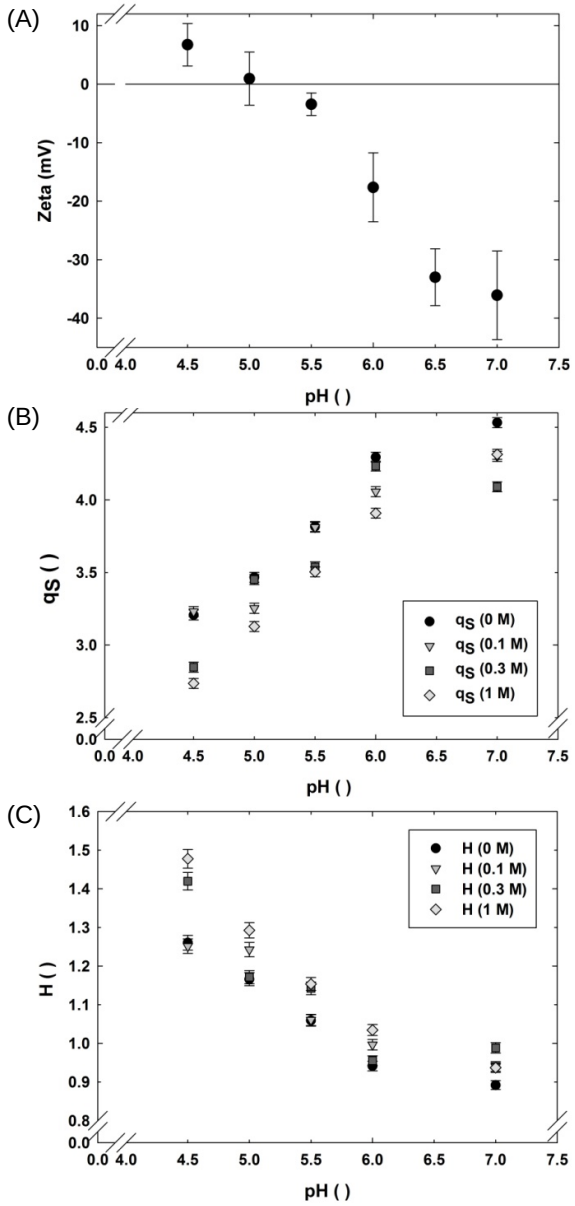

Figure 4.1: Properties according to pH and ionic strength (KCl concentration): (a)Apparent zeta potential; (b)global membrane swelling (q_s); (c) relative membrane swelling (H_s). Error bars represent standard deviation (n = 3).

Similar swelling increase with increasing pH and swelling decrease with increasing ionic strength were previously observed for poly(2-hydroxyethyl methacrylate-co-acrylic acid-co-ammonium acrylate) hydrogels and pH conditions between pH 2 to 8 and 0.05 and 0.15 M NaCl ionic strength [98]. As global swelling reflects the macroscopic properties of the macroporous hydrogel, one cannot distinguish whether the additional water is part of the open pore structure or part of the bulk hydrogel structure.

4.5.3 Membrane Relative Swelling

Membrane relative swelling, estimated from the swelling of the material in aqueous 70% isopropanol to its swelling in an aqueous solution, was developed as an alternative method to water contact angle or protein adsorption for the characterization of the relative hydrophobicity of poly(ethylene glycol)diacrylate hydrogels with different monomer characteristics [92]. In the current study, membrane relative swelling was selected to complement the global swelling characteristics and surface charge characteristics of the material. The highest relative swelling observed at pH 4.8 reflects the small positive charge of the carboxylic acids and the high affinity of the membrane material to aqueous isopropanol for these conditions. The decreasing membrane relative swelling profile with increasing pH (Figure 4.1 (c)) reflects significant contraction of the material in aqueous 70% isopropanol, lower polarity solvent compared to phosphate citrate buffer, which agrees with the increasing negative surface charge of the material with increasing pH (Figure 4.1 (a)). At a given pH, the relative membrane swelling increased with increasing ionic strength. The influence of pH on membrane relative swelling was significant for all ionic strength, whereas the influence of ionic strength on membrane relative swelling was significant only at pH 4.5 ($\alpha = 0.05$). The magnitude of the membrane relative swelling observed in this study according to pH, 0.9 to 1.48 is comparable to those reported for the relative swelling of poly(ethylene glycol)diacrylate hydrogels with different monomer characteristics ranged between 0.9 and 1.29 [92].

4.5.4 Membrane Pore Visualization and Characterization

Visualization and characterization of micron size porous structure can be achieved by FE-SEM but the sample should be water free which for hydrated hydrogel materials implies sample preparation. Water removal of hydrated hydrogel materials is delicate since the structure is sensitive to water movement. In contrast to air drying, freeze drying may alleviate the effect of drying by minimizing the water movement with an initial freezing step.

The effect of air drying and freeze-drying on the morphology of non-hydrated and hydrated membrane samples visualized by FESEM was first evaluated. The visual appearance (Figure 4.2) and average pore diameter estimate (Table 4.1) of non-hydrated membrane samples was not affected by freeze-drying as expected since the membrane samples contained no water. The fibrous polyolefin support structure, which provides mechanical strength to the carboxylic acid functionalized macroporous hydrogel, was clearly visible. In contrast, when hydrated (24 h, pH 4.5), the visual appearance and average pore size of the membrane was affected by the type of drying (Figure 4.3). Freeze-drying of hydrated membranes displayed smaller pores and average pore size (Table 4.1) when compared to hydrated membranes subjected to either air drying or air drying with subsequent freeze-drying. The higher average pore diameter of the air dried membrane (with and without subsequent freeze-drying) suggests collapse of the hydrogel structure during sample preparation and water removal, while the smaller average pore diameter of the freeze-dried membrane suggests negligible collapse of the porous structure. Freeze drying did not affect membrane global swelling or IgG binding (data not shown).

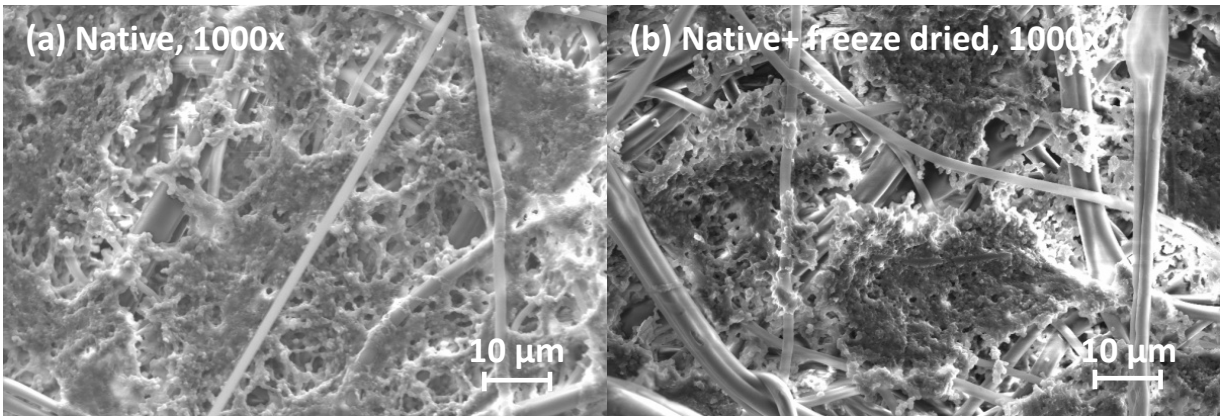

Figure 4.2: FESEM pictures (1000 x magnifications): (a) native non-hydrated membrane and (b) native non-hydrated and freeze-dried membrane.

Since freeze-drying preserved the structure of the hydrated membrane, this preparation method was adopted for the investigation of pH and ionic strength on the surface structure of hydrated membranes (Figure 4.4 and 4.5 and Table 4.1). Small pores were present on the membrane surface at pH 4.5 and 0 M KCl while larger pores were present at pH 6 and pH 7 and 0 and 1 M KCl, reflecting the higher negative charge and increased repulsion of the carboxylic acid groups with increasing pH (Figure 4.1 (a)).

Surface pore diameter estimates ranged from 0 to 1.6 μm (Figure 4.5) and differed

Table 4.1: Estimated average pore diameter (μm) according to pH and ionic strength for native non hydrated membranes and hydrated membranes subjected to different drying conditions.

Hydration	**Membrane preparation**		**Pore size diameter [μm]**[a]
	Air drying	*Freeze drying*	
dry	N/A	-	0.467±0.062
dry	N/A	+	0.476±0.032
pH 4.5 (0 M KCl)	+	-	0.437±0.072
pH 4.5 (0 M KCl)	-	+	0.351±0.025[x]
pH 4.5 (0 M KCl)	+	+	0.422±0.013
pH 4.5 (0 M KCl)	-	+	0.310±0.066*
pH 5 (0 M KCl)	-	+	0.433±0.039
pH 6 (0 M KCl)	-	+	0.448±0.023
pH 7 (0 M KCl)	-	+	0.522±0.036*
pH 4.5 (1 M KCl)	-	+	0.258±0.032*
pH 6 (1 M KCl)	-	+	0.383±0.039
pH 7 (1 M KCl)	-	+	0.439±0.039

[a]Average ± standard deviation (n = 3);
*statistically significant ($\alpha = 0.05$) influence of pH at constant ionic strength; [x]statistically significant ($\alpha = 0.05$) influence of membrane drying step.

according to pH and KCl concentration. Pores with 0.16-0.32 μm diameter represented the bulk of the pores, 30% to 62% at 0 M KCl and 38 to 60% at 1 M KCl. Further analysis was obtained by clustering the pores in three groups, pores with diameter below 0.32 μm, pores between 0.32 and 0.96 μm and pores larger than 0.96 μm. At pH 6 and pH 7, the addition of KCl significantly ($\alpha = 0.05$) reduced the fraction of pores larger than 0.96 μm. Potassium counter ion may shield the negative charge of the carboxylic acid of the larger pores leading to a statistically significant size reduction of these pores. The effect of KCl addition was only significant when considering the pore size frequency but not the average pore size diameter (Table 4.1). The significant influence of KCl addition at pH 7 for pores below 0.32 μm could be an image analysis artifact rather than material characteristic and would need further investigation. At pH 4.5, smaller pores (0-0.32 μm) predominated while

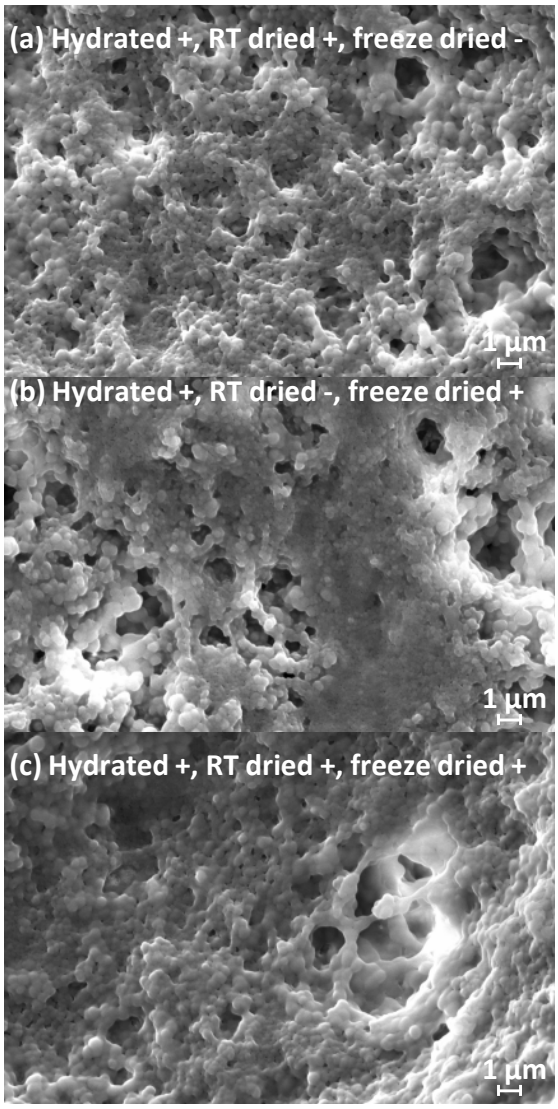

Figure 4.3: FESEM images of hydrated membranes (5000 x Magnification): (a) sample preparation by air drying at room temperature (RT), (b) sample preparation by freezing drying and (c) sample preparation by air drying at RT and subsequent freeze drying.

large pores (> 0.96 μm) were nearly absent with and without KCl addition reflecting the nearly zero surface charge of the material at these pH conditions.

The average membrane pore diameter (Table 4.1) indicates increasing average pore

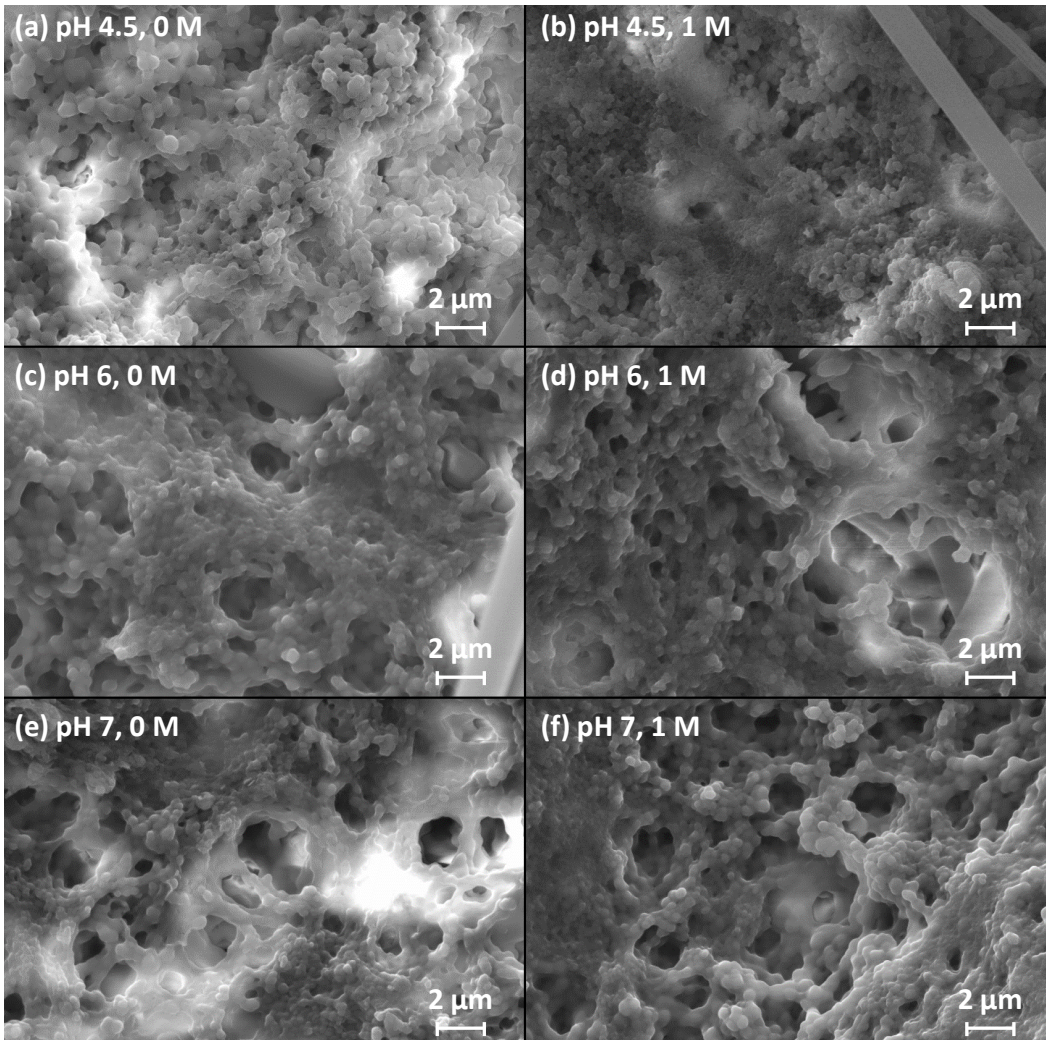

Figure 4.4: FESEM images (5000 x magnification) of hydrated membrane and freeze-dried: (a) pH 4.5 and 0 M KCl; (b) pH 4.5 and 1 M KCl; (c) pH 6 and 0 M KCl; (d) pH 6 and 1 M KCl; (e) pH 7 and 0 M KCl; (f) pH 7 and 1 M KCl.

diameter with increasing pH. At pH 4.5 and 0 M KCl, the average pore diameter was 0.310 μm while at pH 7, 0 M KCl, the average pore diameter increased significantly to 0.522 μm. Comparison of the average pore diameter of the hydrated membrane to the native non-hydrated membrane (0.47 μm) indicates hydrogel contraction at pH 4.5 and hydrogel expansion at pH above 6. The increasing average pore diameter with increasing

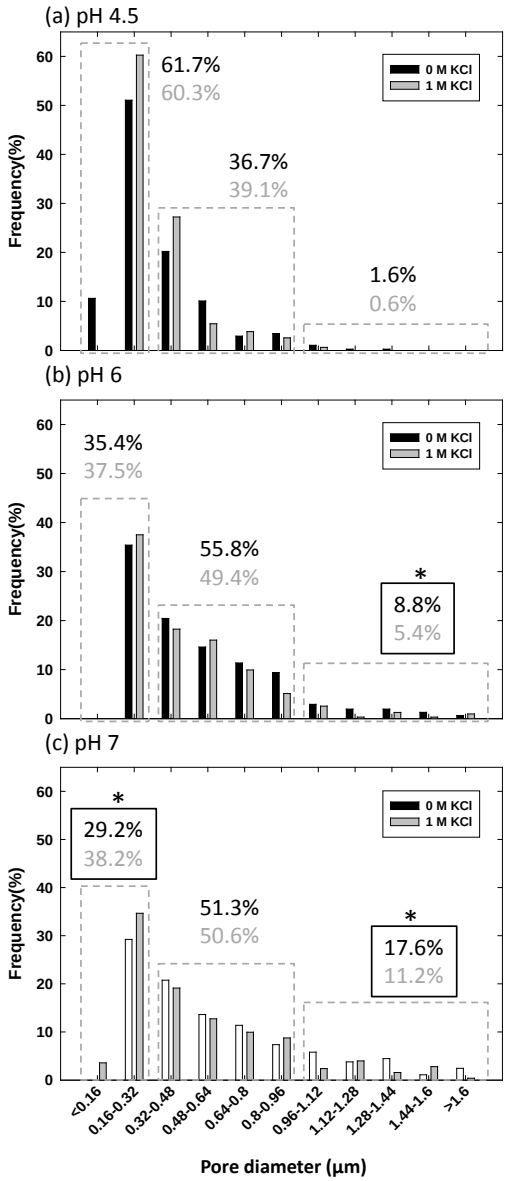

Figure 4.5: Pore diameter distribution according to pH and at 0 M KCl (black bars) and 1 M KCl (grey bars): (a) pH 4.5; (b) pH 6.0; (c) pH 7.0. Numbers denote the frequency of pore diameters in the three pore size regions (<0.32, 0.32-0.96 and >0.96 μm). * Denotes significant ($\alpha = 0.05$) influence of ionic strength on pore size frequency.

pH reflects the increasing negative charge of the carboxylic acids (Figure 4.1 (a)) and the associated increased repulsion, increased water uptake and higher membrane global swelling (Figure 4.1 (b)). The effect of charge shielding by KCl addition at high pH did not translate in statistically significant differences.

Although freeze drying in combination with FESEM and image analysis showed promising results, it is important to be aware of the limits of this approach. Taking FESEM images of membrane surfaces will not capture the tortuosity of the material. Future experiments should include cross-sections of the material. Surface pores might be underestimated due to a limit in contrast and the chosen threshold value. The pore size distributions show that the image program does not capture the smaller range of pores well. The majority of pores however were in the range of 0.16-0.32 μm which is still seven to fourteen times larger than IgG (dimensions 21.9x15.5x1.5 nm), confirming that the large protein will not be hindered by pore size. Future pore size experiments should also be expanded to an alternative technique, confirming the trends and numbers found with FESEM imaging.

The pore diameter estimates obtained in this study for weak cation exchange macroporous materials are of the same order of magnitude with most published pore diameter estimates, 0.26-2 μm (estimates performed over gas flow permporometry) reported for macroporous poly(acrylic acid) grafted cellulose membranes [99] and 0.222 μm (estimated from permeability measurements) at pH 4 reported for hydrated PVDF-PAA membranes [83]. In contrast, the pore diameter estimates in this study are significantly larger (by a factor of 10-100) than those reported previously for dextran-methacrylate hydrogels analysed with FESEM and mercury intrusion porosimetry [44] and polyacrylamide hydrogels analyzed by size exclusion [81]. These differences reflect the distinctive, macroporous character of the weak cation exchange material investigated in this study.

4.5.5 Membrane Interaction with Immunoglobulin G

4.5.5.1 Influence of pH Conditions on IgG Static Binding

Static binding experiments were conducted to explore the charge modulation properties of the macroporous hydrogel weak cation exchange membrane chromatography material according to pH and ionic conditions and relate these to the interactions with IgG. These experiments were not intended for IgG binding capacity optimization. The effect of pH at 0 M ionic strength on IgG static binding capacity with 0.5 g/l initial IgG concentration is presented in Figure 4.6 (a) for narrow pH conditions. The pH significantly influenced IgG binding capacity ($\alpha = 0.05$). The maximum IgG static binding capacity was observed at pH

4.8, 20.1±1.5 mg/ml. Decreased IgG static binding capacity was observed for pH 4.8 and above with minimum IgG static binding capacity, 4.0±0.7 mg/ml, observed at pH 5.5. The significant IgG static binding capacity observed at pH 4.8 appear to result predominantly from the more pronounced positive charge of IgG or non electrostatic interactions with the material. Polyclonal IgG has an overall strong net positive charge in the pH range 4.5-5.5 since its isoelectric point (pI) is 6.5-10 with 77% of the proteins having pI above pH 8 [100]. In contrast, the membrane material at pH 4.8 had an apparent zeta potential nearly zero (+ 1 mV), an average pore diameter significantly larger (Table 4.1) than IgG diameter (approximately 10 nm), its global membrane swelling was lowest (Figure 4.1 (b)) and its relative swelling maximum (Figure 4.1 (c)).

4.5.5.2 Influence of Ionic Strength Conditions on IgG Static Binding

The pH condition where IgG binding capacity was highest, pH 4.8, was selected for assessing the effect of ionic strength on IgG static binding with KCl concentrations up to 100 mM (Figure 4.6 (b)). Maximum IgG static binding capacity, 20.1±1.5 mg/ml, occurred at the lowest ionic strength, 0 M KCl. IgG static binding capacity decreased with increasing ionic strength with a minimum IgG binding, 10.0±0.8 mg/ml, at 100 mM KCl. The influence of ionic strength on IgG binding was statistically significant ($\alpha = 0.05$). The decrease IgG static binding capacity with increasing KCl concentration reflects the shielding role of KCl on the IgG charge. The minor increase of membrane hydrophobicity properties at pH 4.8 (1.17 at 0 M KCl and 1.24 at 100 mM KCl) and the minor decrease of estimated average pore diameter for significantly higher KCl concentration (1 M) (Table 4.1) are believed to have a negligible role in the reduced IgG static binding.

4.5.5.3 Influence of pH and Ionic Strength on IgG Recovery

The recovery of IgG, given as the ratio between the IgG eluted from the membrane and the IgG bound to the membrane, was modulated by pH and ionic strength for binding conducted at pH 4.8 and 0 M KCl (Figure 4.7). The IgG recovery at 1 M KCl increased linearly with increasing pH up to pH 5.5 and subsequently leveled off, with 60% at pH 4.5 and 95% and higher at pH above 5.5 (Figure 4.7 (a)). The effect of pH at 1 M KCl was statistically significant ($\alpha = 0.05$).The effect of ionic strength on IgG recovery (Figure 4.7 (b)) indicates nearly complete IgG recovery for elution at pH 7 and all ionic strength investigated (no significant statistical difference, $\alpha = 0.05$). In contrast, IgG recovery for elution at pH 4.5 was affected significantly by ionic strength. IgG recovery at pH 4.5 increased with ionic strength, from 23% (0.25 M KCl) up to 60% (1 M KCl). Higher ionic strength

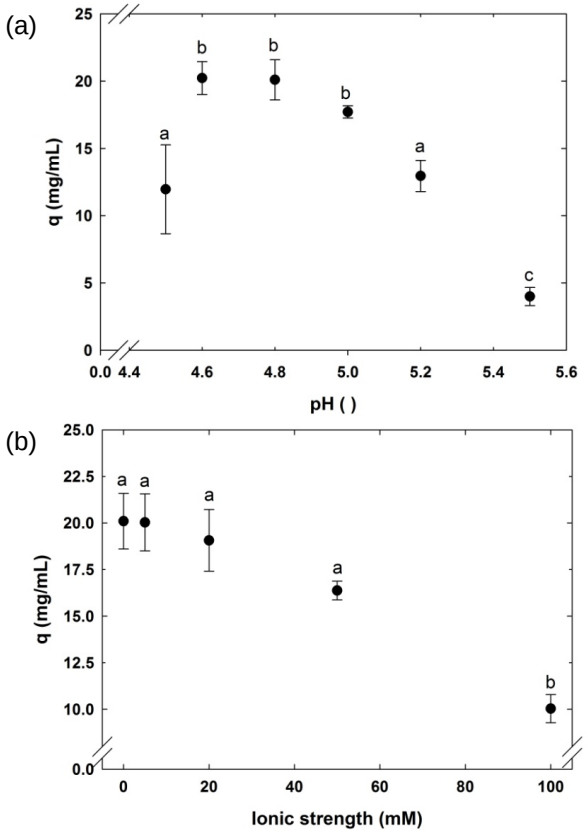

Figure 4.6: IgG static binding capacity (q) (5 h binding time, c_0 (IgG) = 0.5 g/L in phosphate citrate buffer): (a) Effect of pH at 0 M KCl and (b) effect of ionic strength at pH 4.8. Conditions not sharing a common letter are significantly different ($\alpha = 0.05$); Error bars represent standard deviation; n = 3.

conditions (2 M KCl) did not promote any additional IgG recovery (data not shown). The modulation of IgG recovery according to pH and ionic strength suggest that the charge properties of IgG predominate over the charge properties of the membrane material.

The pH and ionic strength conditions selected in this study for IgG elution were similar to previous study with polymethacrylate membrane base functionalized weak materials where lower IgG recovery (up to 67%) was obtained at pH 7 compared to 95% in the current study, illustrating the importance of the material and the need to tailor elution conditions according to material properties [75].

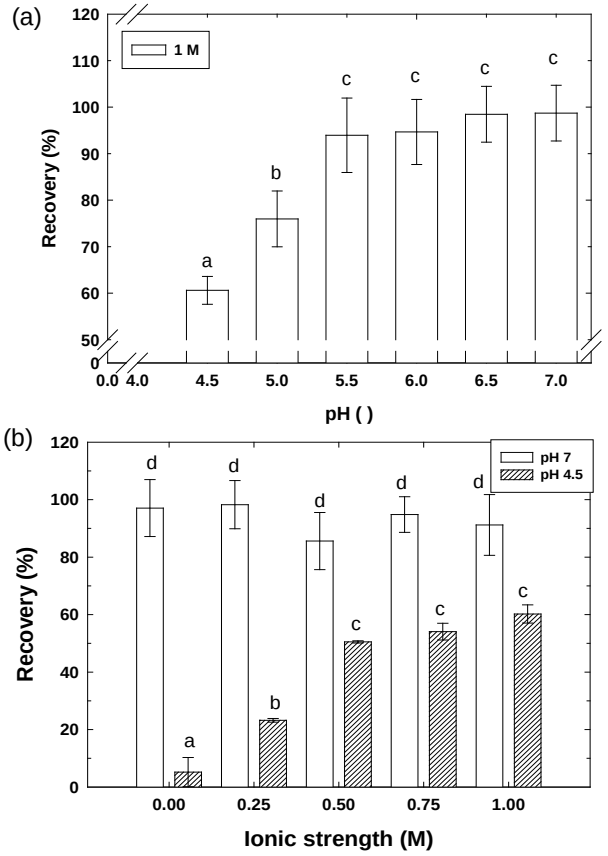

Figure 4.7: IgG recovery and elution conditions: (a) Effect of pH at 1 M KCl; (b) Effect of ionic strength for constant pH conditions (4.5 or 7). IgG binding was conducted at pH 4.8 and 0 M KCl for 5 h and c_0 = 0.5 g/l IgG. Conditions not sharing a common letter are significantly different ($\alpha = 0.05$); Error bars represent standard deviation; n = 3.

4.5.6 Mechanisms During Binding and Elution of IgG with Weak Cation Exchange Hydrogel Material

Electrostatic interactions were observed during IgG binding and elution with weak cation exchange membrane materials. Such interactions were expected to capitalize on the strong positive charge of IgG below its isoelectric point (pH = 8.0 for 77% of the protein content) and the increased negative charge of carboxylic acid ligands of the macroporous hydrogel material at pH above its pKa (pH = 4.7-5.3). Even though the weak acid nature of car-

boxylic acid ligands was confirmed by streaming potential measurements (Figure 4.1 (a)), the strong negative charge of the membrane material at high pH did not dominate IgG binding or hindered IgG elution. Instead, high IgG binding capacity was observed for a narrow pH range, 4.6-4.8, (Figure 4.6 (a)) reflecting the importance played by the strong positive charge of IgG for these pH conditions while the membrane material had small positive charge. Membrane surface charge was important during IgG recovery for most pH conditions except below pH 5.5. When the membrane material possessed strong negative apparent zeta potential at pH 5.5 and higher, nearly complete IgG recovery was obtained with 1 M KCl and pH 5.5 and above (Figure 4.7 (a)) or at pH 7 with no KCl addition (Figure 4.7 (b)). When the membrane material had nearly zero surface charge, pH 4.5, increasing ionic strength was required to disrupt IgG material interactions and increase IgG recovery but complete IgG recovery could not be achieved. The nearly complete recovery of IgG without KCl addition obtained at pH 7 is advantageous for subsequent purification operations.

In terms of membrane material characteristics, its relative swelling was useful in confirming the charge profile of the membrane material but did not assist with understanding of IgG binding and recovery. The membrane average surface pore diameter did not seem to affect and restrict IgG binding and recovery since the estimated average pore diameter is significantly larger than IgG diameter.

Based on the experimental observations obtained in this study, a visual representation of the material surface charge, swelling and average pore diameter and IgG charge according to pH is schematized in Figure 4.8. The hydrogel domain and open macropore domain of the membrane material containing the carboxylic acid groups constitute the active material which interacts with IgG. The recovery conditions at low pH correspond to low global swelling and small average pore diameter of the material and high positive charge of IgG and those at high pH correspond to high global swelling and large average pore diameter of the material and nearly zero charge of IgG.

4.6 Conclusions

This study illustrated the potential of the apparent zeta potential, membrane global swelling and surface pore visualization by FESEM of freeze-dried hydrated membrane samples to better understand charge interactions, water uptake and macropore structure and their relationship to binding and recovery features of IgG with weak cation exchange macroporous hydrogel membrane materials.

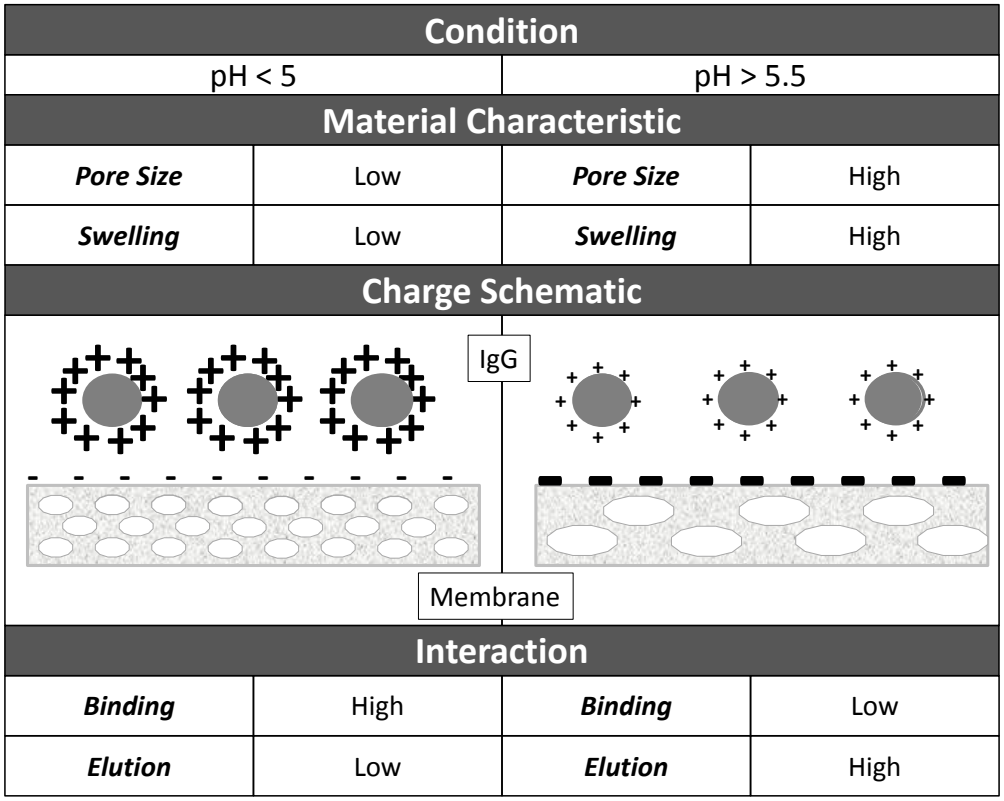

Figure 4.8: Schematic representation of membrane material characteristics and IgG-membrane interactions for low (< 5) and high pH (> 5.5).

Charge properties of IgG were the predominant mechanism responsible for its binding and elution. The strong IgG positive charge dominated the low surface charge of the membrane material for maximum IgG binding at pH 4.8 while the nearly zero charge of IgG at pH 7 dominated the strong negative charge of the material for maximum IgG elution. The potential influence of localized surface charge and hydrophobicity for IgG and membrane material cannot be excluded and should be the focus of future work. FESEM in combination with freeze-drying was successful in preserving the porous structure of hydrated membrane materials and in quantifying the effect of pH and ionic strength on the surface pore structure. It cannot be excluded that the internal pore structure has different properties and should be part of future work.

The water holding capacity (seen in swelling and pore size characteristics) in the bulk hydrogel domain and the open macropore domain according to pH and ionic strength

conditions is anticipated to become more significant when moving to dynamic operations and should be investigated for the design of large scale operations where open pore structure is desired for high convective flow conditions.

4.7 Acknowledgements

Financial support from the Monoclonal Antibody Network (MabNet) of the Natural Sciences and Engineering Research Council (NSERC) is acknowledged. The authors also thank Dr. Peldzus at the University of Waterloo for access to the electrokinetic analyzer and Nina Heinig at the University of Waterloo for help with the Field Emission Scanning Electron Microscope.

Chapter 5

Protein Adsorption, Ion Exchange Capacity and Mass Transfer in Cation Exchange Membranes

5.1 Synopsis

In the previous chapters we looked at characterization of proteins (Chapter 3) and characterization of weak cation exchange membrane macroporous hydrogel material (Chapter 4). Chapter 5 is expanding material characterization to protein equilibrium adsorption characterization, ion exchange capacity (IEC) characterization and internal mass transfer considerations. Two types of cation exchange membrane materials were investigated, weak cation macroporous membrane material and a strong cation exchange membrane chromatography material. Two proteins with distinct size and charge were selected, IgG (as in Chapter 3 and 4) and lysozyme. Set conditions for protein binding and protein elution conditions were employed based on previous work (see Chapter 4).

Static protein binding capacity was developed by Katharina Hassel and conducted by Katharina Hassel and Nicholas Cober. Adsorption model analysis was conducted by Katharina Hassel with support from Rawle Groothuizen. Static IEC experimentation was developed by Nicholas Cober and conducted by Nicholas Cober and Katharina Hassel. Dynamic IEC was developed and conducted by Kayleigh Kuindersma. Dynamic protein binding capacity was established and conducted by Katharina Hassel with experimental support from Nils Wagner. FESEM sample preparation was performed by Katharina Hassel. FESEM imaging was performed by Nina Heinig (Chemistry Department). Data

analysis was performed by Katharina Hassel with contribution from Nicholas Cober (static IEC) and Kamyar Ghofrani and Maximilian Fondyga for FESEM image analysis. Writing was performed by Katharina Hassel with contribution from Nicholas Cober (literature review). Experimental planning, data analysis and writing were supervised, reviewed and revised by Christine Moresoli.

This chapter was formatted for future submission to Journal of Membrane Science, Katharina Hassel, Nicholas Cober and Christine Moresoli, Mass transfer limitations for a novel weak cation exchange hydrogel membrane.

5.2 Abstract

Protein adsorption and ion exchange capacity (IEC) were assessed and compared to better understand mass transfer in two commercial cation exchange membranes, Natrix C macroporous hydrogel membrane and Sartobind S surface grafted membrane. Significant differences were observed for the equilibrium protein binding capacity according to material and for IgG and lysozyme, protein candidates with different size and charge characteristics. Higher equilibrium protein binding capacity was observed for Natrix C membrane compared to Sartobind S even though IEC was lower. IgG isotherm with Natrix C was best captured by the steric mass action adsorption model which accounts for charge and steric effects while the Langmuir adsorption model best captured IgG adsorption with Sartobind S membrane. Mass transfer characteristics also differed according to protein and material type. Ion transport and protein transport increased when the membrane structure was disrupted except for IgG and Natrix C membrane. Convective mass transfer limitations were also identified and could be somewhat or totally removed when operating in dynamic mode. Further work is required to investigate these differences at the microscopic level and explore pH and ionic conditions.

5.3 Introduction

An important element of high purity protein production is their separation and purification. In the past, this has been done with packed bed resin chromatography systems. Since protein transport in these systems is diffusion driven (Figure 5.1 A), processing times can be long and significant pressure drop can be observed [101].

It is therefore desirable to consider alternative technologies for protein separation. Membrane chromatography technologies offer several advantages over traditional packed

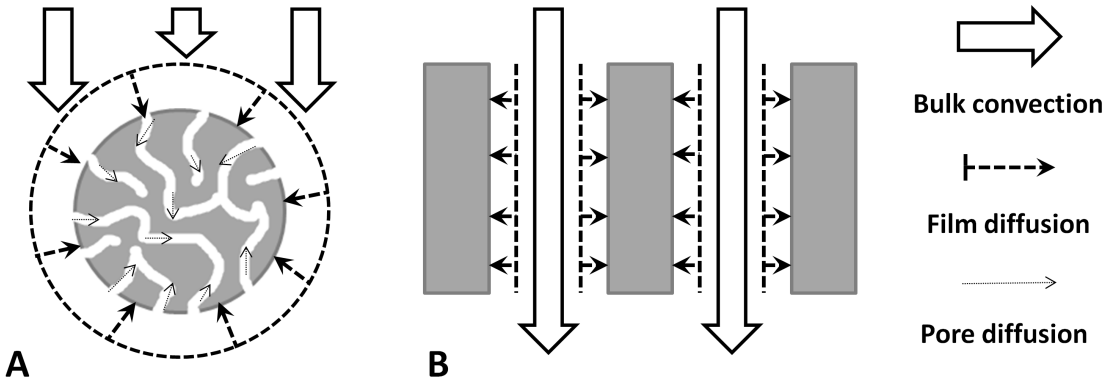

Figure 5.1: Mass transport phenomena in resin (A) and membrane adsorbers (B)

bed resin systems. Membrane chromatography is based on convective transport (Figure 5.1 B) such that processing time is reduced, is easier to scale up and decreased pressure drop can be observed. The high binding capacity and 3D architecture of membrane chromatography materials is conducive to internal mass transfer limitations. The strong non-linear profile of breakthrough curves reported in the literature supports the existence of such mass transfer limitations. But the investigation of mass transfer for protein capture with ion exchange membrane materials is complex due to the interrelationship between mass transfer, protein adsorption and ion exchange considerations [39].

Ion exchange chromatography materials contain either positively or negatively charged functional groups. When functional groups are negatively charged, interactions will take place with positively charged proteins and are referred to as cation exchange chromatography materials. Examples of cation exchange groups include sulphonic or carboxylic acid groups [102,103]. The strength of the electrostatic interaction between the functional group and the target protein differs according to functional group. A strong cation exchange material will be completely ionized for a wide pH range reflecting its charge stability while weak cation exchange material possesses variable ionization according to pH conditions.

Charge characteristics of ion exchange materials can be obtained from their ion exchange capacity (IEC). Titration methods are commonly reported for IEC determination and ion exchange membranes [24–27]. These studies report IEC values between 0.22-2.8 meq/g for strong and weak cation and anion membrane materials.

The purpose of this study was to determine the protein adsorption and ion exchange capacity characteristics of two commercial cation exchange membrane chromatography

materials, weak cation exchange hydrogel macroporous membrane and a strong cation exchange surface grafted membrane. Human immunoglobulin G (IgG), a polyclonal antibody which contains several isoforms with slightly different structure and properties and lysozyme, extracted from hen egg white, were selected because of their different size and charge characteristics.

Further intentions were to investigate potential mass transfer limitations by comparing IEC and protein binding capacity for intact and cut membranes. By cutting the membrane in smaller pieces more surface area is obtained and becomes available for binding compared to the intact membrane

5.4 Material and Methods

5.4.1 Chemicals and Buffers

Hydrochloric acid (Fischer Scientific Canada), sodium hydroxide and potassium chloride obtained from EMD (Billerica, MA, USA) and sodium chloride from BDH Inc. (Toronto, Ontario, Canada) were used. Phosphate citrate buffer was prepared from solutions of 0.1 M citric acid, anhydrous (EMD, Tokyo, Japan) and 0.2 M sodium phosphate, dibasic, heptahydrate (EMD, Darmstadt, Germany). Acetate buffer was prepared with acetic acid (EMD, Darmstadt, Germany) and sodium acetate (EMD, Darmstadt, Germany). Phosphate buffer was prepared with monosodium phosphate (monohydrate), disodium phosphate (heptahydrate) and potassium chloride obtained from Fischer Scientific Canada. Milli-Q water was prepared in house from a Millipore Synergy UV system (EMD Millipore, Darmstadt, Germany). Human immunoglobulin G was purchased from Equitech-Bio, Inc. (Kerrville, TX, USA). Lysozyme chloride was obtained from Neova Technologies (Abbotsford, BC, Canada). Their characteristics are presented in Table 5.1.

5.4.2 Membrane Materials

Weak cation exchange (C) membranes were provided by Natrix Separations Inc. (Burlington, Ontario, Canada) as 25 mm diameter discs (dynamic IEC and dynamic conditions), 47 mm diameter discs (static binding conditions) and flat sheet (static IEC). Strong cation exchange membranes (Sartobind S) were purchased from Sartorius-Stedim (Bohemia, NY, USA) in DIN A4 flat sheet format. Membrane specifications given by the manufacturer are presented in Table 5.1.

Table 5.1: Protein and membrane characteristics

	Proteins	
Characteristics	*Lysozyme*	*IgG*
Charge[a]	+++	+
pI[b]	11	6.5-10
Size (kDa)[c]	14.3	150
Dimensions (nm)[d]	3x3x4.5	21.9x15.5x1.5
Diffusion coefficient (cm^2/s)[e]	$0.5\text{-}2.5*10^{-6}$	$4.4*10^{-7}$
	Membranes	
Characteristics[f]	*Natrix C*	*Sartobind S*
pKa	4.7-5.3	2
Material	Pore filled hydrogel	Surface grafted polymer
Pore size (μm)	0.3	>3
Ionization(%)	50	100
IEC ($\mu eq/cm^2$)	n/a	4-6

[a]at pH 5; [b] [67, 104]; [c] [105, 106]; [d] [107, 108]; [e] [109, 110]; [f]Manufacturer data.

5.4.3 Ion Exchange Capacity (IEC) Estimation

5.4.3.1 IEC by pH - Static Conditions

Titration method was used for the determination of ion exchange capacity [24–27]. Membrane samples were prepared from flat sheet material for three different membrane formats: Intact membranes (cut to 2x2 cm), cut membranes (4 scissor cut pieces of 1x1 cm each) and crumble membranes (12 small scissor cut pieces from a 2x2 cm piece). The mass of each membrane sample was recorded before being placed in 250 ml Erlenmeyer flasks containing 40 ml of 1 M hydrochloric acid solution to ensure that the carboxylic and sulphonic groups were converted to acid form (H^+). The membrane samples were equilibrated for 4 hours at room temperature (21±1°C) with shaking at low speed (shaker Eberbach Corporation Ann Arbor, Michigan, USA). After equilibration, membrane samples were removed and rinsed thoroughly with Milli-Q water to remove any traces of HCl. The membrane samples were then placed in 40 ml of 1 M sodium chloride solution with shaking during 24 h to ensure that all H^+ were released from the membrane and eluted in the solution. The solution and membranes were then transferred into a beaker for titration with 0.1 M sodium hydroxide. The pH of the solution was measured with a pH meter (±0.002) (Mettler Toledo Seven-

multi). The pH of the solution according to volume of sodium hydroxide added was used to determine the equivalence point (pH 7) and the corresponding ion exchange capacity according to Equation 5.1.

$$IEC(\frac{meq}{g}) = \frac{M_{NaOH} * V_{NaOH}}{m_{membrane}} \tag{5.1}$$

Where M_{NaOH} is the molarity of NaOH (mol/l), V_{NaOH} is the volume of NaOH added at the equivalence point (l) and $m_{membrane}$ is the mass of the membrane, prior to hydration (g). The equivalence point was estimated using the 1^{st} derivative method where the maximum value of the first derivative function represented the equivalence point.

5.4.3.2 IEC by Conductivity - Dynamic Conditions

IEC for dynamic conditions was estimated with an AKTA Prime system (GE Healthcare, Sweden) (Fast protein liquid chromatography (FPLC) system) equipped with a conductivity probe as illustrated in Figure 5.2.

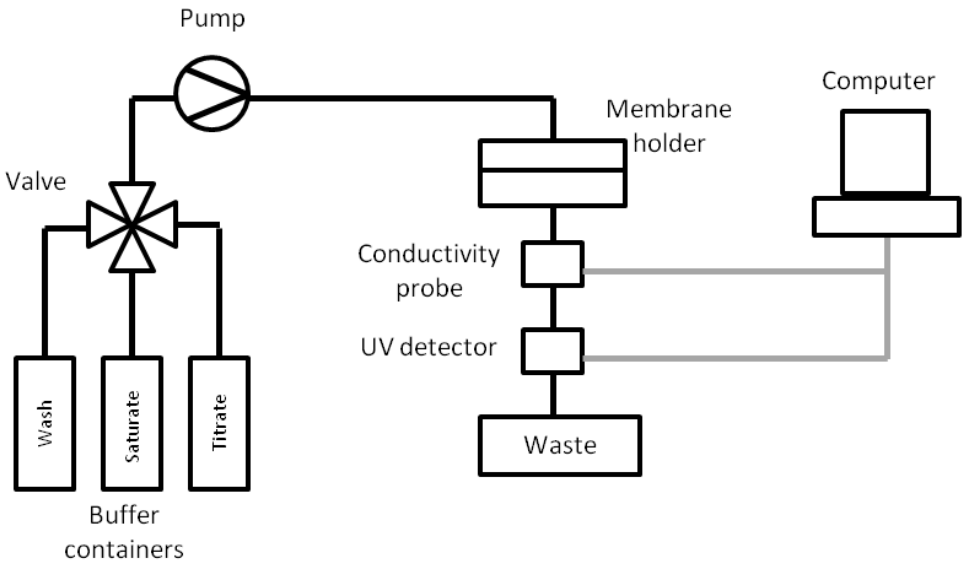

Figure 5.2: AKTA set-up

A 25 mm diameter membrane sample was placed in the membrane holder and then subjected to the conditions presented in Table 5.2; namely equilibration with Milli-Q water,

Table 5.2: Experimental conditions of IEC estimation by conductivity and dynamic mode for 2 ml/min as feed flow rate

Step #	**Time (min)**	**Function**	**FlowRate**	**Solution**
I	0	Equilibration	1 ml/min	Milli-Q Water
II	10	Binding	1 ml/min	0.1 M NaOH
III	35	Washing	1 ml/min	Milli-Q Water
IV	55	Elution	1 ml/min	0.025 M HCL
V	90	End	-	-

saturation with 0.1 M NaOH, thorough rinsing with Milli-Q water and titration with 0.025 M HCl at a flow rate of 2 ml/min.

IEC was estimated from the equivalence point deduced from change in slope of the measured conductivity versus HCl added volume (Figure 5.3) according to Equation 5.2.

$$IEC(\frac{meq}{g}) = \frac{M_{HCl} * V_{HCl}}{m_{membrane}} \tag{5.2}$$

Where M_{HCl} is the molarity of HCl (mol/l), V_{HCl} is the volume of HCl added at the equivalence point (l) and $m_{membrane}$ is the mass of the membrane prior to hydration (g).

5.4.4 Static Protein Binding Capacity

All static protein binding experiments were carried out at room temperature (21±1°C). A membrane disc (47 mm diameter) was cut into eight pieces and each was weighed. A cut section of a membrane disc (dry weight 0.026 ± 0.002 g) was placed in a 20 ml vial. The membrane piece was equilibrated in 5 ml of equilibration buffer (phosphate citrate pH 5) on a shaker (Thermo Scientific, Canada) at 125 rpm for 2 h. Following equilibration the solution was drained, 10 ml of binding buffer were added (equilibration buffer containing 0.5 mg/ml of IgG or lysozyme) and placed on the shaker at 125 rpm for 5 h. The total protein concentration of the solution was quantified before and after binding by spectrophotometry at 280 nm (Spectronic Gensys 5). Experiments were conducted in triplicates. The static protein binding capacity was evaluated by difference between the protein content of the solution before and after binding, assuming that the volume of the solution remained constant (Equation 5.3).

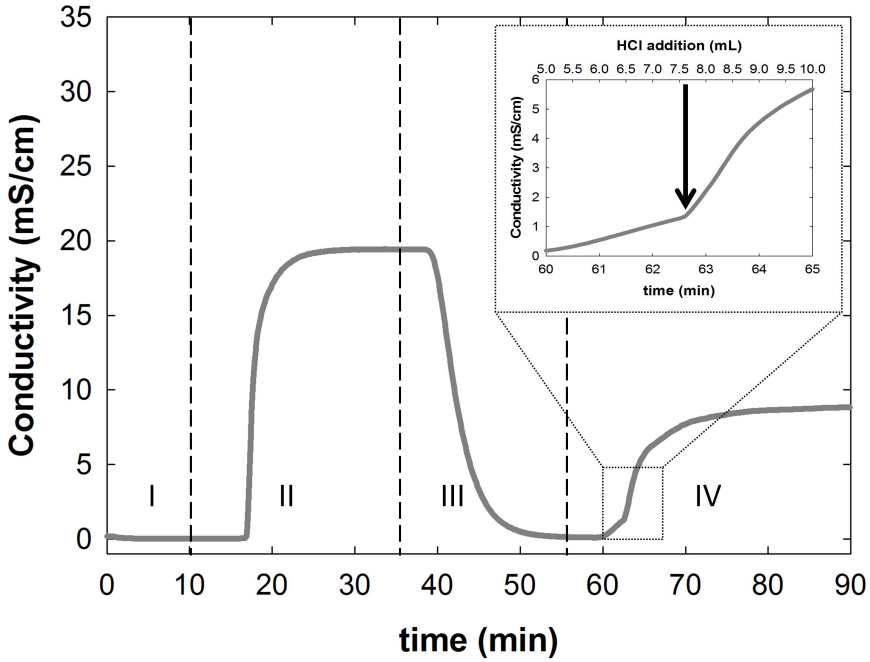

Figure 5.3: Typical conductivity profile during dynamic ion exchange capacity determination. I: Equilibration with Milli-Q water, II: Binding with 0.1 M NaOH, III: Washing with Milli-Q water and IV: Titration with 0.025 M HCl.

$$q(\frac{mg}{mL}) = (c_O - c_f) * (\frac{V_{solution}}{V_{membrane}}) \tag{5.3}$$

Where q is the binding capacity (mg protein/ ml membrane), c_0 is the initial concentration of protein in solution (mg/ml), c_f is the final concentration of protein after binding (mg/ml), $V_{solution}$ is the volume of binding buffer (ml), $V_{membrane}$ is the measured volume of the dried membrane piece (ml).

5.4.5 Protein Isotherms

All protein isotherm experiments were performed as described in the static binding section with the following differences. Protein (IgG and lysozyme) concentration ranged from

0.1 to 4 g/L. Binding time was 24 h for IgG and 72 h for lysozyme respectively. After binding, all solutions were filtered through a 0.45 μm PES syringe filter (Thermo Scientific, Ottawa, ON, Canada) before UV measurements. The binding capacity was estimated with Equation 5.3.

To describe protein adsorption isotherms, four models (Langmuir, Bi-Langmuir, Freundlich and Steric mass-action) were used (overview in Table 5.4.5). All model parameters were estimated with the MATLAB 2014a curve fitting toolbox.

The Langmuir model represents a common model based on the assumption of a monolayer surface coverage without any interaction of the adsorbed species, see Equation 5.4 [111].

$$q(c) = q_{max} * \frac{K_L * c}{1 + K_L * c} \tag{5.4}$$

Where c(mg/ml) is the equilibrium protein concentration in solution, q (mg/ml) is the protein adsorption capacity at equilibrium q_{max} (mg/ml) is the maximum adsorption capacity and K_L is the Langmuir equilibrium constant given by the ratio of adsorption constant (k_a) and the desorption constant (k_d) as illustrated in Table 5.4.5. High K_L values reflect situations where increase of the equilibrium protein concentration is sharper meaning there is a higher interaction between proteins and membrane binding sites. Low K_L values reflect situations where increase of the equilibrium protein concentration is slower and accordingly the affinity between proteins and binding sites is lower. Many situations for protein binding on membranes do not agree with the Langmuir isotherm since the assumptions may not represent reality.

The Bi-Langmuir model is an expansion of the Langmuir model for chromatographic separations that do not possess a homogeneous surface. This model considers two binding sites having different interactions resulting in two independent contributions as seen in Table 5.4.5 and Equation 5.5 [32]:

$$q(c) = q_{max,1} * \frac{K_{B,1} * c}{1 + K_{B,1} * c} + q_{max,2} * \frac{K_{B,2} * c}{1 + K_{B,2} * c} \tag{5.5}$$

$K_{B,i}$ = Bi-Langmuir equilibrium constant for sites 1 and 2 and $q_{max,i}$ = saturation capacity of the material (mg/ml) for sites 1 and 2. The Bi-Langmuir model is selected when the plot q/c versus q is strongly curved.

When considering the influence of one adsorbent on the subsequent adsorption step, the Freundlich model may be more suitable. This isotherm however does not include a q_{max} parameter and therefore cannot predict the equilibrium adsorption capacity of the material easily. It can be described with Equation 5.6 [111], where K_F and n are Freundlich isotherm constants.

$$q(c) = K_F * c^{\frac{1}{n}} \tag{5.6}$$

The steric mass-action (SMA) model describes non-linear adsorption in ion-exchange systems. Assumptions for the model are (1) spherical proteins with uniform size and density, (2) protein binding is dependent on the characteristic charge v (due to the multi-pointed nature of proteins), (3) steric hindrance of the counterions bound to the material occurs and (4) model parameters do not change during adsorption process. Table 5.4.5 shows a representation of principles and involved parameters [34]. Equation 5.7 represents the isotherm.

$$c = \frac{q}{K_{SMA}} * \frac{n * c_S}{A - (v + n * \sigma) * q}^{\frac{v}{n}} \tag{5.7}$$

With c = protein concentration (mg/ml) for a given q = binding capacity (mg/ml), K_{SMA} = equilibrium constant for SMA model, A = ion exchange capacity of monovalent salt counter-ions (mmol/l), n = value of valence of salt counter-ions, c_S = salt counter-ion concentration in bulk phase (mmol/l), v = characteristic charge, σ = protein steric factor. The equation can be simplified by looking at the two limiting cases, concentration approaching zero (Equation 5.8) and concentrations approaching infinity (Equation 5.9).

$$\frac{q}{c} = K_{SMA} * \frac{A}{n * c_S}^{\frac{v}{n}} \tag{5.8}$$

$$q_{max} = \frac{A}{v + n * \sigma} \tag{5.9}$$

Parameters K_{SMA}, v and σ are estimated by making assumptions for A, n, C_S and q_{max} based on the experimental system.

Table 5.3: Overview of four protein adsorption models (Langmuir, Bi-Langmuir, Freundlich and Steric-mass action)

<table>
<tr>
<th>Langmuir</th>
<th>Bi-Langmuir</th>
</tr>
<tr>
<td>
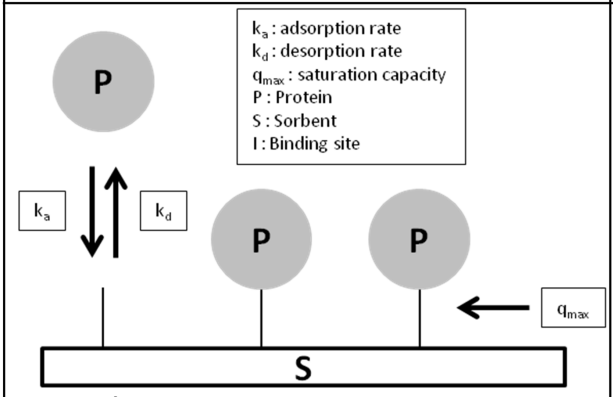

Assumptions:
❖ Monolayer coverage
❖ Binding sites are identical and independent
❖ Proteins are non-interacting
</td>
<td>
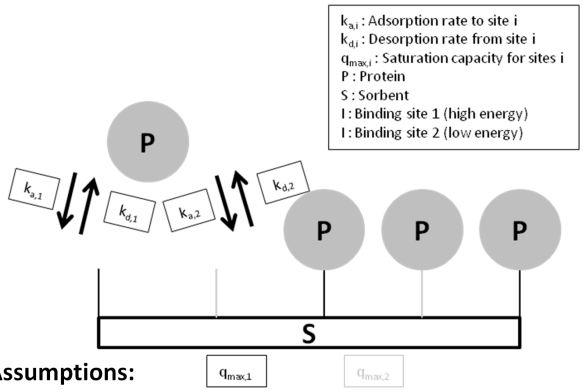

Assumptions:
❖ Monolayer coverage
❖ Two, energetically different, binding sites
❖ Proteins are non-interacting
</td>
</tr>
<tr>
<th>Freundlich</th>
<th>Steric-mass action</th>
</tr>
<tr>
<td>
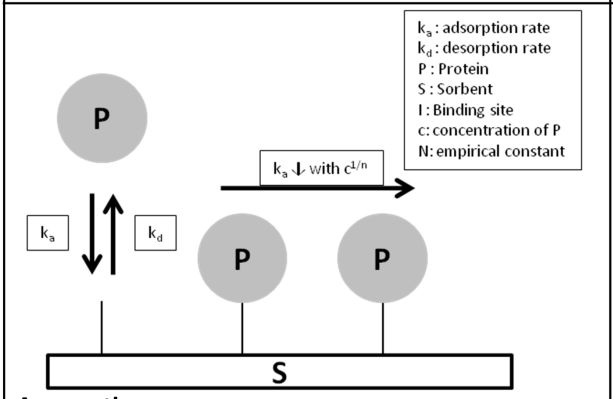

Assumptions:
❖ Bound proteins may change adsorption rate of subsequent proteins
❖ At low protein concentration similar to Langmuir
</td>
<td>
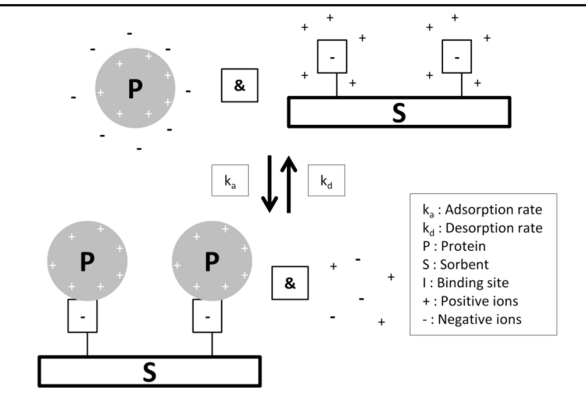

Assumptions:
❖ Accounts for steric shielding
❖ Includes effect of counter-ion concentration
❖ Considers size of proteins (uniform, spherical)
</td>
</tr>
</table>

Table 5.4: Experimental conditions for dynamic protein binding capacity determination

Step #	**Time (min)**	**Function**	**Solution**	**Flow rate (ml/min)**
I	10	Equilibration	Buffer pH 5[a]	1
II	50 (Natrix C) 30 (Sartobind S)	Binding	0.5g/l protein in buffer pH 5[a]	1
III	20	Washing	Buffer pH 5[a]	1
IV	20	Elution	Phosphate buffer pH 7	2

[a]Phosphate citrate buffer (lysozyme) and acetate buffer (IgG)

5.4.6 Dynamic Protein Binding Capacity

Dynamic protein binding experiments were performed with an AKTA Prime system (GE Healthcare, Sweden) equipped with UV detector (Figure 5.2). For IgG experiments, a 50 mM pH 5 acetate buffer and for lysozyme experiments, a pH 5 phosphate citrate buffer was used. Protein concentration in the binding solution was 0.5 g/l for both IgG and lysozyme. Elution conditions for IgG and lysozyme were 0.2 M pH 7 phosphate buffer with 1 M KCl. AKTA steps are summarized in Table 5.4.

Dynamic protein binding capacity was based on 10% breakthrough according to Equation 5.10.

$$q_{DBC10\%} = \frac{c_0 * V_{10\%}}{V_{membrane}} \tag{5.10}$$

Where $q_{DBC_{10\%}}$ is the dynamic protein binding capacity (mg protein/ml membrane) at 10% breakthrough, c_0 is the initial protein concentration in solution (mg/ml), $V_{10\%}$ is the volume of permeate collected at 10% breakthrough (ml) and $V_{membrane}$ is the calculated volume of the dry weight membrane weight (ml).

5.4.7 Scanning Electron Microscopy Imaging

Membrane pore structure was visualized by Field Emission Scanning Electron Microscopy (FESEM). Freeze dried (Epsilon 1-4 Freeze Dryer [Martin Christ, Germany]) membrane samples (prior equilibration in phosphate citrate buffer pH 5) were mounted on FESEM

sample stands, sputter coated with a fine layer of gold particles (FESEM gold coating unit Desk II, Denton Vacuum, USA) and images were acquired with the FESEM (Leo 1530, Carl Zeiss AG, Germany). The working parameters for the FESEM were 10 kV and secondary electron signal (SE2). The magnification was 5000 x and three images at different positions on the membrane sample were taken for each sample. Average pore size diameters were evaluated with Pore Image Processor, Matlab. Details of the image analysis are presented in Chapter 4.

5.4.8 Statistical Analysis

To determine if two data sets were significantly different from each other, the Student t-test was used assuming a two tailed distribution and a confidence level of 95% ($\alpha = 0.05$).

5.5 Results and Discussion

5.5.1 Protein Adsorption at Equilibrium

Significant differences in equilibrium protein binding profile were observed according to membrane material and protein type. For IgG and the Natrix C membrane, equilibrium protein binding capacity increased continuously with increasing protein concentration while for IgG and the Sartobind S membrane material, equilibrium protein binding capacity reached a maximum at approximately 1 mg/ml protein concentration and remained constant with increasing protein concentration (Figure 5.4). IgG binding capacity at the highest protein concentration investigated (4 mg/ml) was significantly higher (three fold) for the Natrix C membrane (125 mg/ml) compared to the Sartobind S membrane (40 mg/ml). The maximum protein binding capacity for IgG and Sartobind S is comparable to those reported in the literature, 19.5 mg/ml in 10 mM potassium phosphate buffer pH 7 [112]. There is no published protein binding capacity available for IgG and the Natrix C membrane.

The effect of protein type on protein binding capacity was obtained by comparing IgG binding to lysozyme binding with the Natrix C membrane. Protein binding capacity for lysozyme was at least twice that of IgG (Figure 5.4). The maximum protein binding capacity observed for lysozyme and Natrix C, 295 mg/ml, is significantly higher than reported values for lysozyme and Sartobind S, 130 mg/ml in pH 5 sodium acetate buffer (Gebauer et al. [49]).

These observations point to significant differences in material architecture and or functional groups density and access which will be discussed in the next section.

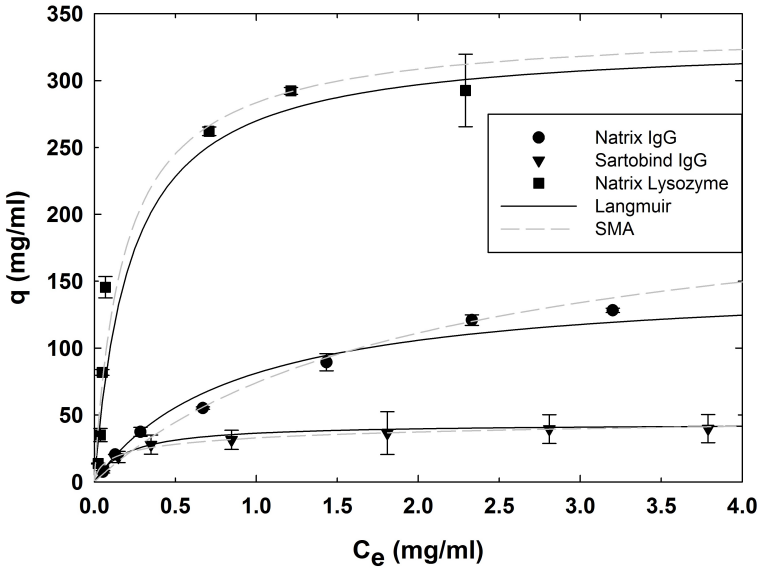

Figure 5.4: Isotherms (n=3) for Natrix C (IgG (•) and Lysozyme (□)) and Sartobind S (IgG (▽)) fitted with Langmuir model (black lines) and SMA model (grey lines). Error bars represent standard deviation.

Protein equilibrium binding was further investigated by comparing protein equilibrium estimated with four different adsorption models and their respective residual sum of squares (SSR) presented in Table 5.5. The highest SSR for all combinations of membrane and protein was obtained for the Freundlich model which indicates poor description of the experimental data. The Langmuir and bi-Langmuir model had relatively similar SSR which suggest that two different types of binding sites did not offer noteworthy improvement on the fit of the experimental data such that the bi-Langmuir model will not be further discussed. In contrast, differences for the fit of the experimental data were observed with the SMA model. (To solve the SMA model the following values were used: $A_{NatrixC} = 450$ mmol/l, $A_{SartobindS} = 900$ mmol/l, n = 1, $C_S = 100$ mmol/l and q_{max} was taken from the Langmuir model (Equation 5.4).) Higher SSR was observed for IgG binding and lysozyme binding with Natrix C and Sartobind S when comparing the Langmuir model to the SMA model. The Langmuir model is known to capture linear isotherms and situations where protein adsorption is not affected by the proteins already adsorbed whereas SMA model captures profound non-linear adsorption with protein adsorption increasing slowly with

increased protein concentration.

Table 5.5: Model parameters for isotherms

Langmuir	q_{max} (mg/ml)	K_L (ml/mg)			SSR
IgG-Natrix	186	0.7			75
IgG-Sartobind	41	5.5			8
Lysozyme-Natrix	319	7.0			4005
Bi-Langmuir	$q_{max,1}$ (mg/ml)	$K_{B,1}$ (ml/mg)	$q_{max,2}$ (mg/ml)	$K_{B,2}$ (ml/mg)	SSR
IgG-Natrix	202	0.4	20	7.6	70
IgG-Sartobind	39	5.5	2	5.5	8
Lysozyme-Natrix	300	7.0	19	7.0	4000
Freundlich		K_F (ml/mg)	n (-)		SSR
IgG-Natrix		71	1.8		166
IgG-Sartobind		30	4.0		60
Lysozyme-Natrix		249	2.8		$1.1*10^4$
Steric mass action		K_{SMA} (ml/mg)	v (-)	σ (-)	SSR
IgG-Natrix		64	0.3	3	0.06
IgG-Sartobind		12	1.3	19	0.27
Lysozyme-Natrix		513	0.8	0.6	0.55

Langmuir fitting showed lysozyme binding having a higher capacity than IgG binding to Natrix C membranes with 319 mg/ml and 186 mg/ml respectively. Membrane ligand could bind more of the smaller protein lysozyme. When comparing IgG binding to Natrix Weak C or Sartobind S, Natrix membranes showed a five times higher binding capacity. Langmuir affinity constant K_L describes the shape of the curve: the larger K_L, the higher the affinity between protein and membrane. In this study Natrix-IgG had the lowest affinity (0.7), both Sartobind-IgG and Natrix-Lysozyme were higher with 5.5 and 7.0 for Sartobind and Natrix respectively. Hence those two isotherm showed the typical, sharp Langmuir shape whereas Natrix-IgG isotherm showed a slow increase to the maximum. Similar values for q_{max} and K_L can be found in literature. Tatarova et al. [111] studied lysozyme binding to Sartobind S membranes and recorded 77.7 mg/ml and 8.3 ml/mg for q_{max} and K_L respectively.

Steric mass action model, assuming protein steric factor and characteristic charge, resulted in small SSR. The smallest steric factor of 0.6 was observed for the Natrix-Lysozyme isotherm since lysozyme is smaller than IgG. The steric factor increased drastically for IgG with 3 and 19 for Natrix C and Sartobind S respectively, reflecting the higher ligand density and hence more sterically hindered counter-ions for Sartobind S (compare 5.5.2. The characteristic charge v, representing the number of charges involved in the ion exchange reaction, was below 1.3. Studies showed that in ion exchange chromatography lysozyme has 3-5 charged amino acids that are predominantly involved in the interaction depending on the protein orientation [113]. No charge mapping for IgG in ion exchange chromatography is known to the authors.

Published protein isotherms fitted with the SMA model indicate a wide range of experimentation, parameters estimation methods and estimates and isotherm shapes. Chen et al. [34] investigated BSA binding with ion exchange resins and different buffers (acetate pH 5.5, phosphate pH 6.8 and Tris-HCl pH 7.4) and reported a broad range of parameters, 47-1712, 2.37-3.10 and 10.0-17.6 for K_{SMA}, v and σ respectively depending on the buffer type. In their study, the shape of the isotherm was affected by the salt counter-ions present in the buffer. Low salt concentration led to a sharp increase of the protein isotherm curve whereas higher salt concentration resulted in less pronounced isotherms. Francis et al. [48] indicated that the SMA model did not provide a good representation of ovalbumin binding on Mustang Q membranes at different feed flowrates.

As SSR are relatively high and fit of the experimental data at high protein concentration is limited for each of the Langmuir model and SMA model, mass transfer limitations may be present and affect the fit of the experimental data with the adsorption models.

5.5.2 Ion Transport – Access to Functional Groups

Ion transport characteristics according to membrane type and static and dynamic conditions were assessed from ion exchange capacity (IEC) (Table 5.6). IEC of Sartobind S was twice that of Natrix C (statistically significant, $\alpha = 0.05$) which is the opposite of the maximum equilibrium protein binding observed for IgG and these two membranes. Thus differences in ion exchange functional groups cannot explain the higher equilibrium protein binding observed for Natrix C. Estimated IEC are in agreement with values reported by the manufacturers and reported in literature for polyvinylchloride based membrane material grafted with anion or cation exchange groups, between 0.22 -2.8 meq/g [24, 25, 27, 29].

Experimental insights of the ion transport in the membrane were obtained by comparing IEC for intact (one 2x2 cm piece), cut (four pieces, 1x1 cm each) and crumble (smallest

pieces from a 2x2 cm piece) membranes. Static IEC increased significantly when comparing intact to cut or crumble format for each membrane type. Relatively similar IEC increase was observed when compared to the intact membrane, 30% and 68% increase for Natrix C and 20% and 59% IEC increase for Sartobind S membranes with decreasing membrane piece sizes. Membrane format influence on IEC was statistically significant ($\alpha = 0.05$) except between Sartobind S intact to cut. The importance of convective flow on IEC was significant. When comparing Natrix C dynamic to static IEC, dynamic IEC was more than doubled showing the positive influence of convective flow. Dynamic IEC with Sartobind S membranes did not yield a measureable equivalence point and needs further investigation.

Table 5.6: IEC (Average±Standard deviation (n=3)) of Natrix C and Sartobind S according to membrane format and operation mode

Mode	**Membrane Format**	**IEC (meq/g)**	
		Natrix Weak C	*Sartobind S*
Static	*Intact (2x2 cm)*	0.461±0.020*	0.956±0.063
	Cut (0.5x0.5 cm)	0.599±0.065*	1.147±0.148
	Crumble (pieces)	0.774±0.048*	1.517±0.109*
Dynamic	*Circular 25 mm diameter disc*	1.62±0.05	N/A

*Denotes statistically significant ($\alpha = 0.05$) influence of membrane format for given membrane type (static mode).

5.5.3 Protein Transport-Access Functional Groups

In the previous section, ion transport in the membranes was discussed. In this section, the focus is on protein transport. Proteins are significantly larger than ions and have not a single charge but a charge distribution; hence their interaction with the membrane material will be more complex and more hindered than ion transport. Differences in protein diffusion mass transport limitations were observed according to protein size, membrane format (intact versus crumble) and membrane type (Table 5.7).

Looking at intact membranes, significantly higher protein binding capacity was obtained for lysozyme compared to IgG. For the Natrix C membranes, lysozyme binding capacity increased 47% compared to IgG. For Sartobind S, lysozyme binding capacity increased 74% compared to IgG. These observations indicate that protein size and charge significantly influenced binding. IgG, a relatively large protein, may have limited access to the binding sites and/or is blocking neighbouring sites once attached while lysozyme, a

Table 5.7: Influence of protein type, membrane format, and membrane type on static and dynamic protein binding capacity q (Average±Standard deviation (n=3))

Protein	**Membrane Format**	**q (mg/ml)**			
		Natrix Weak C		***Sartobind S***	
		Static[a]	*Dynamic*[b]	*Static*[a]	*Dynamic*[b]
IgG	*Intact*	14.9±2.5	115.4±7.2$^{\dagger\diamond}$	13.1±3.1*	17.7±3.3
	Crumble	16.7±1.2	N/A	19.6±3.1*	N/A
Lysozyme	*Intact*	21.8±3.9*	151.3±6.1$^{\dagger\diamond}$	22.7±2.2*	24.6±5.9
	Crumble	38.9±6.9^{*+}	N/A	29.1±0.6^{*+}	N/A

[a]Binding conditions: pH 5, phosphate citrate buffer, c_0=0.5 mg/ml, t=5 h;
[b]binding conditions: pH 5, acetate buffer (IgG) or phosphate citrate buffer (Lysozyme), q_{DBC} at 10% breakthrough;
*significant difference ($\alpha = 0.05$) between membrane format for given protein and static conditions;
$^{+}$significant difference ($\alpha = 0.05$) between membrane type for given protein, membrane format and static conditions;
†significant difference ($\alpha = 0.05$) between protein type for dynamic mode;
$^{\diamond}$significant difference ($\alpha = 0.05$) between static and dynamic mode for given membrane type and protein.

smaller protein, may have easier access and limited blocking effect leading to higher binding capacities. In contrast, different protein binding capacity was observed when comparing intact and crumble membrane for a given combination of protein and membrane type. A statistically significant influence ($\alpha = 0.05$) was observed between membrane format except for Natrix C and IgG. Highest protein binding capacity increase from intact to crumble was with Natrix C and lysozyme with 78% protein binding capacity improvement. For Sartobind S, statistically significantly higher protein binding capacity was observed for IgG and lysozyme, 50% increase for IgG and 28% increase for lysozyme. The differences in protein binding according to membrane format indicate internal protein diffusion limitations for all protein and membrane combinations except IgG and Natrix C. Transport and binding mechanisms appear to be different for IgG compared to lysozyme in Natrix C. For the Natrix C crumble format, the increase from IgG to lysozyme binding was more than twofold. For Sartobind S crumble format the increase in binding capacity for IgG compared to lysozyme was close to 50%. The increased binding capacity due to format could be related to the increased surface area or the improved 3D density arrangement of

material ligands.

Membrane pore size distributions are very important when considering dynamic modes. Materials with small pores might have increased system back pressure or broader peaks but material with larger pores (¿ 1 μm) might be limited in their separation capacity as well due to the protein travel time to the pore wall for adsorption being greater than their total residence time within the membrane [114]. Natrix C and Sartobind S membranes have significantly different average pore sizes with 0.3 and ¿ 3 μm respectively (Table 5.1). Significant enhancement of protein binding capacity was obtained for the Natrix C material when convective flow was introduced in the dynamic operation (Table 5.7). Dynamic protein binding capacity was up to ten times higher than static protein binding capacity and nearly the equilibrium binding capacity for IgG and Natrix C (77%, Figure 5.4). For lysozyme and Natrix C, the dynamic protein binding was approximately seven times higher than the static binding capacity and approximately 46% of the equilibrium binding capacity (330 mg/ml, Figure 5.4). Natrix C average pores were 7-14 times larger compared to IgG and 35-60 times larger than lysozyme. Therefore protein size as well as charge played a role as shown by the significantly higher enhancement of the IgG versus lysozyme binding capacity which reflects differences in transport and binding mechanisms. In contrast, negligible (no statistical significance) enhancement of protein binding capacity was observed for the Sartobind S material when convective flow was introduced (Table 5.7) and dynamic binding capacity remained below the equilibrium protein binding capacity (42%) for IgG (44 mg/ml, Figure 5.4). Sartobind S pore size is over 100x larger than IgG and even though Sartobind S membranes showed a higher IEC than Natrix C, protein binding capacity did not reflect IEC differences. Ligand density is not the only factor influencing maximum protein binding capacity, protein size, charge and material architecture, especially pore size, need to be considered. The observed DBC are of the same order of magnitude as those reported by the manufacturer. IgG binding to Natrix C was given as 100 mg/ml (compare 115 mg/ml this study) and 25 mg/ml lysozyme binding to Sartobind S (compare 24.6 mg/ml this study).

5.5.4 Transport Limitations

As protein capture by ion exchange involves ion displacement during protein adsorption, the presence of ion mass transfer limitations as shown by differences in IEC of intact and crumble membrane will affect protein adsorption. The ion mass transfer limitations (Table 5.6) are not linearly related to the differences in protein binding capacity (Table 5.7) for intact and crumble membranes. This non-linear relationship indicates that protein size and charge characteristics and material porosity may have an important role in protein

adsorption. The pore structure visualized by FESEM can be seen in Figure 5.5. Natrix C shows a dense hydrogel, with an average pore size of 0.458 μm (Figure 5.5 A). Sartobind S shows larger open pores with an average pore size of 0.890 μm (Figure 5.5 B). When ions travel in the material and are exchanged with the functional groups of the membranes, changes in pH (measured during static mode) or changes in conductivity (measured during dynamic mode) can be observed. The number of functional groups will determine the amount of exchanged ions (IEC); pore structure will determine the speed of ions travelling to the functional groups of the membrane. Wang et al. [20] investigated lysozyme binding patterns to Sartobind S membranes with CLSM (Confocal Laser Scanning Microscopy). The binding pattern was similar to pore morphology and lysozyme predominantly bound to the functional layer rather than the cellulose support of the membrane.

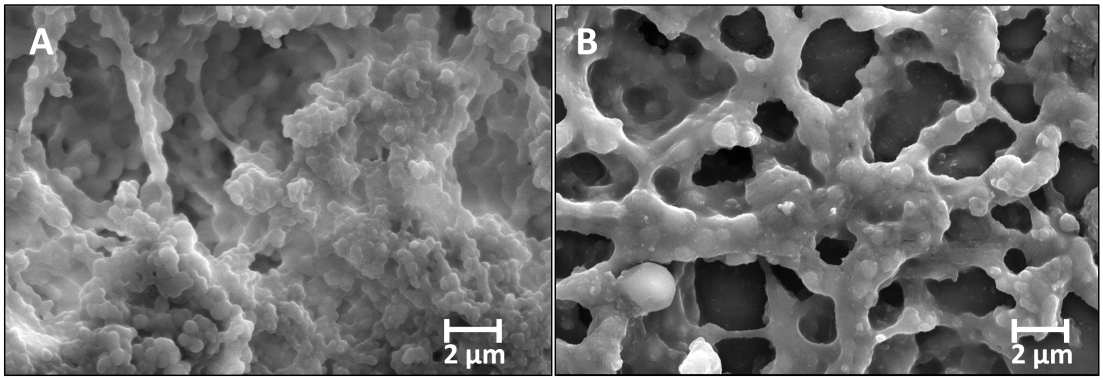

Figure 5.5: FESEM image (5000x magnification) of Natrix Weak C (A) and Sartobind S (B) membrane

The convective flow introduced in the dynamic operation affected IEC (Table 5.6) differently than protein binding capacity (Table 5.7). Since IEC and protein static and dynamic binding capacity increased differently according to membrane type when its architecture was disrupted (intact and crumble format), internal protein transport within macroporous hydrogels or 3D functional membrane materials for commercial cation exchange membranes is present. Based on these experimental observations, a schematic representation of the mass transport phenomena specific to each membrane material pore structure and ion exchange characteristics (Figure 5.6) was developed and includes internal diffusion in addition to bulk convection and film diffusion.

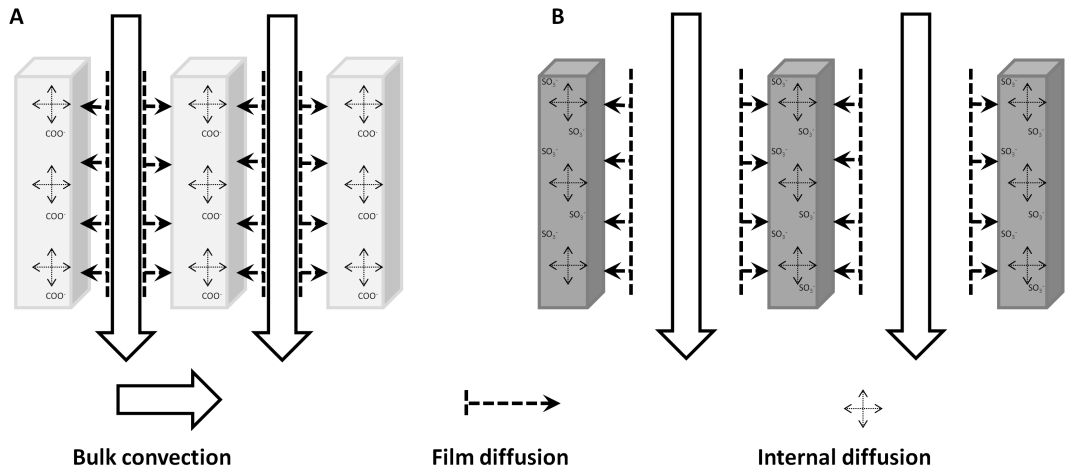

Figure 5.6: Mass transfer in (A) weak cation exchange membranes with narrow pores and low IEC (light grey) and in (B) strong cation exchange membranes with open pores and high IEC (dark grey).

5.6 Conclusions

This study provided insights on mass transfer limitations for two commercial cation exchange membranes with different architecture. Protein binding and ion exchange capacity were examined and related to protein type, membrane material architecture and format. When comparing protein binding capacity, the smaller protein lysozyme always showed higher binding capacity than the larger IgG, confirming binding capacity were not only limited by the ligand density but also by the bound protein and the space occupied by the bound proteins. Protein isotherms showed best fit with the Langmuir model for Sartobind S membranes and the SMA model for Natrix C membranes. None of the models however could describe all regions of the isotherms sufficiently. Membrane format influenced binding, with more accessible binding sites in smaller membrane formats. In the dynamic mode the Natrix C membrane showed superior protein binding than the Sartobind S membrane.

Analysis of ion exchange capacity (IEC) showed that Sartobind S had twice the ligand density compared to Natrix C membranes. By comparing intact, cut and crumble membrane formats, IEC increased significantly for both membrane types with smaller membrane pieces showing the limited ion accessibility for larger membrane pieces and internal diffusion needs to reach maximal capacities. FESEM imaging showed differences between the

two materials, pore filled hydrogel versus surface grafted groups, leading to different pore sizes. Mass transport limitations however were observed in both materials proving that these limitations go beyond visual structure and involve ion binding capacities and protein characteristics. Convective mass transfer limitations were also identified and could be somewhat or totally removed when operating in dynamic mode. Further work is required to investigate these differences at the microscopic level and relate these to pH and ionic conditions.

5.7 Acknowledgements

Financial support from the Monoclonal Antibody Network (MabNet) of the Natural Sciences and Engineering Research Council (NSERC) is acknowledged. The authors would like to thank Marc Aucoin (University of Waterloo) for the access to the AKTA prime system, Nina Heinig at the University of Waterloo for help with the Field Emission Scanning Electron Microscopy and Kayleigh Kuindersma for the development of the dynamic IEC determination.

Chapter 6

Potential of weak cation exchange membranes for the recovery of large proteins and antibodies

6.1 Introduction

The overall objective of this PhD project was to evaluate the potential of Natrix Weak C membranes for the capture of large proteins and antibodies as an alternative to Protein-A resins. The findings of this study are promising; however some questions were left unanswered and will be kept for future work.

The predominant interaction when purifying proteins with composite ion exchange membranes is based on electrostatic attraction and repulsion. However hydrophobic interaction might play a role as well when the support layer of the membrane has hydrophobic tendencies and is not fully covered by the ion exchange hydrogel. Further impacts on the purification may be due to material characteristics (pore size, surface charge, swelling potential), protein characteristics (size, surface charge) and cell culture characteristics (mAb concentration, impurities).

6.2 Influence of Protein and Membrane Characteristics on Purification Behaviour

Hydrophobicity was a concern to the author since the hydrophobic backbone of the material was exposed in some FESEM pictures resulting in a potential addition of hydrophobic interaction beyond cation exchange. Hydrophobic tendencies of antibodies were evaluated with the fluorescence probe ANS. Smallest hydrophobicity numbers were found for IgG and EG2 at pH 7. pH 7 was determined to be the optimal pH for eluting IgG. Furthermore zeta potential measurements showed that at pH 7 the surface charge was highly negative (-40 mV zeta potential) whereas the hydrophobicity of the membrane was again very small. Therefore at high pH, hydrophobicity of proteins and material could be neglected, electrostatic interactions were predominant. Surface charge of IgG, known from its pI above pH 7, was slightly positive at pH 7 and strongly positive at pH 5. pH 5 was determined to be the optimal pH to encourage interaction between the membrane and IgG. At this pH, hydrophobicity of IgG increased twofold compared to pH 7, EG2's hydrophobicity increased four times, hydrophobicity of the material increased by 50%. Even though the proteins' hydrophobicity increased significantly, their positive overall charge coupled with ANS being an anionic dye does not exclude interaction beyond hydrophobic behavior. By using ANS, the study could not achieve decoupling of hydrophobicity and electrostatic interaction. Furthermore the change of material hydrophobicity was small, hence hydrophobicity could also be neglected at low pH, and binding was predominantly determined by the material's zeta potential close to zero and the protein's highly positive overall charge. Concerns of the membrane's base material influencing binding and elution could not be confirmed.

Membrane swelling potential and pore size showed the same trend, increasing values with increasing pH. Lowest pore size of 260 nm at pH 4.5, 1 M KCl, was still ten times larger than IgG (dimensions: 21.9x15.5x1.5 nm), assuring an unhindered passing of the protein through the membrane. Dimension changes of the protein with changing conditions cannot be neglected and should be part of future investigations.

Mass transfer limitations of Natrix Weak C were investigated. Although it was shown that these limitations were present, they could be somewhat removed in the dynamic mode where its open pore structure showed superior behaviour over resins and other commercially available membranes with a 6.5 times higher dynamic binding capacity.

6.3 Influence of Cell Culture Characteristics on Purification Behaviour

An important characteristic moving from production to purification of antibodies is the concentration of mAbs. Increasing titres (≥ 5 g/l) have been observed over the last decades to meet the increasing need of mAb therapeutics. This benefit in upstream improvements however does not translate to benefits in downstream, especially for purifications with resins since their usage is limited by the mass of product to be purified and not the volume [15]. Another characteristic is the quantity of mAb relative to other host cell proteins (HCP). Tait et al. [115] found that less than 20% of total proteins are HCP due to the modifications and improvements done to cell line and cultivation to focus predominantly on mAb production. An increase in impurities would be problematic when considering an alternative purification principle. The Protein-A affinity ligand binds mAbs only whereas cation exchange ligands might interact with mAbs as well as HCP.

6.4 Comparison of Cation Exchange Membranes to Cation Exchange and Protein-A Resins

Table 6.1 is comparing Protein-A and cation exchange resins with cation exchange membranes. The most distinct difference and advantage of cation exchange membranes is its high DBC for IgG with 115 mg/ml compared to 80 mg/ml (cation exchange resins) and 30 mg/ml (Protein-A resins). Yields are comparable for all systems. A crucial factor of antibodies is their purity which is highest with Protein-A resins and explains it predominant use over the years. Some cation exchange resins however have been reported to yield purities of up to 95% which is promising. The purity for Natrix weak C membranes need to be determined, however Suck et al. [116] tested Vivapure IEX spin columns and obtained high purities in a one step purification of an enzyme. Another factor that needs to be pursued further is the volume or annual throughput. So far NatriX C membranes have been used on a laboratory scale (< 1 ml). A serious scale up investigation and testing is needed in order to reach comparable volumes of 10 000 l. Savings however could be substantial once a successful scale up is performed. The company (Natrix Separations) is predicting a 60% cost decrease for the capture step.

Therefore membrane chromatography is superior to resin chromatography in some areas especially when dealing with large proteins and high concentrations. Purity and scale up potential needs to be evaluated for Natrix C membranes before drawing a final conclusion

Table 6.1: Comparison of Natrix Weak C cation exchange membrane to cation exchange and Protein-A resins

	Protein-A Affinity Resin	**Cation Exchange Resin**	**Cation Exchange Membrane (Natrix C)**
$DBC_{IgG,10\%}$ (mg/ml)	$\sim$30[a]	$\sim$80[d]	$\sim$115[g]
Yield (%)	95[b]	95[e]	> 95[g]
Purity (%)	> 98[b]	95[f]	TBD
Time (h)	12[c]	Similar to Protein-A	< 3[g]
Lifetime	200 cycles[c]	Similar to Protein-A	1 use disposable unit[h]
Facility cost (Mm $)	50-300[c]	-	60% decrease in capture step[h]
Throughput (kg/a)	100 - 4 000[c]	-	TBD
Adsorber volume	$>$ 10 000 l[c]	$>$ 10 000 l[c]	$<$ 1 ml (scale up needed)[h]

[a] [117], [b] [118], [c] [119], [d] [85], [e] [120], [f] [121], [g]This study, [h]Manufacturer information

on replacing Protein-A as first capture step. A one step purification with cation exchange membranes will most likely not yield comparable purities therefore an orthogonal sequence of membranes should be envisioned and investigated as a replacement for Protein-A.

6.5 Conclusion

Every purification technology should have a high throughput, high yields and purities as well as produce stable biomolecules at a high speed, with accuracy, reliability and minimal cross-contamination. From this work there are further specific characteristics to consider for future cation exchange membrane development:

- Is the membrane a composite material, if so are there potential interactions from the base material?
- What is the charge profile of the membrane (pKa), determining the potential and limits of purifying different proteins (with different pI)?

- What is the pore size distribution of the material and will the proteins be able to pass unhindered?
- What are static and dynamic binding capacities compared to other commercial products?
- What is the purity of a protein mixture in a one step/orthogonal capture?

Overall, Natrix Weak C membranes are a promising alternative to Protein-A resins for capturing large proteins and antibodies. This thesis showed their superiority to other commercially available membranes with a 6.5 times higher dynamic binding capacity and a 1.5 times higher capacity compared to cation exchange resins found in literature. Two comparison factors remain for investigation: purity and scale up potential.

Chapter 7

Conclusions and Recommendations

The research presented in this thesis focused on the characterization of (1) hydrophobicity of proteins, (2) a weak cation exchange macroporous hydrogel membrane and (3) protein capture by cation exchange membranes.

The first objective was to analyse protein hydrophobicity according to pH and ionic strength (Chapter 3). Fluorescence intensity of proteins with ANS probe is widely used in literature but so far no comparison between studies has been done. To compare results from different studies a standardization step was suggested. This thesis further showed the possibility of expanding the protein concentration range beyond linear range by using the Scott plot (a single reciprocal plot) to evaluate hydrophobicity for proteins. Optimal excitation/emission fluorescence intensity for ANS and BSA were investigated and determined to be 390 nm/470 nm excitation/emission. At pH values close to the isoelectric point of BSA, the hydrophobicity index was lowest and increased with pH further away from the pI. Ion content in the buffer system had a stabilizing effect on the proteins and led to a slightly higher hydrophobicity index. The ANS test was expanded to IgG as polyclonal antibody and EG2 as monoclonal antibody. Results indicated that pH had statistically significant influence on all proteins. The order of magnitude of the hydrophobicity index (H) in the majority of cases was $H_{BSA} > H_{EG2} > H_{IgG}$. The polyclonal antibody IgG showed low fluorescence intensity suggested to be caused by its different Fab sequences resulting in different interactions with ANS. EG2, which has Fc sequences similar to IgG but different Fab sequences, showed a stronger signal. With this knowledge one can postulate that IgG and EG2 at pH 5 will interact with membrane materials via hydrophobic interactions in addition to electrostatic interactions, hence purification conditions close to pH 5 will favor binding. At pH 7, hydrophobicity interaction will be reduced and will favor elution.

The second objective was to characterize a weak cation exchange membrane material by analysing surface charge, swelling behaviour, hydrophobicity, pore size (Chapter 4) and ion exchange capacity (Chapter 5). Membrane surface charge at pH 5 was close to 0 mV which is coherent with the reported pKa of the membrane. With increasing pH, membrane surface charge increased as well. Pore size (analysed with FESEM in combination with freeze-drying to preserve porous structure of the hydrated membranes) and membrane swelling were low at pH 5 and high at pH 7. Membrane hydrophobicity showed an opposite trend with high values at low pH and low values with increasing pH. Membrane surface charge, pore size and hydrophobicity results support binding at pH 5 and elution at pH 7. With decreasing membrane format/increasing surface area, the IEC of Natix C increased significantly revealing mass transfer limitations.

The third objective was to characterize membrane protein interaction. This was achieved by investigating static protein binding and elution conditions (Chapter 4), dynamic protein binding capacity and by modelling protein adsorption (Chapter 5). As the previous findings suggested, highest protein binding was at low pH (pH 5) and low ionic strength. Elution was highest at pH 7 and high ionic strength (1 M). Different adsorption models (Langmuir, Bi-Langmuir, Freundlich and Steric-mass action) were used to describe binding isotherms. However none of the models could describe protein adsorption over the complete range of concentration. This implied that there were mass transport limitations present which the models were not able to capture. To assess these limitations, protein binding for membrane materials with different formats was assessed. Membrane format influenced binding, with more accessible binding sites in smaller membrane formats. When comparing protein binding capacity, the smaller protein lysozyme always showed higher binding capacity than the larger IgG, confirming binding capacities are not only limited by the ligand density but also by the size of the protein and the space it occupies. The dynamic mode operation showed increased protein binding capacity compared to static conditions supporting the presence of mass transfer limitations. Buffer conditions for IgG however needed to be adjusted showing the importance of protein stability in the dynamic mode and should be investigated further.

The results presented in this work led to the formulation of the following recommendations for future work on protein capture by cation exchange membrane chromatography:

1. **Further analysis of mass transfer for Natrix C membrane material**
   Mass transfer limitations for this membrane material were identified. Protein isotherms, gained in static mode, gave a first insight into binding behaviour. It is proposed to move to a dynamic set-up with varying flow rates to expand on the grasp of protein adsorption and mass transfer behaviour.

2. **Influence of pH and ion type on protein adsorption**
   When moving from the static to the dynamic mode, pH and ionic strength conditions from the static mode were applied to the dynamic mode. The effect of pH, ionic strength, flow rate and buffer type for protein binding and elution in the dynamic mode should be investigated to determine highest recovery for the respective protein.

3. **Influence of mAb glycoforms on their capture and recovery**
   So far model proteins, lysozyme and IgG, have been used in the dynamic mode. It is suggested to expand this to monoclonal antibodies with different glycoforms such as those produced by MabNet. The capture of these antibodies with cation exchange membranes could be evaluated to assess the effect of glycoform pattern on their binding and/or recovery.

4. **Protein binding visualization**
   Visualization of interaction between proteins and membrane has been done on a macroscopic level. It is therefore not yet clear which parts of the proteins are interacting with the membrane. An evaluation on microscopic level is recommended. Protein binding visualization could be done by confocal laser scanning microscopy (CLSM), charge mapping or protein crystallization with X-ray analysis. This would give more insight in the type of binding and could lead to further purification optimization.

References

[1] MJ Espiritu, AC Collier, and JP Bingham. A 21st-century approach to age-old problems: the ascension of biologics in clinical therapeutics. *Drug discovery today*, 19(8):1109–1113, 2014.

[2] JK Ryu, HS Kim, and DH Nam. Current status and perspectives of biopharmaceutical drugs. *Biotechnology and Bioprocess Engineering*, 17(5):900–911, 2012.

[3] JG Elvin, RG Couston, and CF van der Walle. Therapeutic antibodies: Market considerations, disease targets and bioprocessing. *International journal of pharmaceutics*, 440(1):83–98, 2013.

[4] S Hober, K Nord, and M Linhult. Protein a chromatography for antibody purification. *Journal of Chromatography B-Analytical Technologies in the Biomedical and Life Sciences*, 848(1):40–47, 2007.

[5] *Immunobiology : the immune system in health and disease*. Garland Pub, New York, 2001.

[6] R Jefferis. Antibody therapeutics: isotype and glycoform selection. *Expert Opinion on Biological Therapy*, 7(9):1401–1413, 2007.

[7] *Molecular biology of the cell*. Garland Science, New York, 2002.

[8] G Kohler and C Milstein. Continuous cultures of fused cells secreting antibody of predefined specificity. *Nature*, 256(5517):495–497, 1975.

[9] A Bell, ZJ Wang, M Arbabi-Ghahroudi, TA Chang, Y Durocher, U Trojahn, J Baardsnes, ML Jaramillo, S Li, TN Baral, M O'Connor-McCourt, R MacKenzie, and J Zhang. Differential tumor-targeting abilities of three single-domain antibody formats. *Cancer letters*, 289(1):81–90, 2010.

[10] JR Birch and AJ Racher. Antibody production. *Advanced Drug Delivery Reviews*, 58(5-6):671–685, 2006.

[11] J Zhang. *Mammalian Cell Culture for Biopharmaceutical Production*. Manual of Industrial Microbiology and Biotechnology. 2010.

[12] B Kelley. Industrialization of mab production technology the bioprocessing industry at a crossroads. *Mabs*, 1(5):443–452, 2009.

[13] M Butler and A Meneses-Acosta. Recent advances in technology supporting biopharmaceutical production from mammalian cells. *Applied Microbiology and Biotechnology*, 96(4):885–894, 2012.

[14] YH Wan, S Vasan, R Ghosh, G Hale, and ZF Cui. Separation of monoclonal antibody alemtuzumab monomer and dimers using ultrafiltration. *Biotechnology and bioengineering*, 90(4):422–432, 2005.

[15] D Low, R O'Leary, and NS Pujar. Future of antibody purification. *Journal of Chromatography B-Analytical Technologies in the Biomedical and Life Sciences*, 848(1):48–63, 2007.

[16] Handbook. *Affinity Chromatography-Principles and Methods*. Amersham Biosciences, 2002.

[17] A Arouri, P Garidel, W Kliche, and A Blume. Hydrophobic interactions are the driving force for the binding of peptide mimotopes and staphylococcal protein a to recombinant human igg1. *European Biophysics Journal with Biophysics Letters*, 36(6):647–660, 2007.

[18] B Huang, FF Liu, XY Dong, and Y Sun. pages pp.4168–4176. Molecular mechanism of the affinity interactions between protein A and human IgG1 revealed by molecular simulations. The Journal of Physical Chemistry B, 2011.

[19] JM Walker. *The Protein Protocols Handbook*. Humana Press, 2009.

[20] M Holtzhauer. *Basic methods for the biochemical lab*. Springer, Berlin ; New York, 2006.

[21] P Kumpalme and S Ghose. pages pp.225–276. Chromatography: The High-Resolution Technique for Protein Separation. R. Hatti-Kaul and B. Matthiasson (Ed.), Isolation and Purification of Proteins, 2003.

[22] JF Kramarczyk, BD Kelley, and JL Coffman. High-throughput screening of chromatographic separations: Ii. hydrophobic interaction. *Biotechnology and bioengineering*, 100(4):707–720, 2008.

[23] Handbook. *Ion Exchange Chromatography - Principles and Methods*. Amersham Biosciences, 1999.

[24] SM Hosseini, SS Madaeni, AR Heidari, and AR Khodabakhshi. Preparation and characterization of poly (vinyl chloride)-blend-poly (carbonate) heterogeneous cation exchange membrane: Investigation of solvent type and ratio effects. *Desalination*, 285:253–262, 2012.

[25] N Gizli, S Cinarli, and M Demircioglu. Characterization of poly(vinylchloride) (pvc) based cation exchange membranes prepared with ionic liquid. *Separation and Purification Technology*, 97:96–107, 2012.

[26] GS Gohil, VK Shahi, and R Rangarajan. Comparative studies on electrochemical characterization of homogeneous and heterogeneous type of ion-exchange membranes. *Journal of Membrane Science*, 240(1-2):211–219, 2004.

[27] PV Vyas, P Ray, GS Trivedi, SK Adhikary, and R Rangarajan. Studies on exchange equilibria of cations between cation-exchange membranes and electrolytic solutions. *Journal of colloid and interface science*, 246(2):366–371, 2002.

[28] J Cheng, Yi Li, TS Chung, SB Chen, and WB Krantz. High-performance protein separation by ion exchange membrane partitioned free-flow isoelectric focusing system. *Chemical Engineering Science*, 63(8):2241–2251, 2008.

[29] RK Nagarale, GS Gohil, VK Shahi, and R Rangarajan. Preparation and electrochemical characterizations of cation-exchange membranes with different functional groups. *Colloids and Surfaces A-Physicochemical and Engineering Aspects*, 251(1-3):133–140, 2004.

[30] XF Li, Z Wang, H Lu, CJ Zhao, H Na, and C Zhao. Electrochemical properties of sulfonated peek used for ion exchange membranes. *Journal of Membrane Science*, 254(1-2):147–155, 2005.

[31] S Brunauer, LS Deming, WE Deming, and E Teller. On a theory of the van der waals adsorption of gases. *Journal of the American Chemical Society*, 62:1723–1732, 1940.

[32] AM Katti and GA Guichon. Fundamentals of nonlinear chromatography - prediction of experimental profiles and band separation. *Advances in Chromatography*, 31:1–118, 1992.

[33] H Yang and MR Etzel. *Evaluation of Three Kinetic Equations in Models of Protein Purification Using Ion Exchange Membranes*. Ind. Eng. Chem. Res., 2003.

[34] WD Chen, HH Hu, and YD Wang. Analysis of steric mass-action model for protein adsorption equilibrium onto porous anion-exchange adsorbent. *Chemical Engineering Science*, 61(21):7068–7076, 2006.

[35] DS Ballantine, RM White, AJ Ricco, GC Frye, ET Zellars, and H Wohltjen. *Acoustic Wave Sensors - Theory, Design, and Physico-Chemical Applications*. Elsevier, 2007.

[36] A Stein and A Kiesewetter. Cation exchange chromatography in antibody purification: ph screening for optimised binding and hcp removal. *Journal of Chromatography B-Analytical Technologies in the Biomedical and Life Sciences*, 848(1):151–158, 2007.

[37] R Ghosh. Protein separation using membrane chromatography: opportunities and challenges. *Journal of Chromatography a*, 952(1-2):13–27, 2002.

[38] I Sellick. pages pp: 50–52. Capturing Large Biomolecules with Membrane Chromatography. Innovations in Pharmaceutical Technology, 2006.

[39] V Orr, L Zhong, M Moo-Young, and CP Chou. Recent advances in bioprocessing application of membrane chromatography. *Biotechnology Advances*, 31(4):450–465, 2013.

[40] A Staby, R Holm Jensen, M Bensch, J Hubbuch, DL Dunweber, J Krarup, J Nielsen, M Lund, S Kidal, T Budde Hansen, and I Holm Jensen. Comparison of chromatographic ion-exchange resins vi. weak anion-exchange resins. *Journal of Chromatography a*, 1164(1-2):82–94, 2007.

[41] TR McCaw, EK Koepf, and L Conley. Evaluation of a novel methacrylate-based protein a resin for the purification of immunoglobulins and fc-fusion proteins. *Biotechnology progress*, 30(5):1125–1136, 2014.

[42] S Frischer-Fruehholz. Sartobind (r): The high speed membrane chromatography. Technical report, Sartorius, 2006.

[43] C Boi. Membrane adsorbers as purification tools for monoclonal antibody purification. *Journal of Chromatography B-Analytical Technologies in the Biomedical and Life Sciences*, 848(1):19–27, 2007.

[44] SH Kim and CC Chu. Pore structure analysis of swollen dextran-methacrylate hydrogels by sem and mercury intrusion porosimetry. *Journal of Biomedical Materials Research*, 53(3):258–266, 2000.

[45] LC Dong, AS Hoffman, and Q Yan. Dextran permeation through poly(n-isopropylacrylamide) hydrogels. *Journal of Biomaterials Science-Polymer Edition*, 5(5):473–484, 1994.

[46] AM Lenhoff. Protein adsorption and transport in polymer-functionalized ion-exchangers. *Journal of Chromatography a*, 1218(49):8748–8759, 2011.

[47] J Wang, F Dismer, J Hubbuch, and M Ulbricht. Detailed analysis of membrane adsorber pore structure and protein binding by advanced microscopy. *Journal of Membrane Science*, 320(1-2):456–467, 2008.

[48] P Francis, E von Lieres, and C Haynes. Zonal rate model for stacked membrane chromatography part ii: Characterizing ion-exchange membrane chromatography under protein retention conditions. *Biotechnology and bioengineering*, 109(3):615–629, 2012.

[49] KH Gebauer, J Thommes, and MR Kula. Breakthrough performance of high-capacity membrane adsorbers in protein chromatography. *Chemical Engineering Science*, 52(3):405–419, 1997.

[50] P van Beijeren, P Kreis, and T Zeiner. Ion exchange membrane adsorption of bovine serum albumin-impact of operating and buffer conditions on breakthrough curves. *Journal of Membrane Science*, 415:568–576, 2012.

[51] P van Beijeren, Pr Kreis, and T Zeiner. Development of a generic process model for membrane adsorption. *Computers & Chemical Engineering*, 53:86–101, 2013.

[52] EE Meyer, KJ Rosenberg, and J Israelachvili. Recent progress in understanding hydrophobic interactions. *Proceedings of the National Academy of Sciences of the United States of America*, 103(43):15739–15746, 2006.

[53] J Kyte and RF Doolittle. A simple method for displaying the hydropathic character of a protein. *Journal of Molecular Biology*, 157(1):105–132, 1982.

[54] CA Haskard and ECY Li-Chan. Hydrophobicity of bovine serum albumin and ovalbumin determined using uncharged (prodan) and anionic (ans(-)) fluorescent probes. *Journal of Agricultural and Food Chemistry*, 46(7):2671–2677, 1998.

[55] P Gagnon. Technology trends in antibody purification. *Journal of Chromatography A*, 1221:57–70, 2012.

[56] N Alizadeh-Pasdar and ECY Li-Chan. Comparison of protein surface hydrophobicity measured at various ph values using three different fluorescent probes. *Journal of Agricultural and Food Chemistry*, 48(2):328–334, 2000.

[57] M Cardamone and NK Puri. Spectrofluorometric assessment of the surface hydrophobicity of proteins. *Biochemical Journal*, 282:589–593, 1992.

[58] DI Cattoni, SB Kaufman, and FL Gonzalez Flecha. Kinetics and thermodynamics of the interaction of 1-anilino-naphthalene-8-sulfonate with proteins. *Biochimica Et Biophysica Acta-Proteins and Proteomics*, 1794(11):1700–1708, 2009.

[59] D Matulis and R Lovrien. 1-anilino-8-naphthalene sulfonate anion-protein binding depends primarily on ion pair formation. *Biophysical journal*, 74(1):422–429, 1998.

[60] DM Togashi and AG Ryder. A fluorescence analysis of ans bound to bovine serum albumin: Binding properties revisited by using energy transfer. *Journal of Fluorescence*, 18(2):519–526, 2008.

[61] G Weber and LB Young. Fragmentation of bovine serum albumin by pepsin .1. origin of acid expansion of albumin molecule. *Journal of Biological Chemistry*, 239(5):1415–1423, 1964.

[62] XY Mao, PS Tong, S Gualco, and S Vink. Effect of nacl addition during diafiltration on the solubility, hydrophobicity, and disulfide bonds of 80% milk protein concentrate powder. *Journal of dairy science*, 95(7):3481–3488, 2012.

[63] F Moreno, M Cortijo, and J Gonzalez-Jimenez. The fluorescent probe prodan characterizes the warfarin binding site on human serum albumin. *Photochemistry and photobiology*, 69(1):8–15, 1999.

[64] A Kato and S Nakai. Hydrophobicity determined by a fluorescence probe method and its correlation with surface-properties of proteins. *Biochimica et biophysica acta*, 624(1):13–20, 1980.

[65] RB Martin. Disadvantages of double reciprocal plots. *Journal of chemical education*, 74(10):1238–1240, 1997.

[66] CJ Taves, A Kusumi, and JL Winkelhake. Human aglycosyl-igg exhibits increased hydrophobicity binding fluorescence studies with 8-anilinonaphthalene-1-sulfonic acid (ans). *Biochemical and biophysical research communications*, 124(2):605–613, 1984.

[67] CW Parker and CK Osterlan. Hydrophobic binding sites on immunoglobulins. *Biochemistry*, 9(5):1074–1082, 1970.

[68] T Rispens, CMM Lakemond, NIL Derksen, and RC Aalberse. Detection of conformational changes in immunoglobulin g using isothermal titration calorimetry with low-molecular-weight probes. *Analytical Biochemistry*, 380(2):303–309, 2008.

[69] S Determann, JM Lobbes, R Reuter, and J Rullkotter. Ultraviolet fluorescence excitation and emission spectroscopy of marine algae and bacteria. *Marine Chemistry*, 62(1-2):137–156, 1998.

[70] S Salgin, U Salgin, and S Bahadir. Zeta potentials and isoelectric points of biomolecules: The effects of ion types and ionic strengths. *International Journal of Electrochemical Science*, 7(12):12404–12414, 2012.

[71] K Takeda, A Wada, K Yamamoto, Y Moriyama, and K Aaki. Conformational change of bovine serum-albumin by heat-treatment. *Journal of protein chemistry*, 8(5):653–659, 1989.

[72] VP Shanbhag and CG Axelsson. Hydrophobic interaction determined by partition in aqueous 2-phase systems - partition of proteins in systems containing fatty-acid esters of poly(ethylene glycol). *European Journal of Biochemistry*, 60(1):17–22, 1975.

[73] LA Sklar, BS Hudson, and RD Simoni. Conjugated polyene fatty-acids as fluorescent-probes - binding to bovine serum-albumin. *Biochemistry*, 16(23):5100–5108, 1977.

[74] JX Zhou and T Tressel. Basic concepts in q membrane chromatography for large-scale antibody production. *Biotechnology progress*, 22(2):341–349, 2006.

[75] C Charcosset. Membrane processes in biotechnology: An overview. *Biotechnology Advances*, 24(5):482–492, 2006.

[76] C Charcosset. Purification of proteins by membrane chromatography. *Journal of Chemical Technology and Biotechnology*, 71(2):95–110, 1998.

[77] L Zhong, J Scharer, M Moo-Young, D Fenner, L Crossley, CH Honeyman, S Suen, and CP Chou. Potential application of hydrogel-based strong anion-exchange membrane for plasmid dna purification. *Journal of Chromatography B-Analytical Technologies in the Biomedical and Life Sciences*, 879(9-10):564–572, 2011.

[78] N Fraud, J Lim, A Sinclair, and U Gottschalk. Technical and economic benefits of membrane chromatography during polishing steps. *Biopharm International*, 23(8):44–52, 2010.

[79] RF Childs, AM Mika, J Zhou, EN Komkova, M Kim, and TK Dey. *Composite Materials comprising Supported Porous Gels*. 2008.

[80] W Jiang, RF Childs, AM Mika, and JM Dickson. Pore-filled cation-exchange membranes containing poly(styrenesulfonic acid) gels. *Desalination*, 159(3):253–266, 2003.

[81] D Valade, LK Wong, Y Jeon, Z Jia, and MJ Monteiro. Polyacrylamide hydrogel membranes with controlled pore sizes. *Journal of Polymer Science*, 51:129–138, 2012.

[82] AW Chan and RJ Neufeld. Modeling the controllable ph-responsive swelling and pore size of networked alginate based biomaterials. *Biomaterials*, 30:6119–6129, 2009.

[83] S Hernandez, JK Papp, and D Bhattacharyya. Iron-based redox polymerization of acrylic acid for direct synthesis of hydrogel/membranes and metal nanoparticles for water treatment. *Industrial & Engineering Chemistry Research*, 53:1130–1142, 2013.

[84] I Tatarova, R Faber, R Denoyel, and M Polakovic. Characterization of pore structure of a strong anion-exchange membrane adsorbent under different buffer and salt concentration conditions. *Journal of Chromatography a*, 1216:941–947, 2009.

[85] A Staby, JH Jacobsen, RG Hansen, UK Bruus, and IH Jensen. Comparison of chromatographic ion-exchange resins - v strong and weak cation-exchange resins. *Journal of Chromatography A*, 1118(2):168–179, 2006.

[86] TM Pabst, EJ Suda, KE Thomas, P Mensah, N Ramasubramanyan, ME Gustafson, and AK Hunter. Binding and elution behavior of proteins on strong cation exchangers. *Journal of Chromatography A*, 1216(45):7950–7956, 2009.

[87] AV Mamchenko and LG Chernova. Analysis of the potentiometric titration curves of weakly basic anionites. *Adsorption Science & Technology*, 18(10):881–891, 2000.

[88] G Bayramoglu, H Avni Oktem, and M Yakup Arica. A dye-ligand immobilized poly(2-hydroxyethylmethacrylate) membrane used for adsorption and isolation of immunoglobulin g. *Biochemical engineering journal*, 34(2):147–155, 2007.

[89] C Boi, S Dimartino, S Hofer, J Horak, S Williams, GC Sarti, and W Lindner. Influence of different spacer arms on mimetic ligand (tm) a2p and b14 membranes for human igg purification. *Journal of Chromatography B-Analytical Technologies in the Biomedical and Life Sciences*, 879(19):1633–1640, 2011.

[90] S Hofer, A Ronacher, J Horak, H Graalfs, and W Lindner. Static and dynamic binding capacities of human immunoglobulin g on polymethacrylate based mixed-modal, thiophilic and hydrophobic cation exchangers. *Journal of Chromatography A*, 1218(49):8925–8936, 2011.

[91] P DePhillips and AM Lenhoff. Determinants of protein retention characteristics on cation-exchange adsorbents. *Journal of Chromatography A*, 933(1-2):57–72, 2001.

[92] LW McLaughlin. Mixed-mode chromatography of nucleic-acids. *Chemical reviews*, 89(2):309–319, 1989.

[93] BHJ Hofstee. Protein-binding by agarose carrying hydrophobic groups in conjunction with charges. *Biochemical and biophysical research communications*, 50(3):751–757, 1973.

[94] MJ Ariza, A Canas, and J Benavente. Electrokinetic and electrochemical characterizations of porous membranes. *Colloids and Surfaces A-Physicochemical and Engineering Aspects*, 189(1-3):247–256, 2001.

[95] A Pourjavadi and H Salimi. New protein-based hydrogel with superabsorbing properties: Effect of monomer ratio on swelling behavior and kinetics. *Industrial & Engineering Chemistry Research*, 47(23):9206–9213, 2008.

[96] DJ Munoz-Pinto, B Grigoryan, J Long, M Grunlan, and MS Hahn. An approach for assessing hydrogel hydrophobicity. *Journal of Biomedical Materials Research Part a*, 100A(10):2855–2860, 2012.

[97] R Tzoneva, B Seifert, W Albrecht, K Richau, T Groth, and A Lendlein. Hemocompatibility of poly(ether imide) membranes functionalized with carboxylic groups. *Journal of Materials Science-Materials in Medicine*, 19(10):3203–3210, 2008.

[98] S Yarimkaya and H Basan. Swelling behavior of poly(2-hydroxyethyl methacrylateco-acrylic acid-co-ammonium acrylate) hydrogels. *Journal of Macromolecular Science Part A-Pure and Applied Chemistry*, 44(7-9):939–946, 2007.

[99] J Wang, R Faber, and M Ulbricht. Influence of pore structure and architecture of photo-grafted functional layers on separation performance of cellulose-based macroporous membrane adsorbers. *Journal of Chromatography a*, 1216(37):6490–6501, 2009.

[100] K Wrzosek and M Polakovic. Effect of ph on protein adsorption capacity of strong cation exchangers with grafted layer. *Journal of Chromatography A*, 1218(39):6987–6994, 2011.

[101] U Gottschalk. Bioseparation in antibody manufacturing: The good, the bad and the ugly. *Biotechnology progress*, 24(3):496–503, 2008.

[102] TW Xu. Ion exchange membranes: State of their development and perspective. *Journal of Membrane Science*, 263(1-2):1–29, 2005.

[103] T Sata. *Exchange Membranes: preparation, characterization, modification and application*. The Royal Society of Chemisrty, Cambridge, UK, 2004.

[104] X Jin and YL Hsieh. ph-responsive swelling behavior of poly(vinyl alcohol)/poly(acrylic acid) bi-component fibrous hydrogel membranes. *Polymer*, 46(14):5149–5160, 2005.

[105] K Shakir, MK Walsh, and SA Mohammed. Characterization of iraqi sheep milk lysozyme with respect to molecular weight and hydrolytic activity. *Dairy Science & Technology*, 93(6):699–705, 2013.

[106] P Parhi, A Golas, N Barnthip, H Noh, and EA Vogler. Volumetric interpretation of protein adsorption: Capacity scaling with adsorbate molecular weight and adsorbent surface energy. *Biomaterials*, 30(36):6814–6824, 2009.

[107] A Vinu, M Miyahara, KZ Hossain, M Takahashi, VV Balasubramanian, T Mori, and K Ariga. Lysozyme adsorption onto mesoporous materials: Effect of pore geometry and stability of adsorbents. *Journal of Nanoscience and Nanotechnology*, 7(3):828–832, 2007.

[108] S Kim, CA Kim, HB Pyo, and MY Jung. Synthesis of anionic sulfate functionalized polystyrene latex and protein adsorption for application as a biosensor. *Journal of Nanoscience and Nanotechnology*, 9(12):7171–7176, 2009.

[109] YC Kim and AS Myerson. Diffusivity of lysozyme in undersaturated, saturated and supersaturated solutions. *Journal of Crystal Growth*, 143(1-2):79–85, 1994.

[110] MT Tyn and TW Gusek. Prediction of diffusion-coefficients of proteins. *Biotechnology and bioengineering*, 35(4):327–338, 1990.

[111] I Tatarova, P Drevenak, A Kosior, and M Polakovic. Equilibrium and kinetics of protein binding on ion-exchange cellulose membranes with grafted polymer layer. *Chemical Papers*, 67(12):1527–1536, 2013.

[112] J Wang. Macroporous ion-exchange membrane adsorbers: correlation between membrane structure, separation conditions and performance in bioseparation, 2009.

[113] AS Freed and SM Cramer. Protein-surface interaction maps for ion-exchange chromatography. *Langmuir*, 27(7):3561–3568, 2011.

[114] MB Tennikov, NV Gazdina, TB Tennikova, and F. Svec. Effect of porous structure of macroporous polymer supports on resolution in high-performance membrane chromatography of proteins. *Journal of Chromatography a*, 798(1-2):55–64, 1998.

[115] AS Tait, CEM Hogwood, CM Smales, and DG Bracewell. Host cell protein dynamics in the supernatant of a mab producing cho cell line. *Biotechnology and bioengineering*, 109(4):971–982, 2012.

[116] K. Suck, J. Walter, F. Menzel, A. Tappe, C. Kasper, C. Naumann, R. Zeidler, and T. Scheper. Fast and efficient protein purification using membrane adsorber systems. *Journal of Biotechnology*, 121(3):361–367, 2006.

[117] C Jiang, J Liu, Ml Rubacha, and AA Shukla. A mechanistic study of protein a chromatography resin lifetime. *Journal of Chromatography a*, 1216(31):5849–5855, 2009.

[118] GS Blank, G Zapata, R Fahrner, M Milton, C Yedinak, H Knudsen, and C Schmelzer. Expanded bed adsorption in the purification of monoclonal antibodies: a comparison of process alternatives. *Bioseparation*, 10(1-3):65–71, 2001.

[119] N Hammerschmidt, A Tscheliessnig, R Sommer, B Helk, and A Jungbauer. Economics of recombinant antibody production processes at various scales: Industry-standard compared to continuous precipitation. *Biotechnology Journal*, 9(6):766–775, 2014.

[120] J Feuser, M Halfar, D Lutkemeyer, N Ameskamp, MR Kula, and J Thommes. Interaction of mammalian cell culture broth with adsorbents in expanded bed adsorption of monoclonal antibodies. *Process Biochemistry*, 34(2):159–165, 1999.

[121] T Ishihara and T Kadoya. Accelerated purification process development of monoclonal antibodies for shortening time to clinic design and case study of chromatography processes. *Journal of Chromatography a*, 1176(1-2):149–156, 2007.

Appendices

Appendix A

Pore Size Analysis with FESEM

A.1 Flow Sheet for Pore Size Analysis

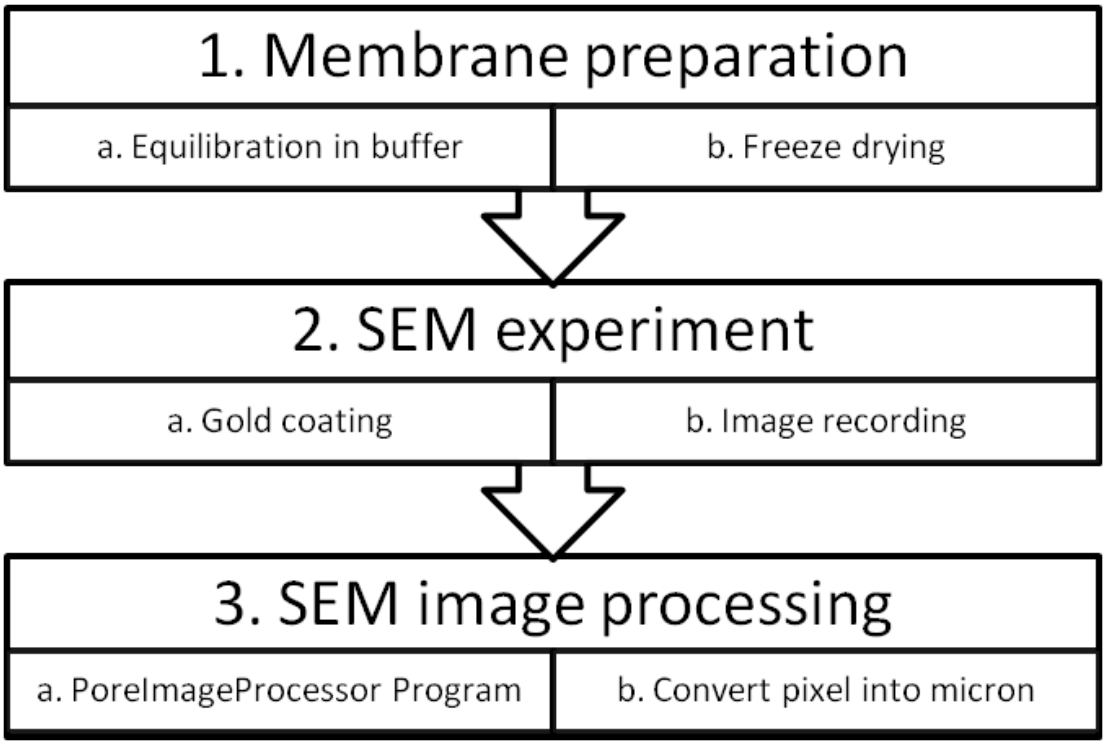

Figure A.1: 3 major steps for the FESEM experiment and data analysis

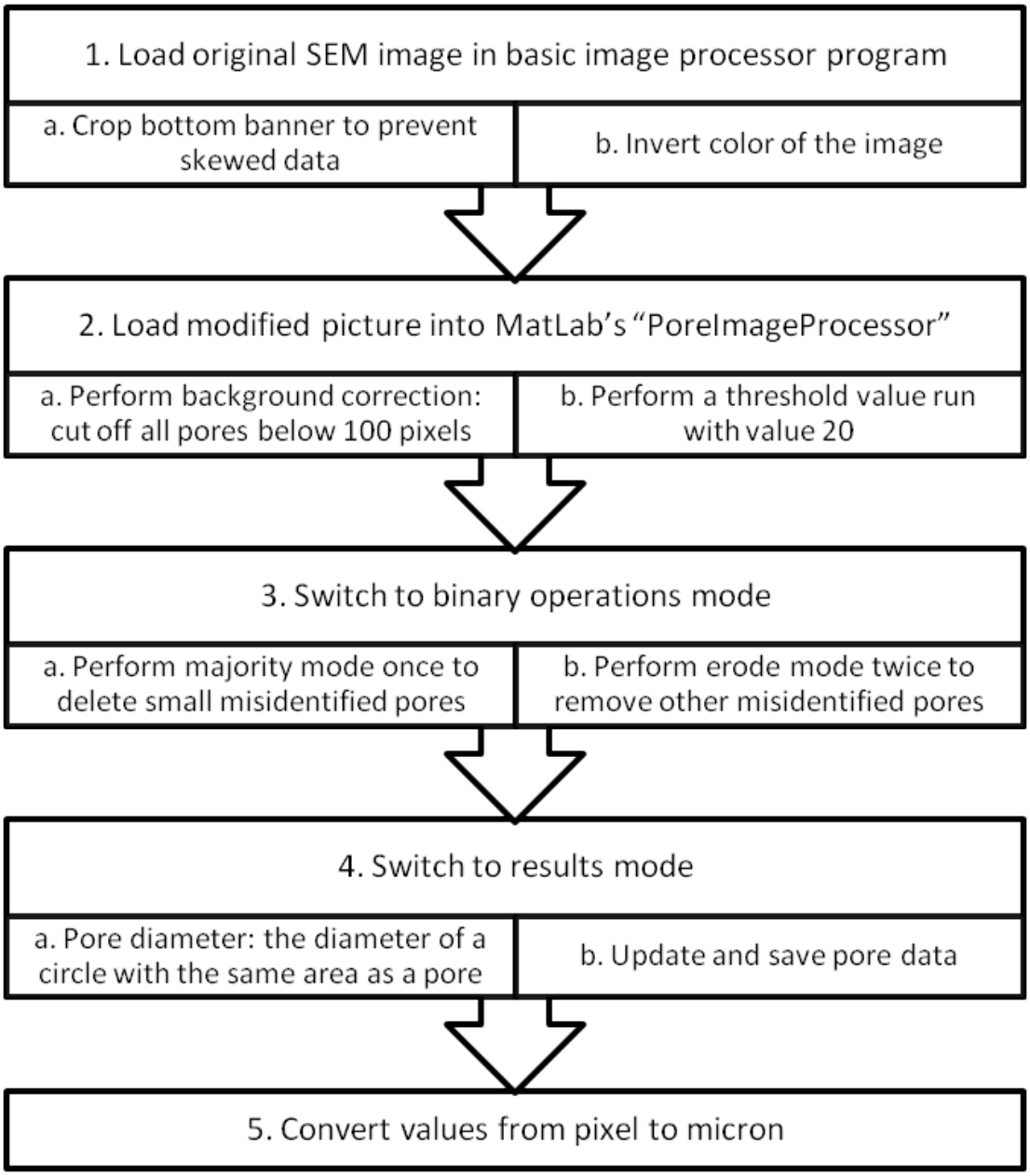

Figure A.2: Detailed description of the FESEM image analysis

A.2 Processed FESEM images

The following figures show the transformation from original FESEM images to pore recognition. Figures A.3-A.22 are used in Chapter 4, Table 4.1.

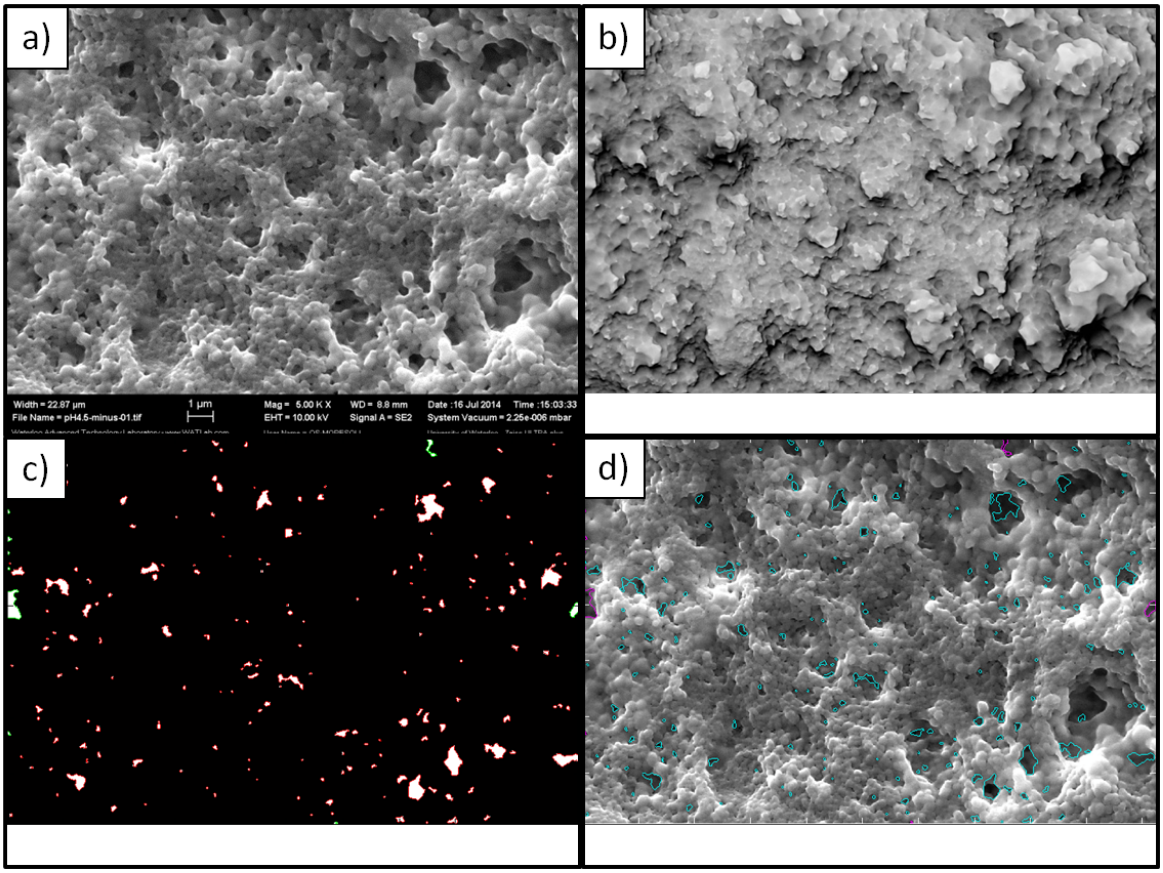

Figure A.3: 2014-07-16-pH 4.5-minus-01, a) Original image b) Cropped & background corrected image c) Pore recognition d) Pores over original image

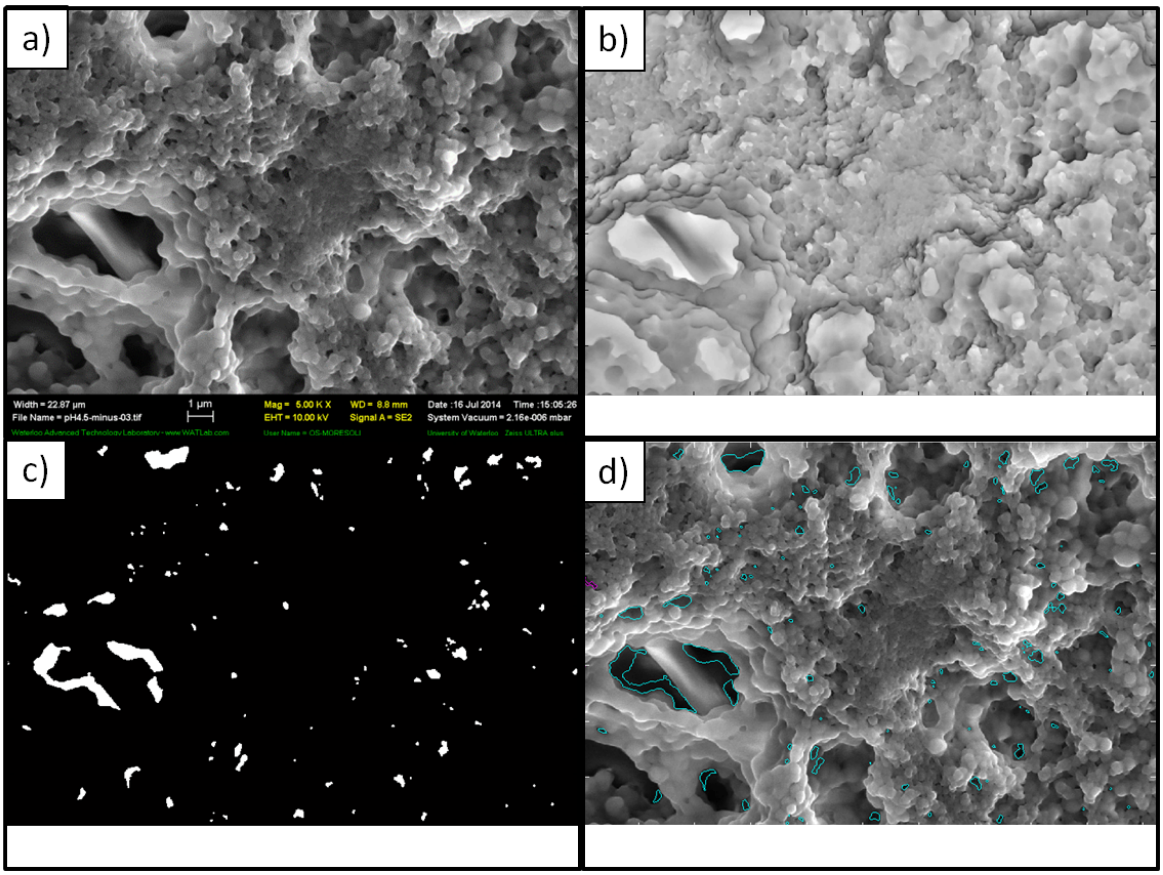

Figure A.4: 2014-07-16-pH 4.5-minus-03, a) Original image b) Cropped & background corrected image c) Pore recognition d) Pores over original image

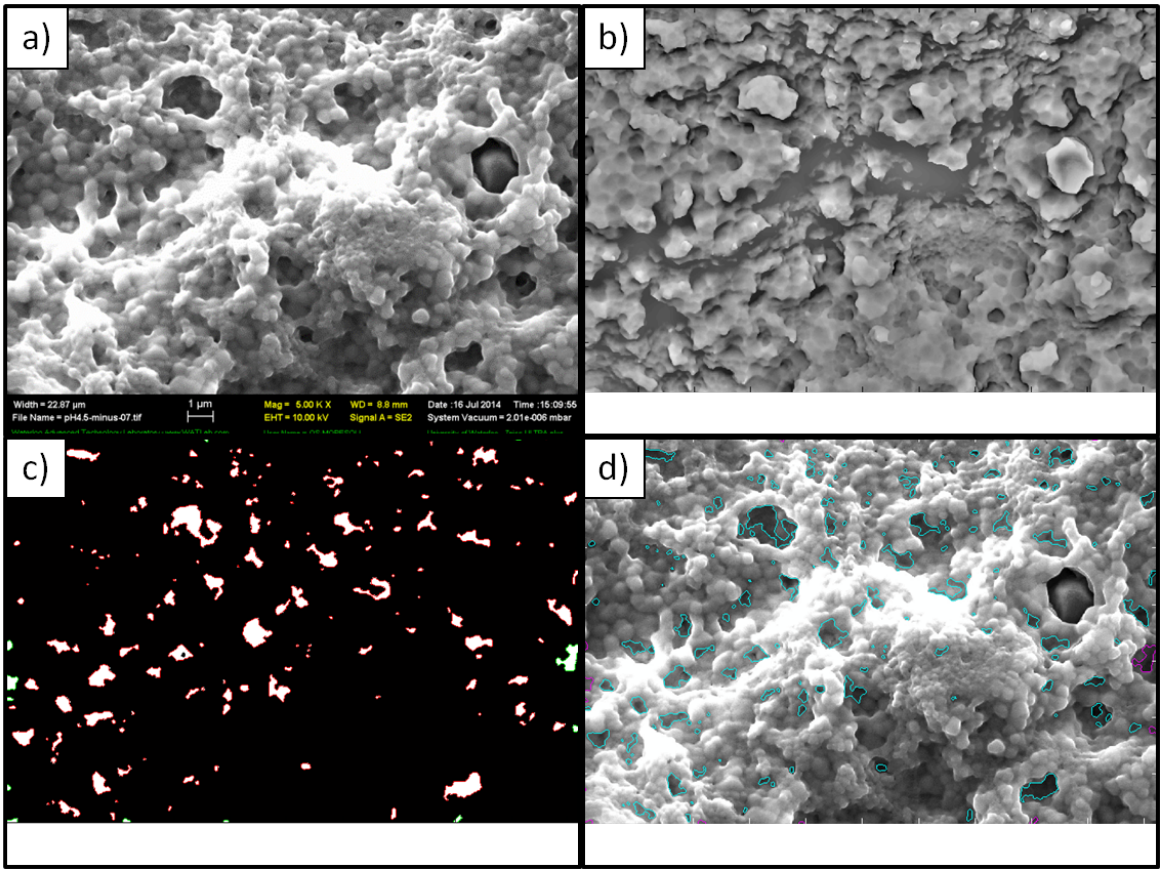

Figure A.5: 2014-07-16-pH 4.5-minus-07, a) Original image b) Cropped & background corrected image c) Pore recognition d) Pores over original image

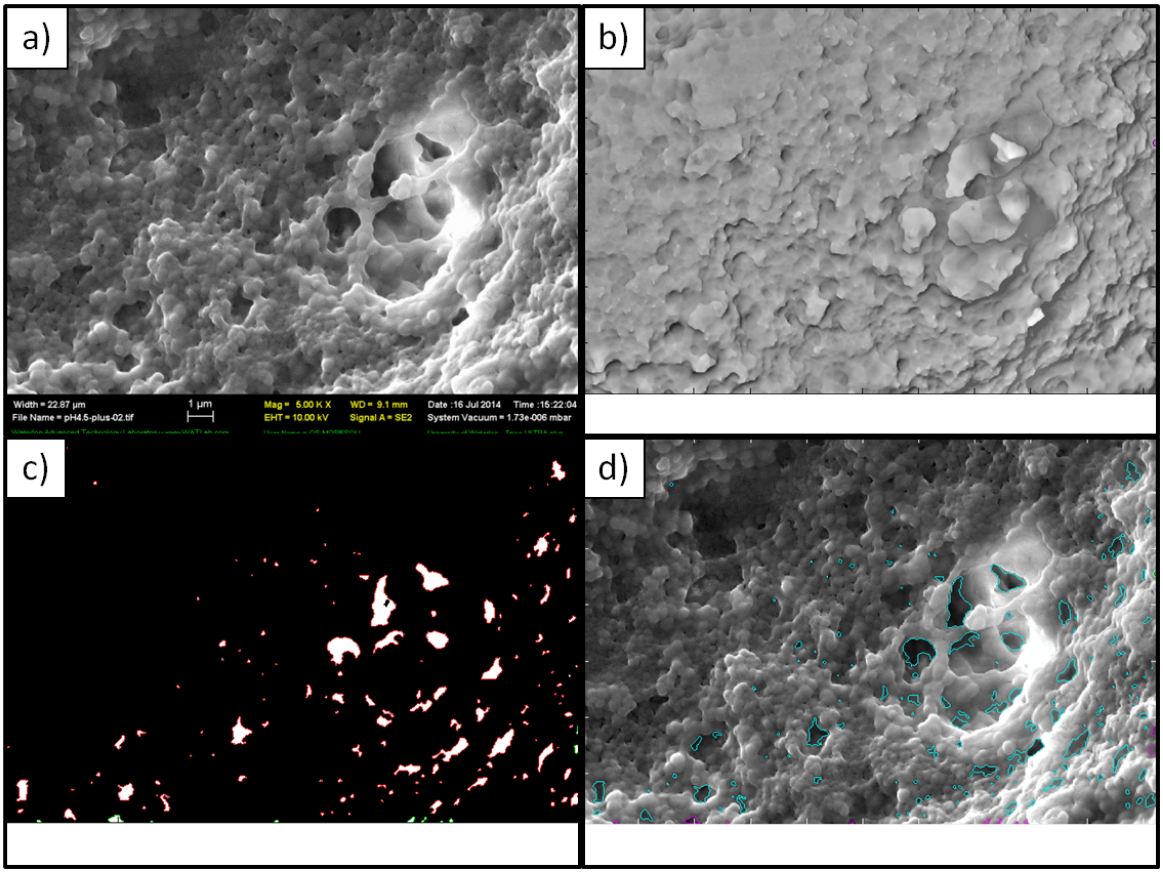

Figure A.6: 2014-07-16-pH 4.5-minus-02, a) Original image b) Cropped & background corrected image c) Pore recognition d) Pores over original image

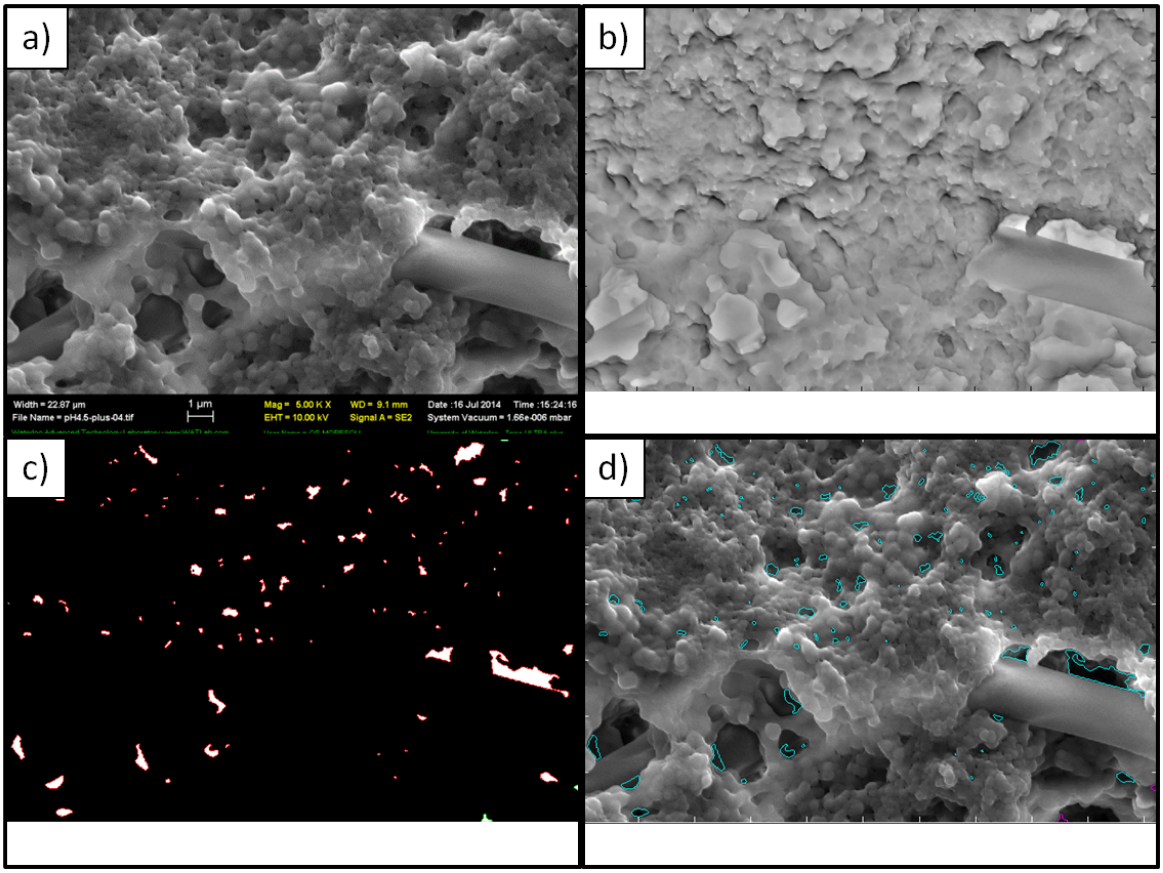

Figure A.7: 2014-07-16-pH 4.5-minus-04, a) Original image b) Cropped & background corrected image c) Pore recognition d) Pores over original image

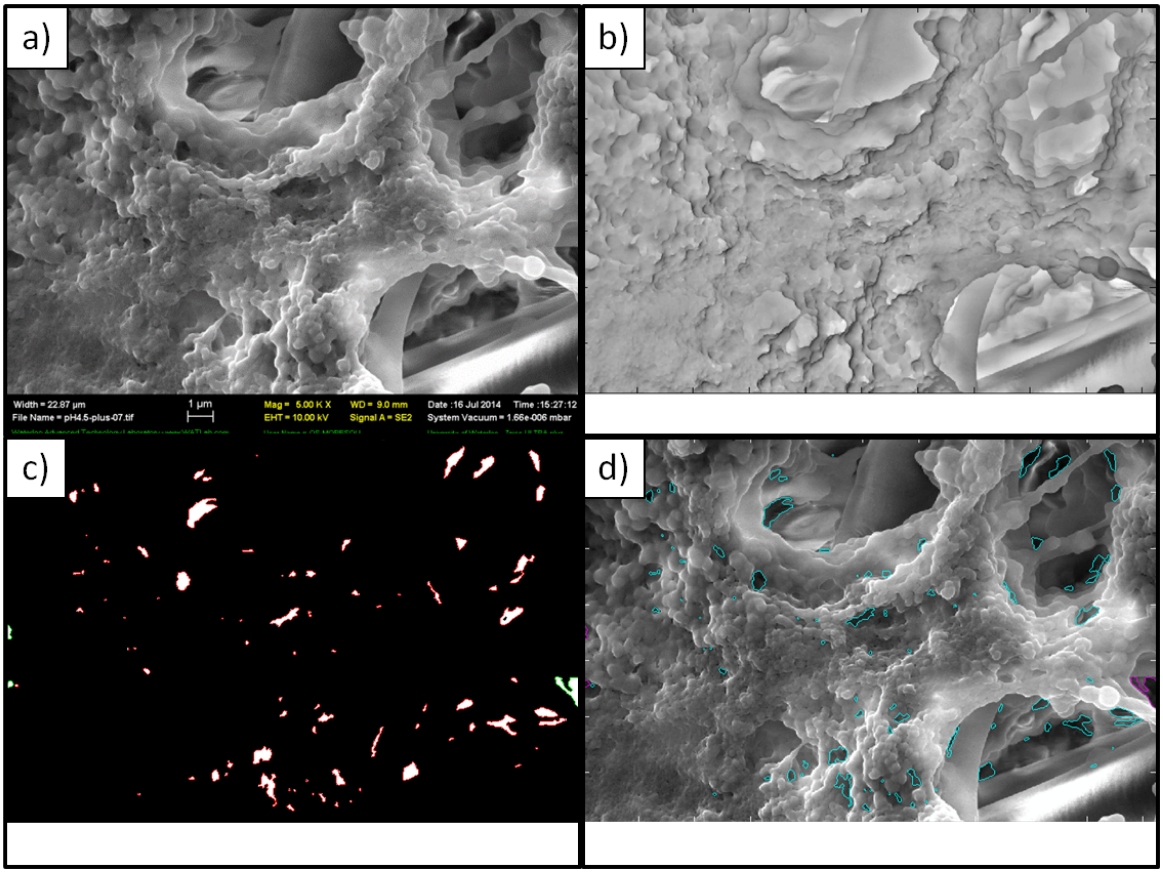

Figure A.8: 2014-07-16-pH 4.5-minus-07, a) Original image b) Cropped & background corrected image c) Pore recognition d) Pores over original image

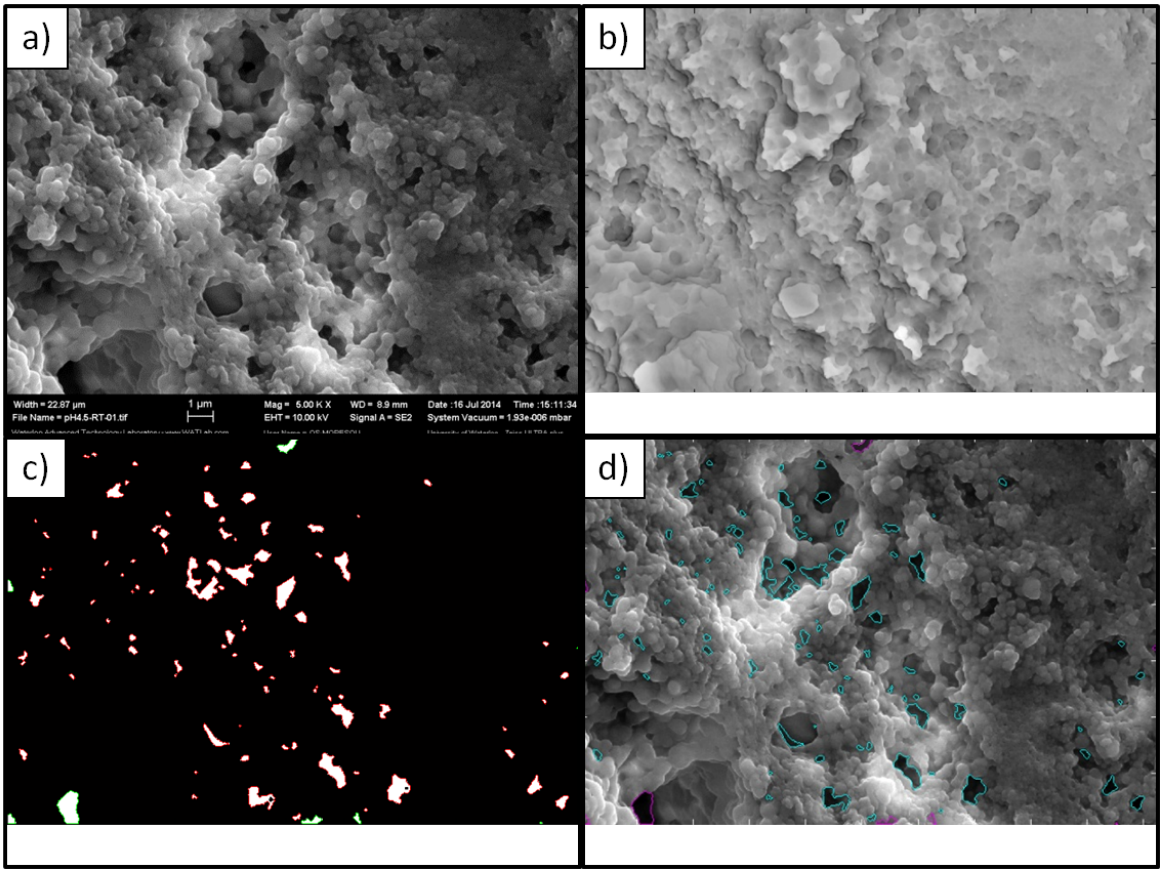

Figure A.9: 2014-07-16-pH 4.5-RT-01, a) Original image b) Cropped & background corrected image c) Pore recognition d) Pores over original image

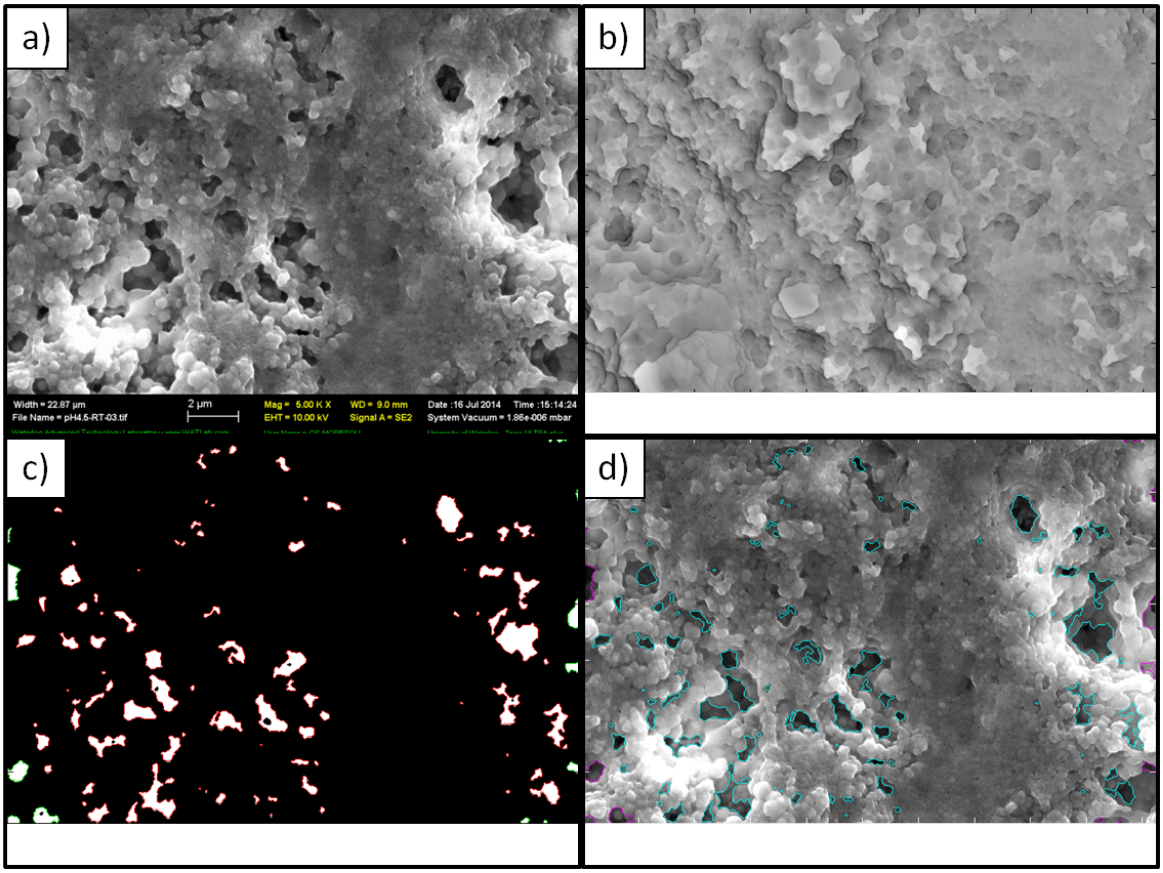

Figure A.10: 2014-07-16-pH 4.5-RT-03, a) Original image b) Cropped & background corrected image c) Pore recognition d) Pores over original image

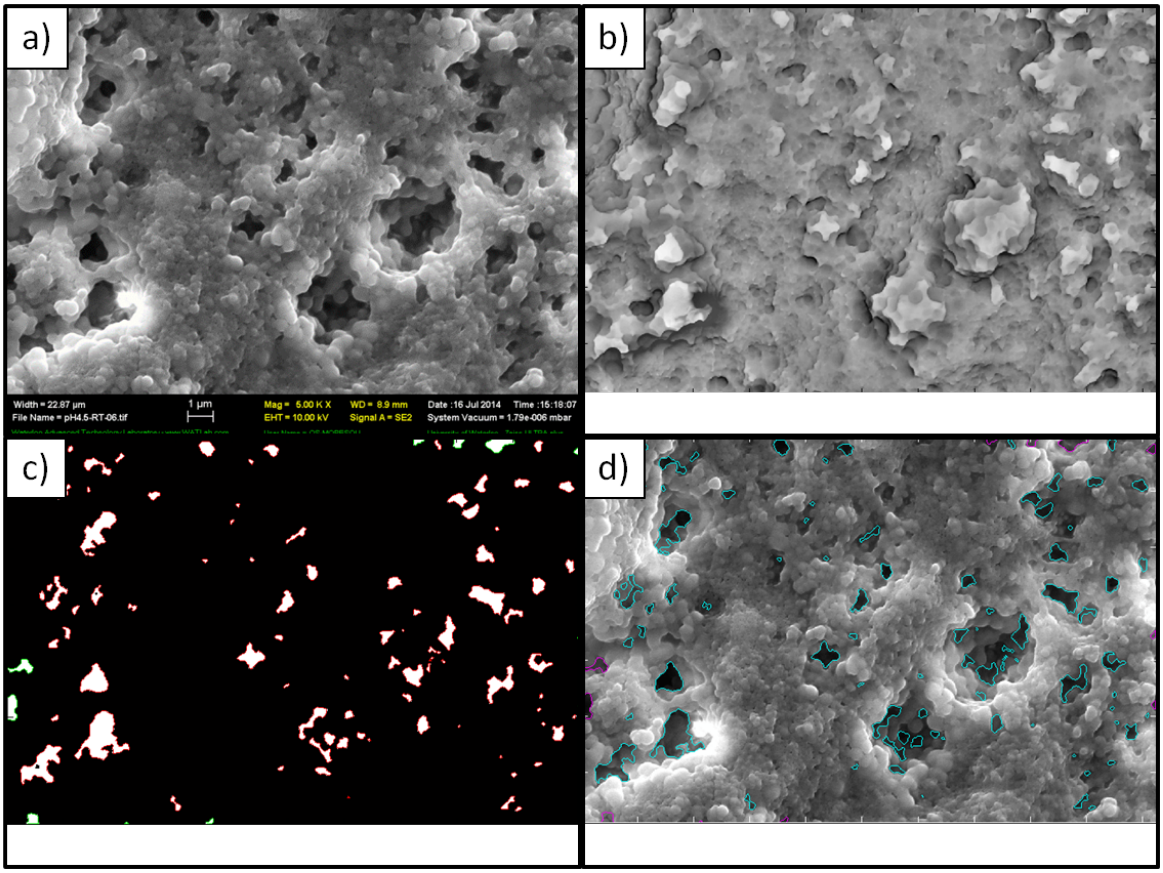

Figure A.11: 2014-07-16-pH 4.5-RT-06, a) Original image b) Cropped & background corrected image c) Pore recognition d) Pores over original image

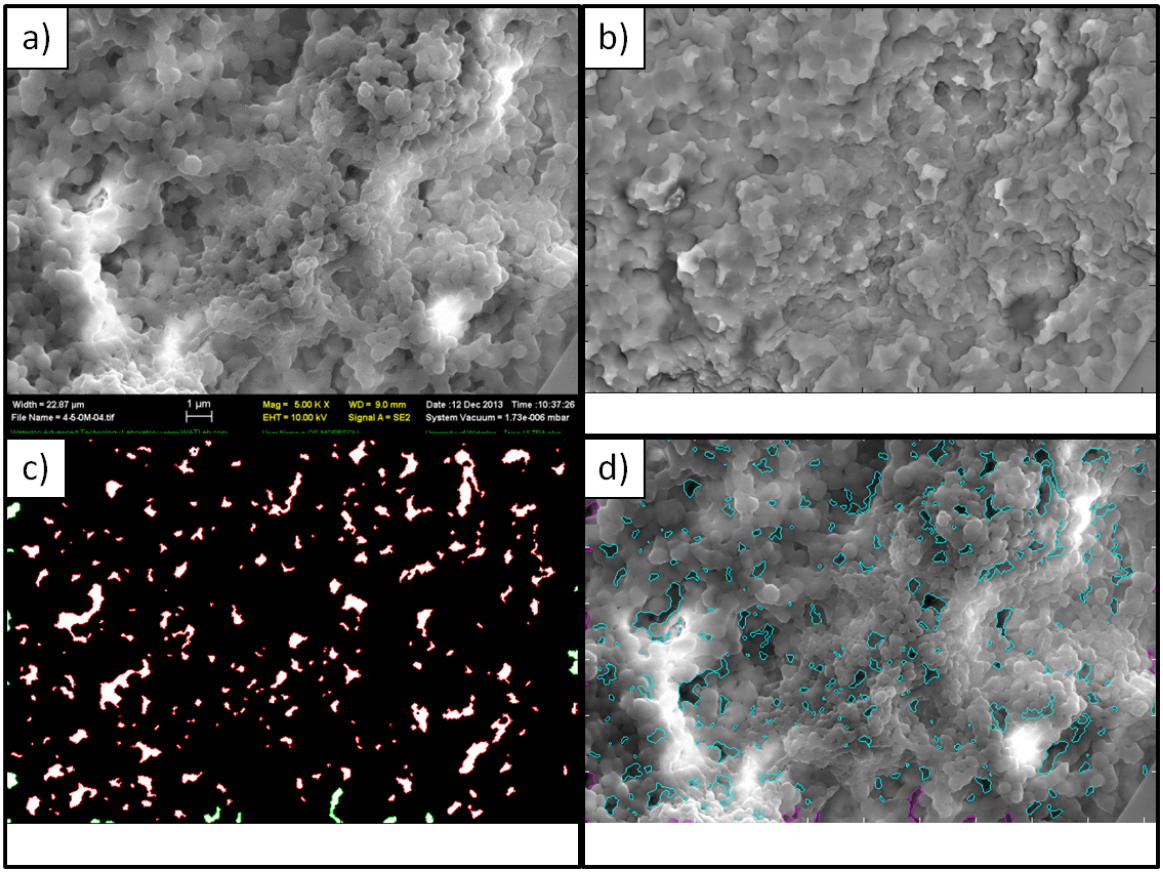

Figure A.12: 2014-04-03-pH 4.5-0M-04, a) Original image b) Cropped & background corrected image c) Pore recognition d) Pores over original image

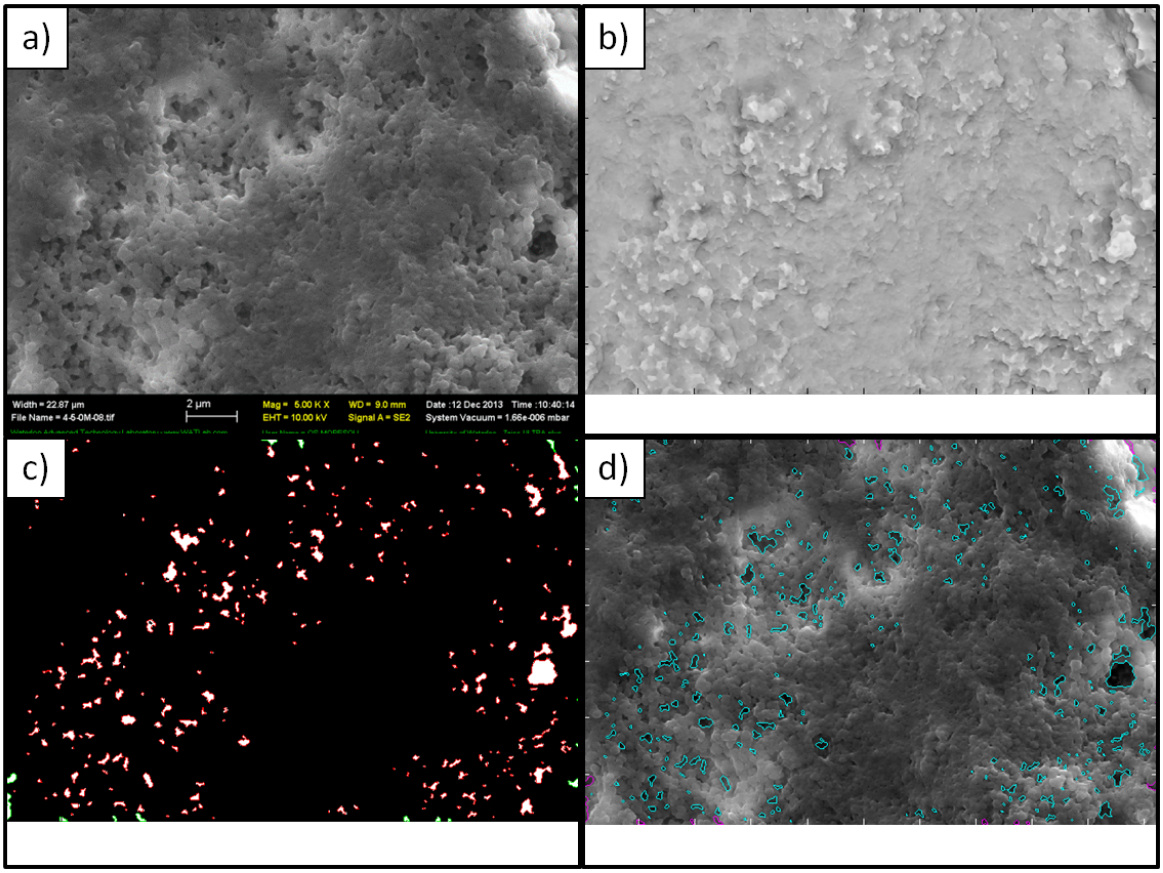

Figure A.13: 2014-04-03-pH 4.5-0M-08, a) Original image b) Cropped & background corrected image c) Pore recognition d) Pores over original image

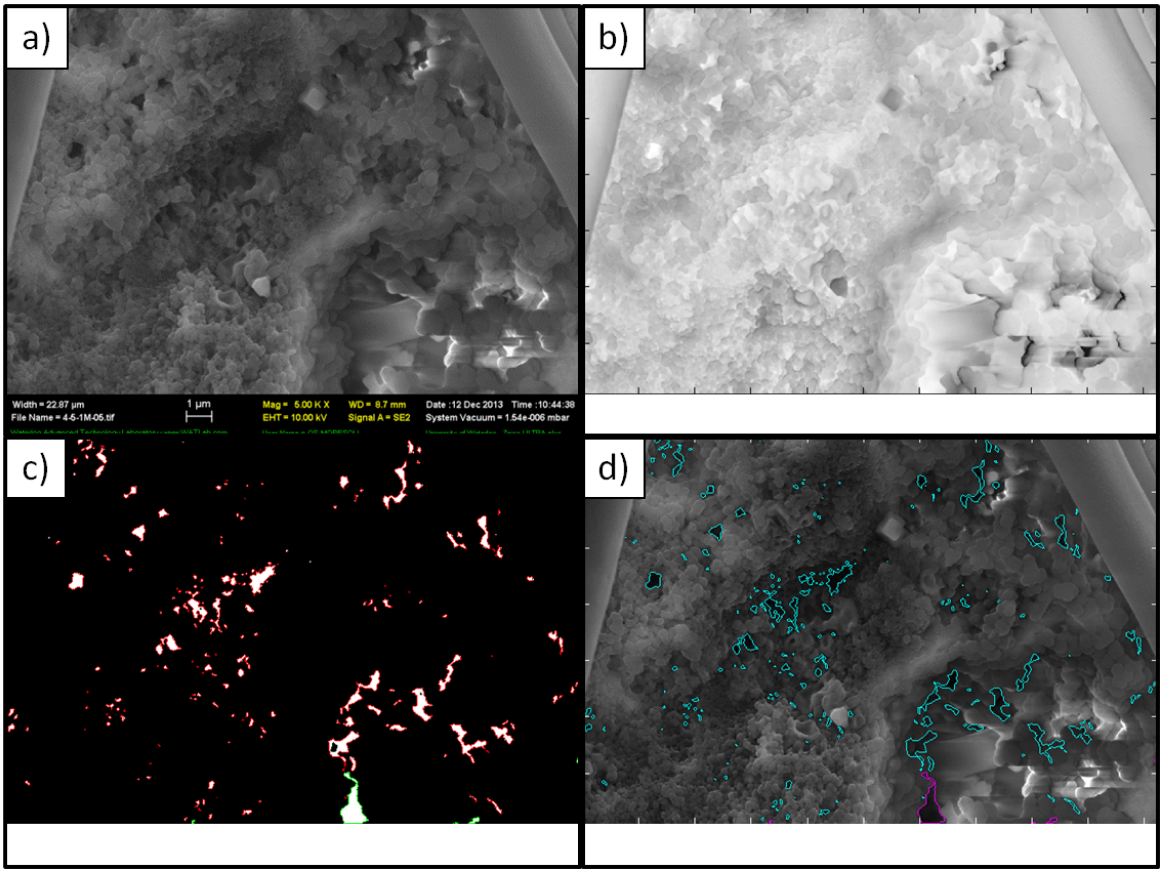

Figure A.14: 2014-04-03-pH 4.5-1M-05, a) Original image b) Cropped & background corrected image c) Pore recognition d) Pores over original image

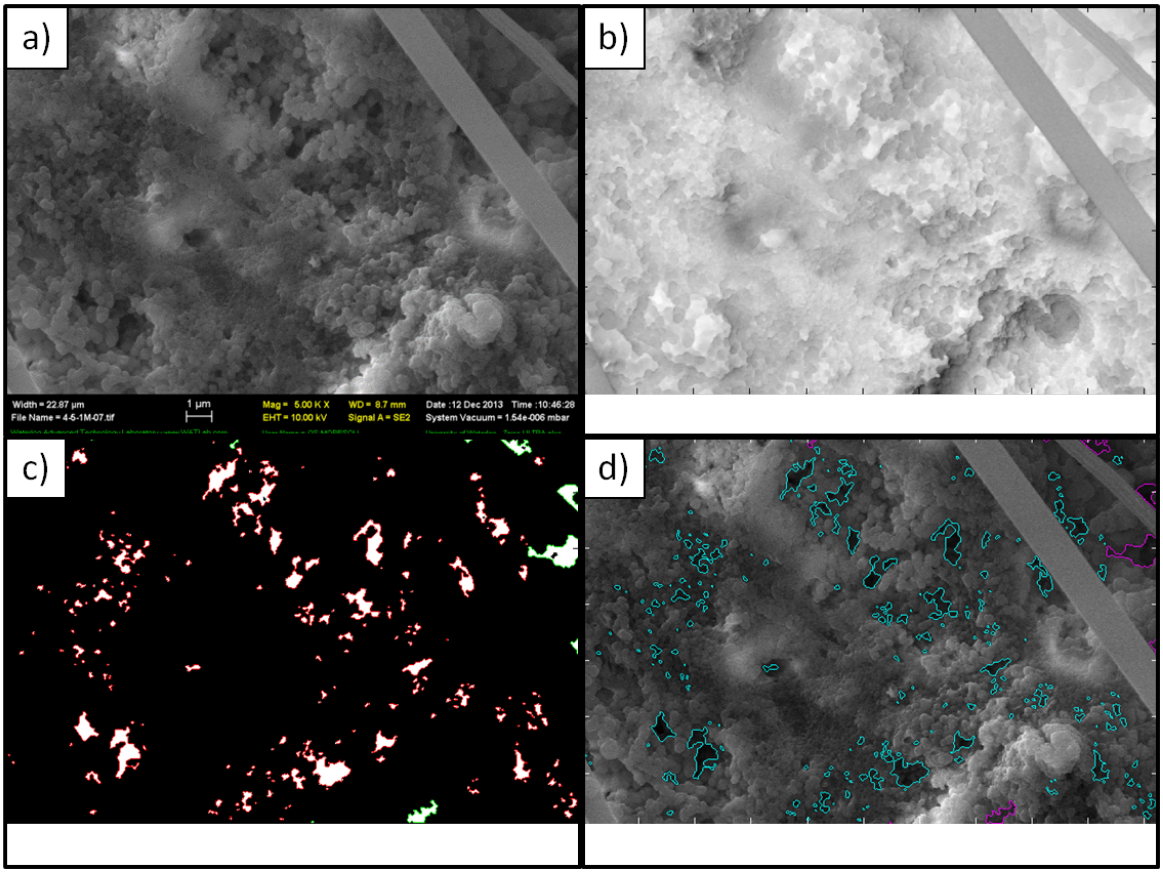

Figure A.15: 2014-04-03-pH 4.5-1M-07, a) Original image b) Cropped & background corrected image c) Pore recognition d) Pores over original image

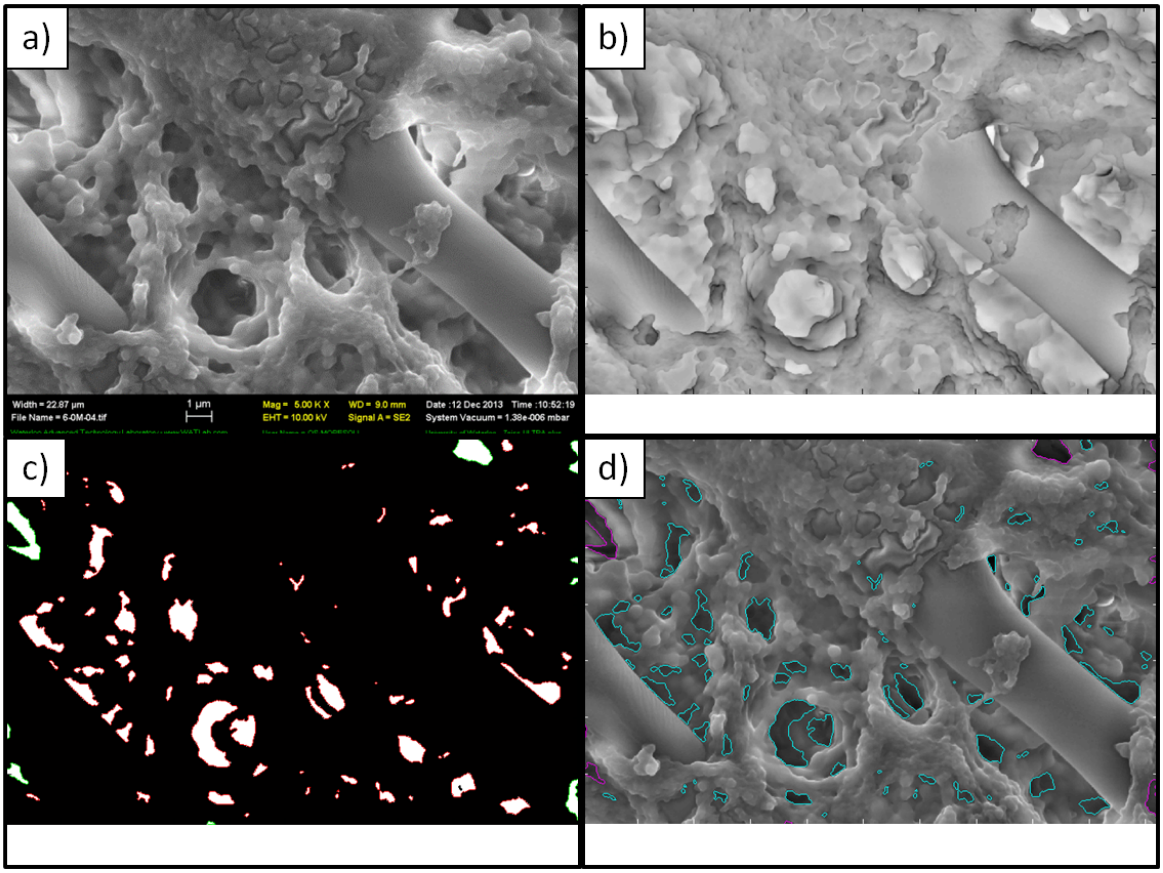

Figure A.16: 2014-04-03-pH 6-0M-04, a) Original image b) Cropped & background corrected image c) Pore recognition d) Pores over original image

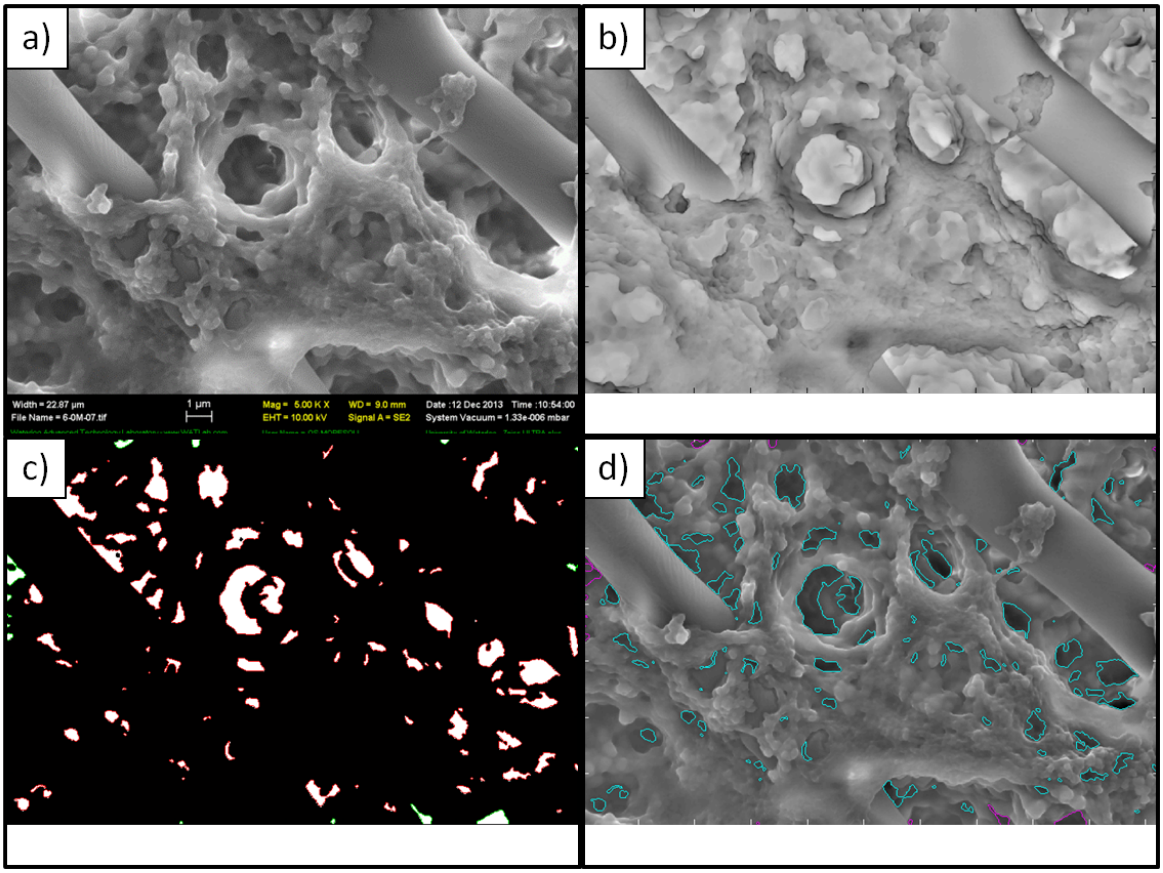

Figure A.17: 2014-04-03-pH 6-0M-06, a) Original image b) Cropped & background corrected image c) Pore recognition d) Pores over original image

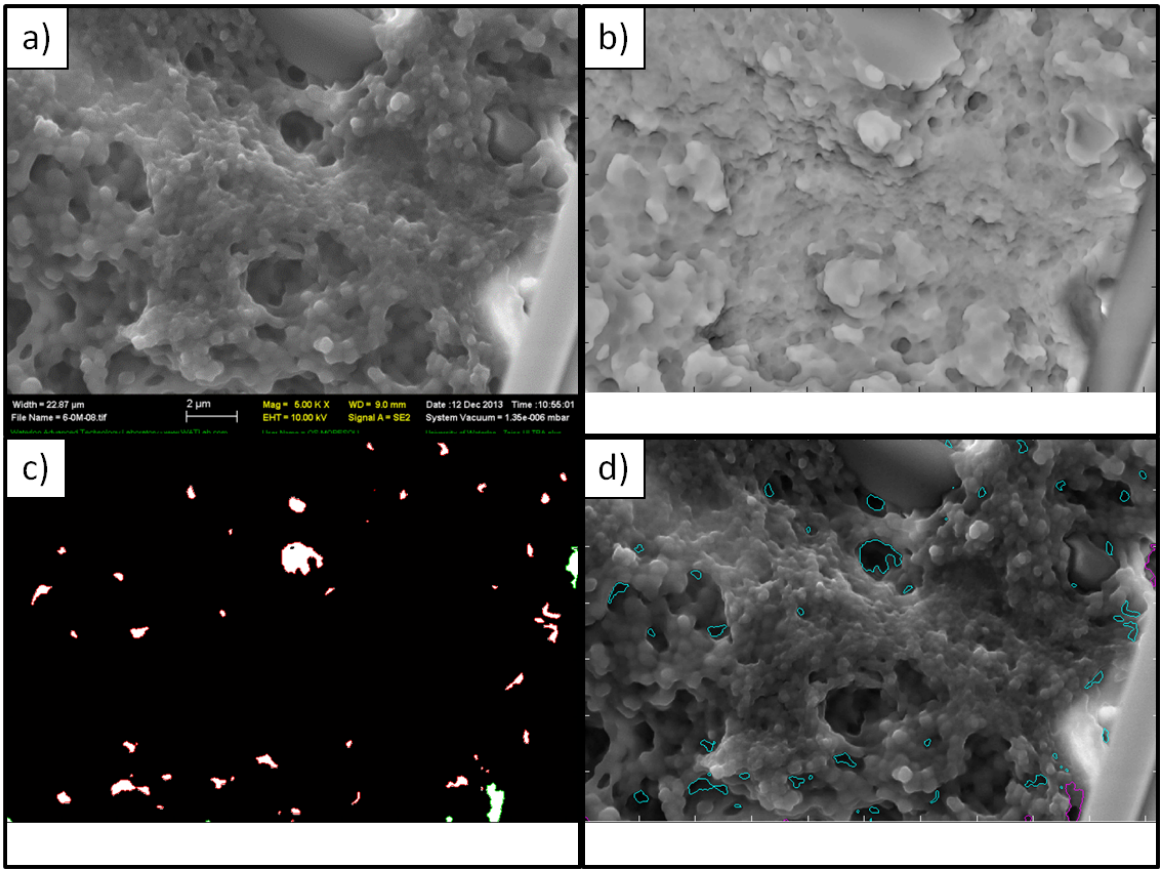

Figure A.18: 2014-04-03-pH 6-0M-08, a) Original image b) Cropped & background corrected image c) Pore recognition d) Pores over original image

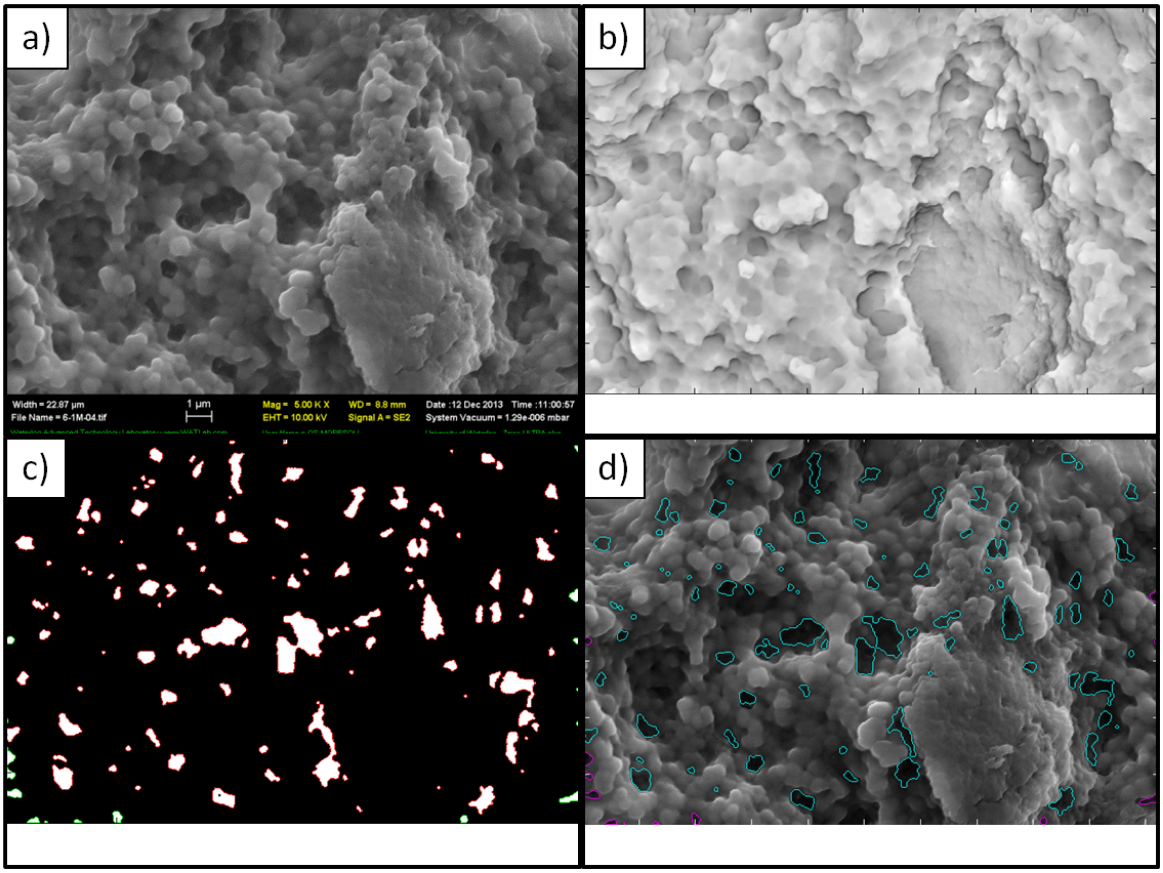

Figure A.19: 2014-04-03-pH 6-1M-04, a) Original image b) Cropped & background corrected image c) Pore recognition d) Pores over original image

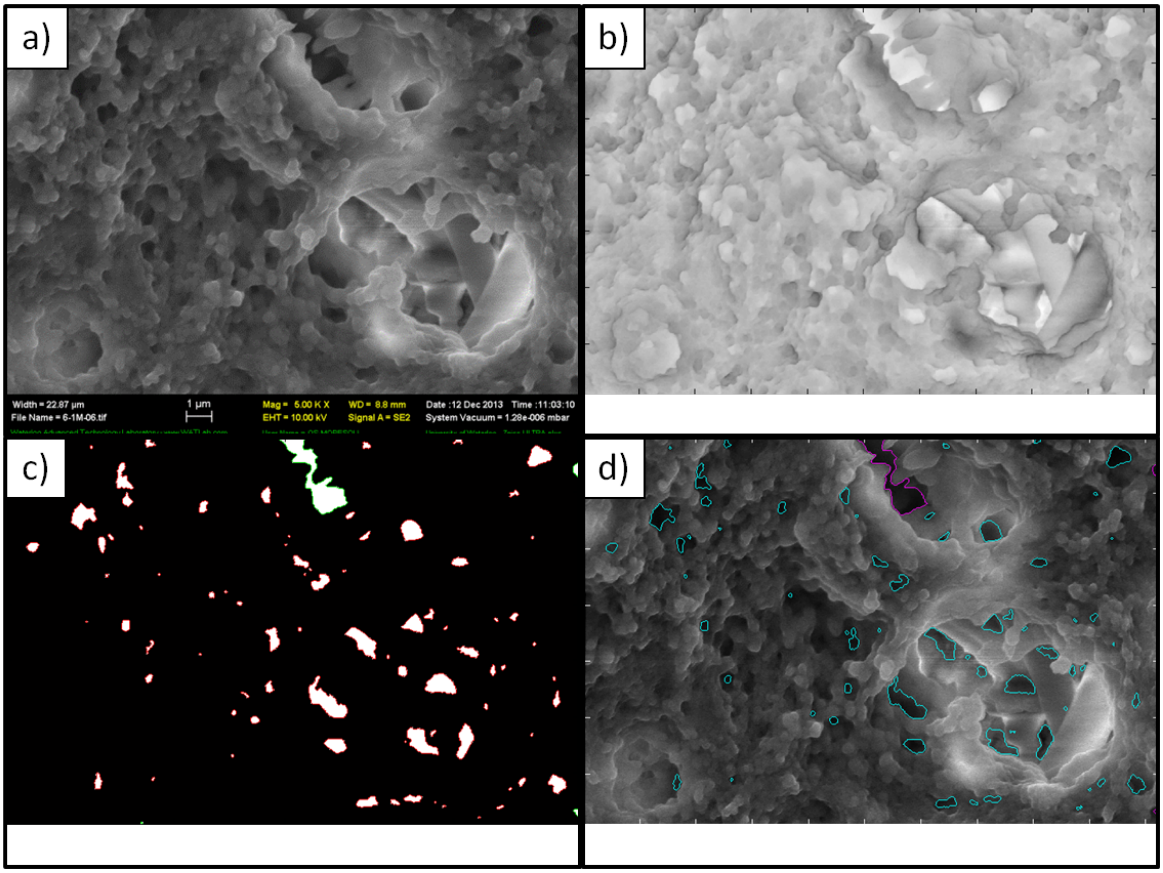

Figure A.20: 2014-04-03-pH 6-1M-06, a) Original image b) Cropped & background corrected image c) Pore recognition d) Pores over original image

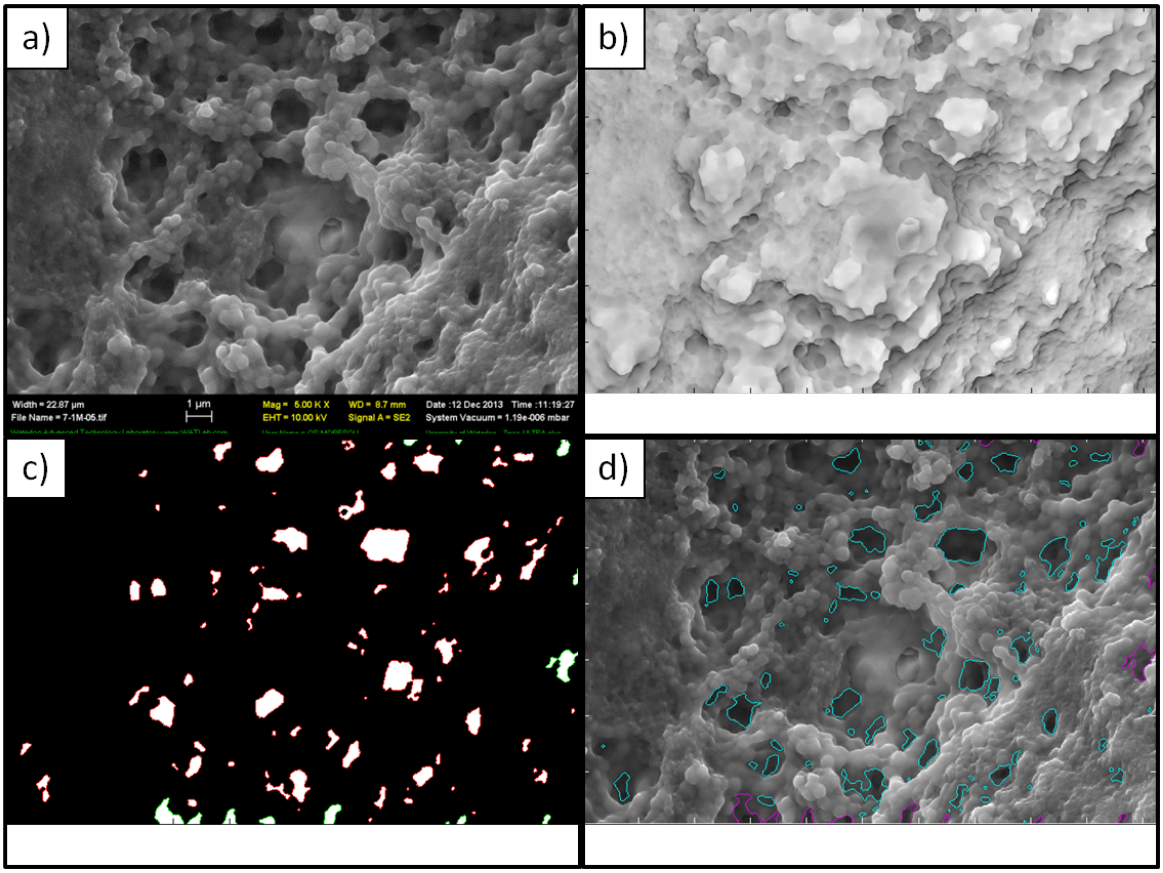

Figure A.21: 2014-04-03-pH 7-1M-05, a) Original image b) Cropped & background corrected image c) Pore recognition d) Pores over original image

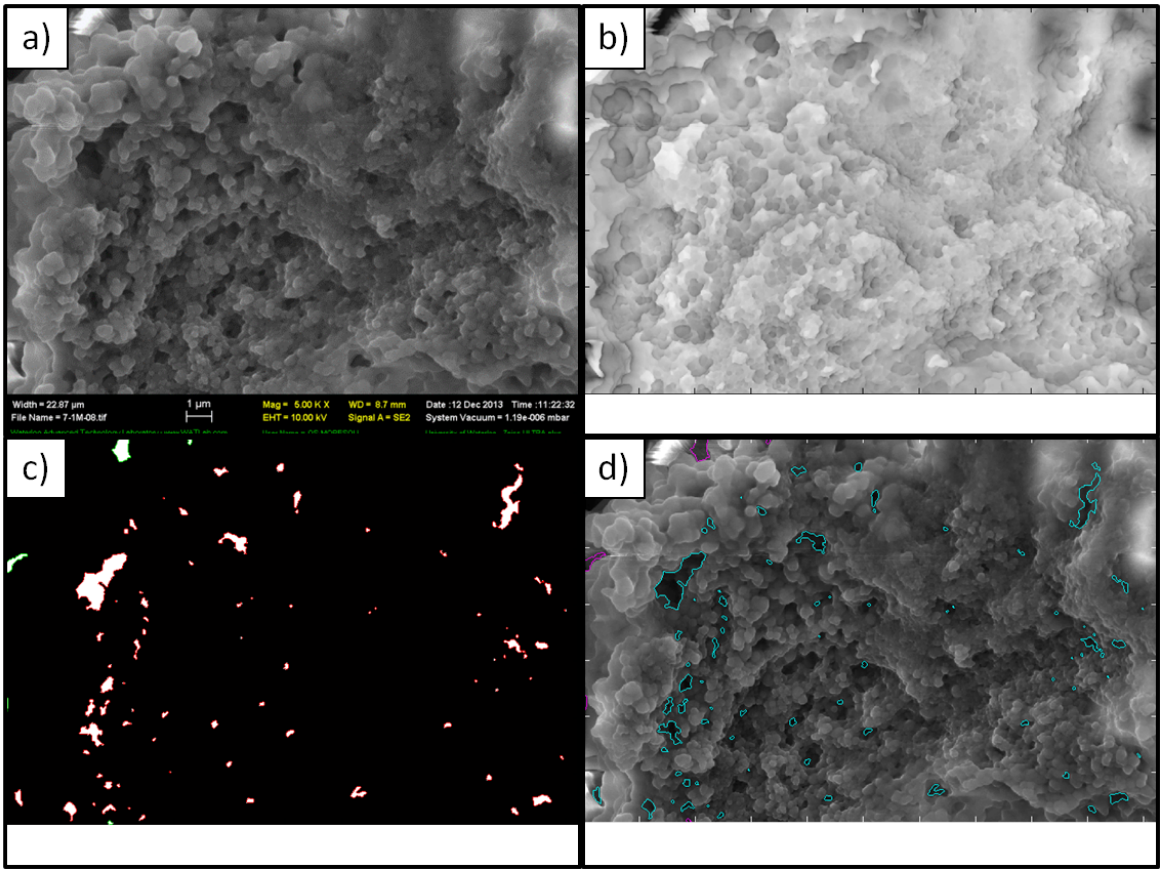

Figure A.22: 2014-04-03-pH 7-1M-08, a) Original image b) Cropped & background corrected image c) Pore recognition d) Pores over original image

Figures A.23 and A.24 are used in Chapter 5, Figure 5.5.

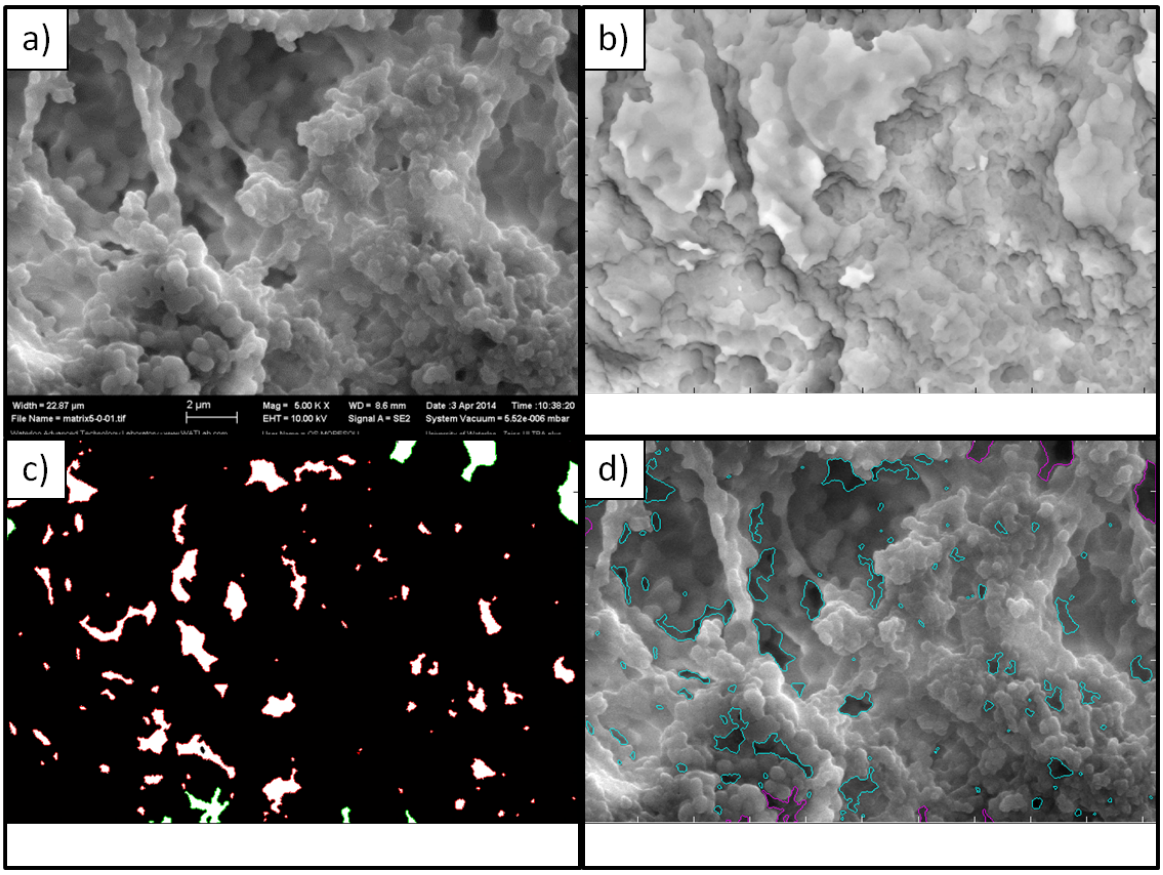

Figure A.23: 2014-04-03-pH 5-0M-01, a) Original image b) Cropped & background corrected image c) Pore recognition d) Pores over original image

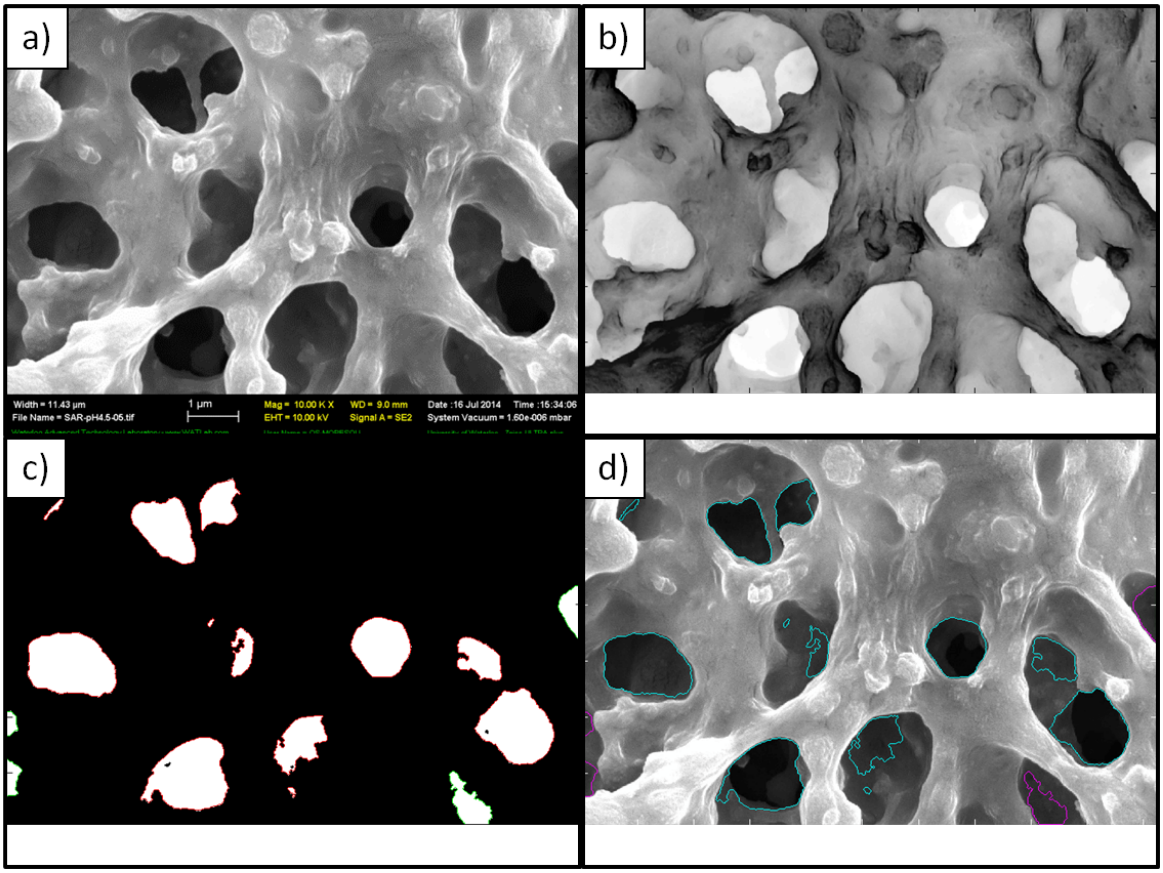

Figure A.24: 2014-04-03-SAR-pH 5-0M-01, a) Original image b) Cropped & background corrected image c) Pore recognition d) Pores over original image

Appendix B

MATLAB Code

B.1 MATLAB Code for Analysing an EEM

```
clc
%program to obtain contour plots of EEM spectra of blanks

n_lines=126;
%number of columns of data (=number of measured emission wavelengths)

%at first, the matrices are filled with zeros:
sample1_a=zeros(n_lines,21); %21 represents the number of excitation wavelengths

%Matlab doesn't recognize "." as a character in variable names
sample2_a=zeros(n_lines,21);

sample3_a=zeros(n_lines,21);

%read in the data:

filename_a='filename.xls';
% Put the Excel file in the same folder
Matrix_a=xlsread(filename_a);
column_number_a=numel(Matrix_a,'1',':');
%gives the number of columns the Matrix has

sample1_a=Matrix_a(:,2:4:column_number_a);
% the numbers 2 and 4 above might need to change. 2 represents the column
% of the first measurement, and 4 represents the number of columns between
% measurements of the same pH
% **numbers above are for 2 samples**
sample2_a=Matrix_a(:,4:6:column_number_a);
% read note above

em_vector=Matrix_a(:,1);  %in column 1, you'll find the emission wavelengths
ex_vector=[300:10:500];

[X,Y]=meshgrid(ex_vector,em_vector);
vect_contours = 0:20:600;
%this sets the space between contours and the highest value of the contours

%plots:
figure(1)
contour(X,Y,sample1_a,vect_contours)
xlabel('excitation wavelength in nm','Fontsize',12)
ylabel('emission wavelength in nm','Fontsize',12)
zlabel('fluorescence intensity in a.u.','Fontsize',12)
colorbar

figure(2)
contour(X,Y,sample2_a,vect_contours)
xlabel('excitation wavelength in nm','Fontsize',12)
ylabel('emission wavelength in nm','Fontsize',12)
zlabel('fluorescence intensity in a.u.','Fontsize',12)
colorbar
```

B.2 MATLAB Code for Analysing a Chromatogram

```
%Matlab code for AKTA weak c membrane chromatography evaluation with one type of Protein
%Use method #24 for c0 determination
%Use method #27 for chromatography; export UV-, conductivity- and pressure
%curves and logbook; no fraction collection
%Use method #37 for chromatography with fraction collection of
%binding/wahing/elution


%Code written by Kamjar Ghofrani 2013
%Edited by Nils Wagner 2014
%Edited by Katharina Hassel 2014

clear all
clc

cfile='2014Nov19_lysC0'; %Define excel sheet with c0 determination
chromfile='2014Nov19_lys3'; %Define excel sheet with AKTA Data
elurate=2; %Flow rate (ml/min) during elution
bindrate=1; %Flow rate (ml/min) during bind/equ/wash steps
deadvolume=3.38; %Deadvolume of the AKTA system in ml (determined by Kayleigh Kuindersma)
proc= 0.5;
bindvolume=50;
%Protein concentration in mg/ml

%Only reliable results, when washing step complete and no leakage
%occurs! Control permeate volume!
%-------------------------------------------------------------------------------

maxabsor=xlsread(cfile,'B4:B10000'); %Importing c0 absorption data
c0=max(maxabsor(390:end))-min(maxabsor(390:end))
 %Determines c0 (Use AKTA method #24 to collect data!)

t=xlsread(chromfile,'A4:A10000'); %Imports time
absor=xlsread(chromfile,'B4:B10000'); %Imports absorption data
bindabsor=xlsread(chromfile,'B4:B416'); %Imports absorption data without elution step
IMPORTANT: needs to be changed when changing protocol

u=abs(t-(xlsread(chromfile,('G12:G12'))+deadvolume/bindrate));
bindstart=find (u==(min(u))) %Imports req.starting time of binding from field G12 and
considers the system's dead volume in order to determine real starting time of binding.

clear u
u=abs(t-(xlsread(chromfile,('G14:G14'))+deadvolume/bindrate));
%Imports req. ending time of binding and adsjusts it
bindend=find (u==(min(u)));

%bindend=find(absor==max(absor(500:4800)))

clear u
u=abs(t-(xlsread(chromfile,('G17:G17'))+deadvolume/elurate));
%Imports req. starting time of elution and finds real starting time.
elustart=find (u==(min(u)))
```

```
clear u
u=abs(t-xlsread(chromfile,('G17:G17')));
elureq=find (u==(min(u)));


c10=abs(bindabsor(30:end)-(c0/10)); %finding 10% breakthrough time by minimizing abs
[30:end] excludes wrong determination of absorption caused by bubbles.
k=find(c10==min(c10))+29; %add 29 to k again to be consistent with time
%finding 10% breakthrough time

vpermeate= bindrate*(t(k)-t(bindstart));
Qdbc = proc*vpermeate/0.09%Formula to calculate DBC

cnorm=absor/c0; %normalize absorbance values

tnorm=t/max(t); %creating normalized time

tbind=t(bindstart:bindend); %create vector for binding time
tbind0=t(bindstart:bindend)-t(bindstart);
%create vector for binding time starting with 0.
tbindnorm=tbind0/max(tbind0); %normalizing
cbind=cnorm(bindstart:bindend); %create vector for bindinding absorption

figure(4); %plot binding curve
plot(tbindnorm, cbind);
title('Breakthrough Curve')
xlabel('Time, Normalized')
ylabel('Absorption, Normalized')

vol=[t(1:elureq);((elurate*(t(elureq+1:end)))-((elurate-1)*(t(elureq))))];
%Total volume at every time
volbind = vol(bindstart:bindend)-vol(bindstart);
%Vector for volume starting with 0 when binding starts
volbindnorm = volbind/max(volbind);

volnorm = vol/max(vol);

bindrange = volnorm(bindend)-volnorm(bindstart)
elurange  = volnorm(end)-volnorm(elustart)
figure(5)
plot(volnorm,absor/c0)
title('Full Chromatogram')
xlabel('Volume, norm')
ylabel('Absorption, Normalized')

Aelu=trapz(volnorm(elustart:end),cnorm(elustart:end)); %Area under elusion curve
Abind=bindrange-(trapz(volnorm(bindstart:bindend),cnorm(bindstart:bindend))); %Area
above binding curve
rec=Aelu/Abind
pbound = Abind/bindrange;
mgbound=pbound*proc*bindvolume;
```

Appendix C

Protein Amino Acid Sequences

Table C.1: 1-Letter code for amino acids

1-Letter	Amino Acid
A	Alanine
C	Cysteine
D	Aspartic Acid
E	Glutamic Acid
F	Phenylalanine
G	Glycine
H	Histidine
I	Isoleucine
K	Lysine
L	Leucine
M	Methionine
N	Asparagine
P	Proline
Q	Glutamine
R	Arginine
S	Serine
T	Threonine
V	Valine
W	Tryptophan
Y	Tyrosine

C.1 1-Letter Amino Acid Code

This Appendix section will display amino acid sequences of proteins used. The sequences are given in the 1-letter-code. Table C.1 can be used to translate letters into amino acids.

C.2 Amino Acid Sequence of BSA

Taken from: http://www.ncbi.nlm.nih.gov/protein/CAA76847.1

```
  1 mkwvtfisll llfssaysrg vfrrdthkse iahrfkdlge ehfkglvlia fsqylqqcpf
 61 dehvklvnel tefaktcvad eshagceksl htlfgdelck vaslretygd madccekqep
121 ernecflshk ddspdlpklk pdpntlcdef kadekkfwgk ylyeiarrhp yfyapellyy
181 ankyngvfqe ccqaedkgac llpkietmre kvltssarqr lrcasiqkfg eralkawsva
241 rlsqkfpkae fvevtklvtd ltkvhkecch gdllecaddr adlakyicdn qdtissklke
301 ccdkplleks hciaevekda ipenlpplta dfaedkdvck nyqeakdafl gsflyeysrr
361 hpeyavsvll rlakeyeatl eeccakddph acystvfdkl khlvdepqnl ikqncdqfek
421 lgeygfqnal ivrytrkvpq vstptlvevs rslgkvgtrc ctkpesermp ctedylslil
481 nrlcvlhekt pvsekvtkcc teslvnrrpc fsaltpdety vpkafdeklf tfhadictlp
541 dtekqikkqt alvellkhkp kateeqlktv menfvafvdk ccaaddkeac favegpklvv
601 stqtala
```

C.3 Amino Acid Sequence of IgG

C.3.1 IgG heavy chain

Taken from: http://www.ncbi.nlm.nih.gov/protein/CAA75030.1

```
  1 mefglrwvfl vailkdvqcd vqlvesgggl vqpggslrls caasgfayss fwmhwvrqap
 61 grglvwvsri npdgritvya davkgrftis rdnakntlyl qmnnlraedt avyycargtr
121 fleltsrgqm dqwgqgtlvt vssastkgps vfplapssks tsggtaalgc lvkdyfpepv
181 tvswnsgalt sgvhtfpavl qssglyslss vvtvpssslg tqtyicnvnh kpsntkvdkk
241 vepkscdkth tcppcpapel lggpsvflfp pkpkdtlmis rtpevtcvvv dvshedpevk
301 fnwyvdgvev hnaktkpree qynstyrvvs vltvlhqdwl ngkeykckvs nkalpapiek
361 tiskakgqpr epqvytlpps rdeltknqvs ltclvkgfyp sdiavewesn gqpennyktt
421 ppvldsdgsf flyskltvdk srwqqgnvfs csvmhealhn hytqkslsls pgk
```

C.3.2 IgG light chain

Taken from: http://www.ncbi.nlm.nih.gov/protein/CAA75031.1

```
  1 mdmrvpaqll gllllwlrga rcdiqltqsp sslsaavgdr vtiacrasqs iadylnwyqq
 61 kpgkapklli ygssslqsgv psrfsgsgsg tdftlsissl qpgdfatyyc qqshtspftf
121 gggtkvqmkr tvaapsvfif ppsdeqlksg tasvvcllnn fypreakvqw kvdnalqsgn
181 sqesvteqds kdstyslsst ltlskadyek hkvyacevth qglsspvtks fnrgec
```

C.4 Amino Acid Sequence of EG2

Taken from: Bell et al., 2010, doi:10.1016/j.canlet.2009.08.003

```
  1 QVQLVESGGG LVQAGDSLRV SCAASGRDFS DYVMGWFRQA PGKEREFVAA ISRNGLTTRY ADSVKGRFTI
 71 SRDNDKNMVY LQMNSLKPED TAVYYCAVNS AGTYVSPRSR EYDYWGQGTQ VTVSSAEPKS CDKTHTCPPC
141 PAPELLGGPS VFLFPPKPKD TLMISRTPEV TCVVVDVSHE GPEVKFNWHV DGVEVHNAKT KPREEQYNSY
211 VVSVLTVLHQ DWLNGKEYKC KVSNKALPAP IEKTISKAKG QPREPQVYTL PPSRDELTKN QVSLTCLVKG
281 FYPSDIAVEW ESNGQPENNY KTTPPVLDSD GSFFKKLTVD KSRWQQGNVF SCSVMHEGLH NHYTQKSLSL
351 SPGK
```

C.5 Amino Acid Sequence of Lysozyme

Taken from: http://www.ncbi.nlm.nih.gov/protein/AAC37312.1

```
  1 mkaliilgfl flsvavqgkv fercelartl kklgldgykg vslanwlclt kwessyntka
 61 tnynpssest dygifqinsk wwcndgktpn avdgchvscs elmendiaka vacakhivse
121 qgitawvawk shcrdhdvss yvqgctl
```